INTERNATIONAL SYMPOSIUM
PRESERVATION OF MONUMENTS & HISTORIC SITES
SEPTEMBER 2026 | ATHENS, GREECE

ΕΛΛΗΝΙΚΗ ΕΠΙΣΤΗΜΟΝΙΚΗ ΕΤΑΙΡΕΙΑ ΕΔΑΦΟΜΗΧΑΝΙΚΗΣ & ΓΕΩΤΕΧΝΙΚΗΣ ΜΗΧΑΝΙΚΗΣ

Τα Νέα της Ε Ε Ε Ε Γ Μ

205

4th International Symposium
Preservation of Monuments and Historic Sites

16 – 18 Σεπτεμβρίου 2026
Εθνικό Ίδρυμα Ερευνών, Αθήνα

Αρ. 205 – ΝΟΕΜΒΡΙΟΣ 2025

SIMSG ISSMGE

ISRM

ISSN: 2732-7248

Π Ε Ρ Ι Ε Χ Ο Μ Ε Ν Α

ΑΡΘΡΑ

November 1861:
Chalmers' under Channel railway

In 1861 The Engineer reported on an early proposal to build a subsea railway across the English Channel

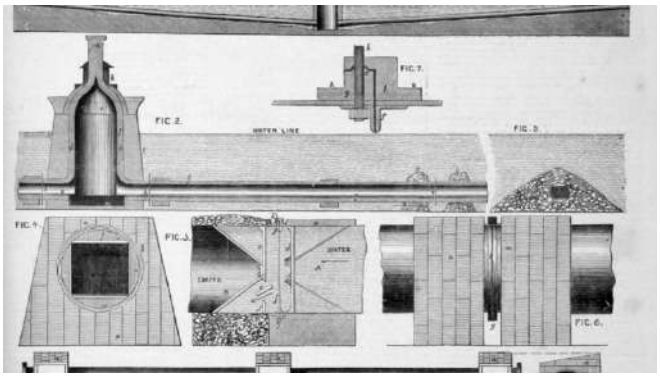

Over the years The Engineer has reported on several schemes to connect the UK to mainland Europe and, as we know, only one project has been successful so far.

Tunnels and bridges have been proposed and in 1880 work started on experimental tunnels in Folkstone that were dug by hand and an early tunnel boring machine.

Nineteen years earlier, The Engineer reported on how a certain James Chalmers of Montreal had 'patented the means whereby he proposes to open a railway communication under the channel.'

Chalmers' idea was somewhat unique in that he'd connect sections of tube and submerge them, rather than dig a tunnel.

The Engineer said: "The shape and form of the tubular roadway may be varied, but it is preferred that such tubular roadway for deep water should be of a circular section, having a rectangular inner way formed therein, as thereby the pressure of the water at great depths may be divided between the tubes by allowing the leakage of the outer or circular tube to collect between it and the inner one, until it obtains such pressure as the inner or square tube may safely carry, then drawing it off through valves into the inner tube, thus relieving by reaction the pressure on the outer or circular tube.

"The length or sections of a tubular way have each bulkheads or partitions, one near each end, which are of a strength to resist the pressure of the water when the length or section is submerged, and when it has been emptied of water."

Each end of a length or section of the tubular way would be formed with inner flanges, as well as with an outer flange. The construction of a tubular roadway could be commenced from shore or bank, and Chalmers thought it preferable to start at a spot 'intermediate of the two shores or banks of the River, Sea, or other water'.

In the tower, suitable steam engines, pumps and machinery are to be constructed, in order to pump away the water in the tower, and to keep it free from water

"In order to commence the works at a point intermediate of the two shores or banks, a tower is first submerged of such dimensions as to descend to the bottom of the water, and to ascend to some height above its upper surface, provision being made for connecting the ends of the tubular ways on opposite sides of the tower in like manner to that in which the ends of the lengths or sections of the tubular way are connected end to end, when they are submerged," said The Engineer.

Our Victorian predecessor continued: "In the tower, suitable steam engines, pumps and machinery are to be constructed, in order to pump away the water in the tower, and to keep it free from water. The lengths or sections of the tubular roadway are in succession floated out to positions they are to occupy, and are then submerged and coupled up, and their inner flanges riveted or connected by screw bolts and nuts, and, as each length section of the tubular roadway is in succession coupled up, the water used therein to aid in submerging it is allowed to flow from it into the sections previously submerged, and thence to the tower where the water is raised and pumped away.

To have a clear way through the lengths of tubular roadway between the tower and the length next to the one last submerged, the bulkheads or partitions were removed as the work proceeded. The outermost bulkhead or partition would remain until another length had been submerged and fixed to the end of the one previously submerged.

When compiling our archive pieces, it is common practise to investigate the career of the main protagonist, but Chalmers left little trace of himself to study. Luckily, The ICE Archive helped to fill in the blanks. They pointed out that Chalmers was quite an inventor, having invented the Chalmers Target, armour for naval warships detailed in Ships of War—Petition of Mr James Chalmers - Hansard - UK Parliament. The ICE Archive told us also that he wrote a book about naval construction. We might also assume he wrote 'The Channel Railway, connecting England & France' prior to his untimely death at the age of 49.

His passing warranted a small obituary in the January 1, 1869 edition of The Engineer, which noted that Chalmers left his widow and family in 'very straightened circumstances'.

"It is to be hoped his exertions on behalf of the public service will not be overlooked by the government," said The Engineer.

(Jason Ford / THE ENGINEER, 18 Nov 2024, https://www.theengineer.co.uk/content/archive/november-1861-chalmers-under-channel-railway)

THE UNDER-CHANNEL RAILWAY.

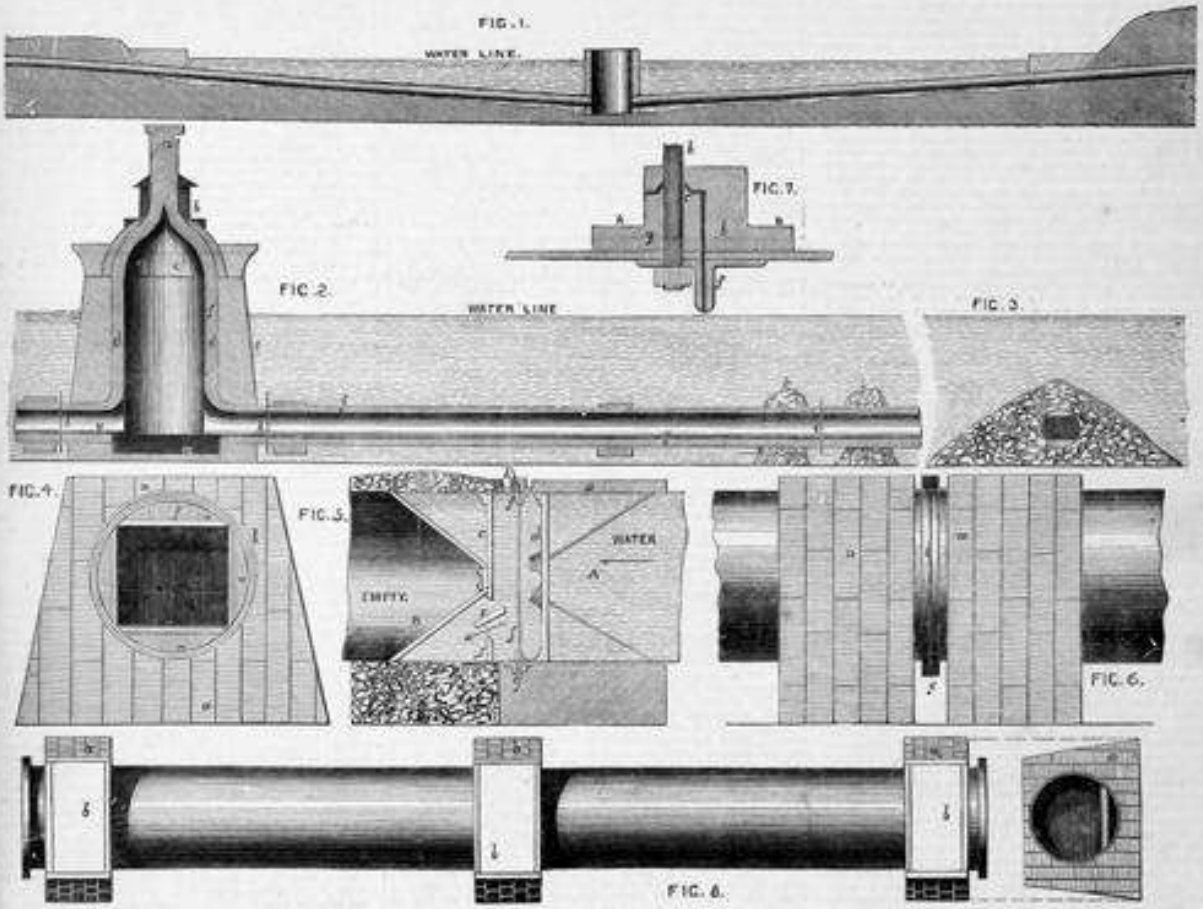

Mr. James Chalmers, of Montreal, has patented the means whereby he proposes to open a railway communication under the Channel. In his specification he says that his invention has for its object improvements in constructing roadways under water, and consists in submerging tubes of suitable dimensions and construction, in place of having recourse to tunnelling, as heretofore. The shape and form of the tubular roadway may be varied, but it is preferred that such tubular roadway for deep water should be of a circular section, having a rectangular inner way formed therein, as thereby the pressure of the water at great depths may be divided between the tubes by allowing the leakage of the outer or circular tube to collect between it and the inner one, until it obtains such pressure as the inner or square tube may safely carry, then drawing it off through valves into the inner tube, thus relieving by reaction the pressure on the outer or circular tube. The lengths or sections of a tubular way have each bulkheads or partitions, one near each end, which are of a strength to resist the pressure of the water when the length or section is submerged, and when it has been emptied of water. Each end of a length or section of the tubular way is also formed with inner flanges, as well as with an outer flange. The construction of a tubular roadway may be commenced from either shore or bank, but it is believed that generally it will be preferable to commence at a spot intermediate of the two shores or banks of the river, sea, or other water, through and submerged to which a tubular roadway is to be constructed. In order to commence the works at a point intermediate of two shores or banks, a tower is first submerged of such dimensions as to descend to the bottom of the water, and to ascend to some height above its upper surface, provision being made for connecting the ends of the tubular ways on opposite sides of the tower in like manner to that in which the ends of the lengths or sections of the tubular way are connected end to end, when they are submerged. In the tower suitable steam engines, pumps, and machinery are to be constructed, in order to pump away the water in the tower, and to keep it free from water. The lengths or sections of the tubular roadway are in succession floated out to the positions they are to occupy, and are then submerged and coupled up, and their inner flanges rivetted or connected by screw bolts and nuts, and, as each length or section of the tubular roadway is in succession coupled up, the water and therein to aid in submerging it is allowed to flow from it into the sections previously submerged, and thence to the tower where the water is raised and pumped away. And in order to have a clear way through the sections or lengths of tubular roadway between the tower and the length next to the one last submerged, the bulkheads or partitions are removed as the work proceeds, the outermost bulkhead or partition remaining till another section or length has been submerged, and has been affixed to the end of the one previously submerged, and the work is so carried on, that the pressure of the outer water acts on the last submerged section or length of the tubular way, to force it against the end of the one previously submerged and fixed. In order to retain the sections or lengths of the tubular way from floating when they are empty, each section is formed with hollow chambers, which are open above but enclosed on all sides, and at the bottom these chambers surround the tubular way, and by having deposited therein a quantity of stones retain them from rising when once submerged and got correctly into position, the chambers being loaded before running off the water contained in the section or length, and before releasing the section or length from the tackle used in submerging it. A section or length of the tubular way having been floated into the position where it is to be submerged, it is made fast to the tackle employed, and a quantity of water is allowed to enter, but not sufficient to cause it to sink; the section or length retaining a quantity of its buoyancy, is gradually drawn down under the water by means of tackle, and brought with its end against the end of the section or length previously submerged and fixed. The tackle used for submerging the sections consists of chains, which are passed through blocks or suitable apparatus anchored or fixed below the water in such manner as to bear the strain of submerging the sections or lengths of the roadway, and such tackle and apparatus is so arranged and worked that the section or length which for the time is being lowered shall be submerged to the proper depth, and the depth and position of it indicated as the work proceeds. In order to ascertain when the end of a length or section of the tubular roadway has been brought into position, or nearly so, there are openings in the bulkheads or partitions fitted with strong glass, through which, by the aid of strong light from within the fixed part of the tubular way, the presence of the end of the section or length which is being brought into position may be seen, and as soon as the ends have come together correctly, the sea pressure will be greatly increased by withdrawing some of the water which is in the space between the two bulkheads or partitions of the two sections or lengths of the tubular way which have by the working of the tackle been brought together.

Fig. 1 shows a section or profile of a channel or river, and of the outline of a tubular roadway; Fig. 2 shows a section of ventilator; such ventilator will be best constructed of iron and stone, c and d being two circular vertical shafts or tubes with stonework built between them. The bottom m may (in order to give strength) be a double cellular bottom, the cells may be filled with concrete when built, launched, and such is its place. The water between the shells a and d may be pumped out, and the stonework built. e is the ventilator or chimney that draws the smoke and foul air from the flues f, f, which are used when the width of the water is great; h is space for a light-house where one is required, as in a navigable channel; g, g, level of the roadway, the space between the bottom m and the roadway is for drainage; k, k, junctions of tubes to ventilator, they will be joined in the same manner as they are joined to each other, as hereafter described; b, i, one length or section of tubular roadway such as may be submerged at a time. When the surface or bottom is ascertained to be uneven, the chamber k can either be shortened by reducing the height, or lengthened by adding blocks of timber, as shown under chamber k, and the other chambers may be partly open to the bottom, allowing material to pass through and form a bottom on the bed of the stream or channel, as is shown at the chamber l; or when it is desirable to make something more permanent than a simple iron tube, by lining it with brick or otherwise, the whole tube may be covered by an embankment as in section Fig. 8. When required at great depths the tubes may be double, a rectangular within a cylindrical tube, and water may be allowed to collect in the spaces w, w, w, (Fig. 4) between them until it attains such a pressure as the inner or square tube may safely carry, then drawn off through valves into the inner tube. The space f is reserved for ventilation where required. a, a, a, a, Figs. 4, 5, 6, and 8, are the bosses or chambers for loading down the tubes, and b, b, b, Fig. 6, are the open parts to receive the loading. These bosses will be best made of iron plates, rivetted together and attached to the tubes by angle iron. Fig. 5 shows method of joining the tubes together under water. Fig. 6 shows an elevation of the ends of two tubes joined together. Fig. 7 shows a method of guiding the ends together. The bolt k is fastened inside of tube A when secured in its place. This bolt has attached to its end a wire cable (see Fig. 5) which, while a tube B is on the surface of the water, is passed through a hole in flange k, and as the tube B descends to its place the bolt k guides the flange k till it rests on the cone c; a circular cone surrounds the bolt hole in the flange g, and the flange k is a semicircular projecting flange, which overlaps the flange g, and guides the end of the tube B to the end of the one previously fixed in its place; when the ends are firmly brought together they are joined, as in Fig. 5. Tube A is shown to be fixed in its place, and fixed from water inside of the partition c. Through the dead lights in the said partition c, aided by strong reflecting lamps, it will be seen when the flanges of the ends of the tubes A and B come together; then the valve c is opened, allowing the water between the partitions c and d to escape through tube A, when the water pressure on tube B will force the flanges k and g together, and as they have an elastic or compressible substance between them a water-tight joint will thus be made, and men will be able to pass into the space between the partitions c and d, and by bolting the flanges f, f, together they will make a permanent joint. The tube B is then to be loaded down, the bolt k will be withdrawn, the partition d will be removed. The operations will be repeated at the other end of the tube B, when another length of tube is lowered. The tube B is furnished with a partition c and valve c, the same as in tube A, and the work thus continued until the tubes reach the shore. When the depth is not great a plain cylindrical tubular passage may be formed strengthened by angle or T-iron, with floor and ceiling, as in section Fig 8, or with floor only, as in section Fig. 6.

Railways in Italy.—A private letter from Turin gives a favourable account of the progress of the Bologna and Ancona Railroad. "M. Salamanca," it says, "had engaged to open for traffic on the 1st of January, 1862, this line, which is not less than 200 kilometres. Half of it is working since the 5th inst., and the whole will be open during the first fortnight of November. In two years M. Salamanca will have connected Rome with Naples and Turin. What, I ask you, can diplomacy do against such an union? You are aware that in Portugal also he is the constructor of the lines which will unite Lisbon with Oporto, and Portugal with the Spanish lines. Here again is another union which must be henceforth taken into account. The line from Naples to Rome will be finished next year, and in the meantime the two capitals will be drawn closer to each other, so that in a couple of months there will be a very limited number of kilometers remaining to be finished."

Artesian Wells.—A communication has been received on this subject by the Academy of Sciences from M. Gaudin, in which he replies to the question often asked, whether the supply of the Artesian wells, bored in the neighbourhood of Paris, can ever be exhausted? The stratum of green sandstone interposed between the strata of chalk and Jurassic limestone is of the average thickness of 160ft.; consequently, taking the depth of 1,802ft. of the Artesian well at Passy as a criterion, there remains a depth of 870ft. of sand. A cubic metre of sand, closely examined, weighs 1,600 kilogrammes, while compact quartz weighs 2,600 kilogrammes; hence the stratum of sand, even supposing it to be closely packed, has interstices amounting to one-third of its bulk in the aggregate, so that every cubic metre (35½ cubic feet) of sand under water contains 333 litres (73½ gallons) of water. Now, the layer of sand existing under the chalk may be represented by a disc of 100 miles radius, and its thickness to 200. The cubic contents of this disc are, therefore, 141,372,500,000,000 gallons, which, divided by 22,000,000,000, then by 365, gives the quotient 175, being the number of years requisite to exhaust the supply of water at the rate of 19,000,000 cubic metres (22,000,000,000 gallons) per day! This would be correct, supposing the quantity of water to remain stationary, and never to receive any increment by the infiltration of rainwater and that of rivers. This our author calculates at half a metre per annum, and hence arrives at the conclusion that the annual increase of the water is double the quantity expended, so that the Artesian wells in or about Paris are, and must ever be, inexhaustible.

Deformation Behaviour of Secant Pile Walls in Layered Soil–Rock Profiles: Lessons Learned from Deep Excavations in Copenhagen

E. Panagiotis, I. Rocchi, F. Petrella, E. Paulatto & V. Zania

Abstract

The performance of deep excavations in layered stiff ground conditions (overconsolidated soil overlying rock) remains largely unexplored, with few published case studies available, hindering the understanding of performance and key indicators for deep excavations in such ground conditions. This study addresses this gap by comprehensively investigating seven deep excavations for a new metro line in Copenhagen. These excavations utilized temporary retaining walls constructed via the bottom-up method in stiff, layered ground conditions embedded in limestone. Through a long-term instrumentation program, the major factors influencing deformation behaviour were examined, including secant pile wall deflections, anchor and strut axial forces, and groundwater levels inside and outside the pits. During the cantilever stage, the maximum normalized deflections ($u_{h,max}/H_e$) ranged from 0.05 to 0.25%, aligning closely with other reported case studies in the literature. Ground stiffness emerged as the critical factor affecting wall deflections, both in the cantilever and supported stages. The relationship between soil stiffness and deflections transitioned from linear to non-linear as construction progressed. Predictive equations for supported cases are derived based on monitoring data, and 3D effects were estimated in four excavations, consistently with existing studies in layered soft soil. This paper expands the literature on secant pile wall behaviour in stiff ground conditions, offering theoretical support for similar projects.

1 Introduction

Underground structures have been extensively constructed for high-rise buildings and subways, adjacent to either existing transportation networks (subways, tunnels) or surrounding buildings, to meet the increasing demand for space in densely populated areas, which is limited due to the rapid urbanization that occurred in recent decades. One of the crucial design aspects of deep excavations is to minimize wall deformations and ground movements, eliminating risks to nearby structures and economic and human losses. This is achieved by monitoring the excavation-induced ground movements and wall deformations. In this context, field data are commonly used to validate predictions obtained with numerical analyses. Field observations have furthermore been used either independently or in conjunction with numerical studies to develop semi-empirical preliminary design tools to provide upper boundary estimates for excavation-induced wall deflections as a function of excavation depth (Peck 1969; Clough and O'Rourke 1990; Ou et al. 1993, Gaba et al. 2017).

Peck (1969) and Clough and O'Rourke (1990) reported maximum displacement normalized to excavation depth at around 0.2–0.3% in stiff clays and sands and 0.5–2% in soft to medium clays, where wall stiffnesses varied. Gaba et al. (2017) recommended in CIRIA 760 an upper bound of 0.25% for unsupported excavations in stiff soils, which aligns closely with the values for stiff clays reported by Clough and O'Rourke (1990). Based on 153 case studies where stiff soil was present at dredge level, Long (2001) reported an average maximum normalized horizontal displacement of 0.36% for cantilever walls, whereas for propped and anchored walls this value decreased to 0.18%. Published studies on layered stiff ground conditions (soil overlying rock) are, however, limited. Yoo (2001) compiled field data from 62 deep excavations in layered ground conditions of soils overlying rock strata in Korea. This study suggested an average maximum normalized wall deflection of 0.12%, while Moorman (2004) reported a value of 0.25% for supported excavations in rocks. Seo et al. (2009) reported average normalized lateral deflections of 0.14% and 0.18% based on data from two sites with comparable ground conditions, which is consistent with the findings of Yoo (2001). It is worth mentioning that Long et al. (2012), who compiled data from 30 deep excavations in layered ground conditions (soft and stiff soils overlying rock), observed even stiffer wall responses for the supported stages compared to the ranges reported in the aforementioned studies, with an average normalized deflection of 0.075%.

To elucidate the factors governing the performance of deep excavations (i.e., ground conditions, types of retaining walls, construction method, support stiffness, etc.), Mana and Clough (1981) introduced the effective stiffness parameter, which is a function of flexural stiffness of wall (EI), the vertical spacing between the supports (s_v) and the unit weight of the soil (γ). Clough et al. (1989) expanded this work through plane strain finite element analyses, replacing the unit weight of soil with the water unit weight to define the support system stiffness (k_s) and including the factor of safety against basal heave. Clough and O'Rourke (1990) found that when basal stability is an issue (i.e. soft to medium clays), the key design parameter in controlling the ground movements is the support system stiffness (k_s), but that this has little influence on stiff clays, because of their lack of need for stiff support systems. For stiff clays, the soil modulus and the coefficient of lateral earth pressure were found to have a more significant impact on ground movements. Additional factors, such as the three-dimensional nature of an excavation, the effects of different support types were also found to play a role but were not considered in Clough and O'Rourke's (1990) chart. To address this gap, Bryson and Zapata-Medina (2012) proposed a new relative stiffness ratio (R) parameter to predict lateral movements, which accounts for the relative stiffness resistance (soil and wall stiffness), the relative bending resistance (vertical and horizontal support spacing, wall moment of inertia) and the excavation stability number (excavation depth, undrained shear strength). This parameter was used with the safety factor against basal heave to construct a new design chart by Bryson and Zapata-Medina (2012), which estimates the lateral wall movements on cohesive soils.

Because of the scarcity of published studies on layered stiff ground conditions (soil overlying rock), these semi-empirical design charts do not incorporate observations on layered soil-rock profiles, and therefore their use may result in potential overdesign and unnecessary project costs. To address this gap, Yoo (2001) suggested an upper-bound equation for predicting normalized maximum lateral wall deflections based on k_s, despite reporting no clear effect of the wall type, except for the observation that diaphragm walls showed relatively smaller deflections compared to the others. Furthermore, they reported a significant influence of soil stiffness on observed wall deflections based on numerical analyses, even though this was not incorporated in the proposed predictive expression for wall deflection. It is important to highlight that none of the reported studies on monitoring data presents a quantitative assessment of the impact of soil stiffness on the deformation behaviour of retaining walls, and the soil elasticity parameters are not reported for the entire stratigraphy. This absence of data hinders further interpretation of results and underscores the need for comprehensive reporting on soil stiffness and analysis of its role on wall deflections in future studies within this domain.

The aim of this research is to improve secant pile walls deformation prediction in layered stiff ground conditions (overconsolidated soil overlying rock), through the analysis of a detailed instrumentation program. To achieve this objective, field measurements of seven deep excavations in the Copen-

hagen area were analysed, where stiff soil layers overlie limestone. The deep excavations herein discussed were performed as part of the extension of the Copenhagen's metro line to Sydhavn, and they are situated in the vicinity of existing infrastructure and buildings. Deformation of secant pile walls, axial forces of anchors and struts, and groundwater levels inside and outside the excavations were systematically monitored throughout the construction and are discussed hereafter. The primary factors affecting the deformation behaviour of the walls during the construction process, including the influence of soil stiffness and 3D effects, are investigated. The findings enrich the existing limited database of secant pile walls performance in layered soil-rock profiles and provide evidence-based support for a more reliable and sustainable design and construction of similar projects in the future.

2 Case Studies and Subsurface Conditions

The excavation case studies presented are Havneholmen (HOL), Enghave Brygge (EBR), Ørstedværket (ØVK), Sluseholmen (SLU), Mozards Plads (MOP), Gåsebæk (GÅB), and Ny Ellebjerg (NEL), where EBR and ØVK are adjacent. The extension of the metro consists of five new underground stations (HOL, EBR, SLU, MOP, and NEL) and two shafts (ØVK and GÅB) that are connected by 4.5 km of twin-tube tunnels. The plan view of the new Copenhagen metro line (M4), indicating the locations of the five metro stations is illustrated in Fig. 1.

Fig. 1

Plan view of Copenhagen's M4 metro line, with case study areas also displayed

2.1 Geology of Copenhagen area and Site Descriptions

The typical geological profile in Copenhagen consists of Quaternary deposits that overlie the Paleogene deposits, which are mainly Danian limestone and locally Selandian greensand. The Danian limestone comprises the Copenhagen Limestone, which is subdivided into the Upper (UCL), Middle (MCL) and Lower Copenhagen Limestone (LCL), and the Bryozoan Limestone (BL). The Copenhagen Limestone overlies the Bryozoan Limestone and is characterized by alternating indurated and less indurated beds and can be generally described as a weak rock with very hard layers or nodules of flint (Paulatto & Carstensen 2017). The upper part of the Copenhagen limestone is typically disturbed or highly fractured by glacial processes, except in areas where the Greensand locally overlies it. The Bryozoan limestone is characterized by asymmetrical mound structures with amplitudes typically raining from 5 to 10 m (Frederiksen et al. 2003). The Quaternary deposits consist of some transitional and true glacial deposits that are subdivided into low permeability (10^{-5}-10^{-9} m/s) tills (upper (ML1) and lower (ML2) clay till /sand till (MS2)) and intermediate to high permeability (10^{-3}-10^{-6} m/s) meltwater deposits (upper (DS1) and lower (DS2) sand and gravel (DG1)). The classification of glacial deposits is based on soil behaviour in a natural moist state, rather than grading (Frederiksen et al. 2003). For instance, any soil that exhibits plastic behaviour at natural water content is classified as clay till, even though the clay fraction might be as low as 15%. Finally, the Quaternary deposits are covered by late and post glacial deposits and fill layers. The fill layer is heterogeneous and consists primarily of sand, gravel and clay and occasionally organic material or building debris.

2.2 Site Conditions and Geotechnical Characterization

The ground conditions at the construction sites and the characteristic geotechnical parameters for the different soil units were determined based on the extensive ground investigations that were carried out as part of the construction of the Copenhagen's metro lines. The design stratigraphies at each of the seven excavations are presented in Fig. 2. Moreover, the determination of the design properties for the fill layer was based on the SPT results, incorporating existing formulations suggested by Stroud (1989) for normally consolidated material. The range of SPT blow counts for all soil units is presented in Table S1 for reference. For the glacial deposits (ML1, ML2, and MS2), both drained and undrained triaxial tests (CAU-CAD) were utilized. Geotechnical properties of Copenhagen and Bryozoan limestones were defined based on triaxial and unconfined compressive strength tests, along with Optical and Acoustic Televiewer (OATV) observations. Great attention was paid to characterizing the rock units, since all excavations are embedded in at least 50% within them. The characteristic values of soil/rock parameters that were adopted in the design phase are presented in Table S1.

Fig. 2

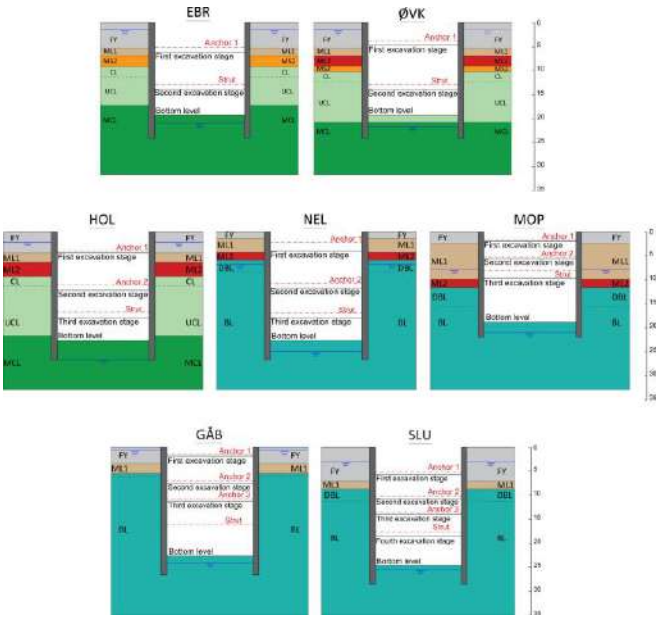

Typical cross sections of the seven deep excavations. The ground design profiles, and the temporary supports are also displayed. Depth measurements are shown in meters. FY: Fill layer, ML1: Upper clay till, ML2: Lower clay till, MS2: Glacial sand till, CL: Disturbed upper Copenhagen limestone, UCL: Upper Copenhagen limestone, MCL: Middle Copenhagen limestone, DBL: Disturbed Bryozoan limestone and BL: Bryozoan limestone

The wall deformation behaviour is anticipated to be influenced by ground stiffness, and the scope of this study is to

analyse this effect. Hence selecting an appropriate representative ground stiffness value is important. As emphasized in various studies (Atkinson 2000), the soil stiffness is stress-dependent and degrades with strain evolution. However, the observed intrinsic variability in ground stiffness in the present soil units (coefficient of variation, COV = 40%; see Panagiotis et al. (2024) for details) outweighed the significance of stiffness degradation. Therefore, a probabilistic approach was adopted for the quantification of the soil and rock stiffness parameters. While this approach may not precisely represent the actual soil stiffness at the specific magnitude and shape of wall deflection, it does account for the variability of the elastic modulus at a stress level of 50% of the strength (E_{50}). An overview of the marginal distributions and their hyper-parameters for all ground units is provided in Table 1, and a graphical illustration of the marginal distributions is shown in Fig. 3.

Table 1 Marginal Distribution and their hyper-parameters for all ground units as inputs for wall deflection probabilistic analysis. (* does not include GÅB)

Table 1 Marginal Distribution and their hyper-parameters for all ground units as inputs for wall deflection probabilistic analysis. (* does not include GÅB)

From: Deformation Behaviour of Secant Pile Walls in Layered Soil–Rock Profiles: Lessons Learned from Deep Excavations in Copenhagen

Groundunit	Distribution	Parameter A	Parameter B	Characteristic [MPa]	Stations
FY	Uniform	6	30	–	All stations*
FY	Weibull	74.28	1.89	58	GÅB
ML1	Weibull	55.01	3.13	48.7	All stations
ML2	Weibull	55.01	3.13	48.7	All stations
MS2	Weibull	55.01	3.13	48.7	All stations
CL/DBL	G1 (Intact): Lognormal	8.035	0.241	2,900	All stations
UCL/MCL	G2 (Intact): Lognormal	9.61	0.404	12,600	All stations
BL Normal	G3 (Intact):	36,126	5545	36,000	All stations
	GSI (Normal)	60	3	60	All stations

Fig. 3

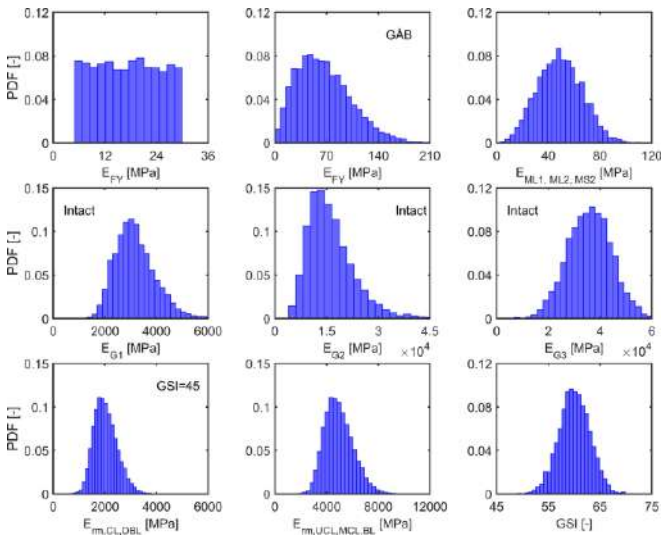

Probability distribution functions of elastic modulus for various units and GSI for the limestone, as implemented in the probabilistic analysis of lateral wall deflections

The marginal distributions of stiffness for the glacial deposits were established using a probabilistic analysis of triaxial data from the ML1 unit (Panagiotis et al. 2024). This distribution was then applied to the ML2 and MS2 units after being validated through a comparison between simulated and actual triaxial test results. Similarly, a probabilistic analysis was conducted on stiffness values derived from analyzing the triaxial tests on intact rock samples with varying degrees of induration. The marginal distributions for each induration level were defined individually. The Copenhagen Limestone is characterized by layering, with each layer exhibiting a distinct degree of induration. Therefore, the estimation of rock mass stiffness involved calculating a weighted average of the rock stiffness based on the induration percentages observed during the site investigation from borehole and OATV logging at each station (E_{50}). This value was then transformed into rock mass stiffness using Eq. 1, as suggested by Hoek and Diederichs (2006), where the disturbance factor, D, was set to 0.25, and the Geological Strength Index (GSI) was defined probabilistically (see Table 1), based on the OATV logging.

$$E_{rm} = E_{50}\left(0.02 + \frac{1-\frac{D}{2}}{1+e^{\frac{(60+15\cdot D-GSI)}{11}}}\right) \quad (1)$$

Finally, the marginal distributions of stiffness for the fill layer were based on N-values obtained from SPT tests. Due to the limited amount of available data, it was deemed more reliable to assign a uniform distribution for the majority of the stations, rather than defining a distinct distribution. However, at the GÅB station, where the majority of SPT N-values were notably higher compared to other stations—indicating a coarser fill composition—a Weibull distribution was fitted to the recorded data.

For each construction stage, the equivalent soil stiffness was estimated based on Eq. 2, where E_i is the soil stiffness of each soil layer, h_i is the thickness of the ith layer and H_e is the excavation depth (i represents the number of layers that were found within the excavation depth). The soil stiffnesses used for the estimation of the are the ones defined probabilistically (Table 1).

$$E_{s,eq} = \frac{E_1 \cdot h_1 + E_2 \cdot h_2 + \ldots E_n \cdot h_n}{H_e}, H_e = h_1 + h_2 + \ldots h_n \quad (2)$$

3 Construction Sequence and Instrumentation

The excavation pits reported in this paper are rectangular in shape, with a width of approximately 20 m and length of 60–120 m. The excavation depth ranges from 18.85 to 24.60 m. The excavations retaining system consists of 1.2 m diameter secant pile walls, supported by ground anchors and steel struts in the temporary case, as shown in Fig. 2 for all cases. The excavations were all completed using the bottom-up construction method, where new anchors or struts were installed as the excavation progressed. After reaching the final excavation depth, the base slab was cast, and after a few days the bottom struts were removed. The characteristics of the piles are the same among the excavations except for the pile length that is a function of the excavation depth and/or the target groundwater cut-off level. The primary pile spacing is 1.8 m and the cracked bending stiffness of the wall is 1745 MNm^2. The excavation and secant pile wall characteristics for all the case studies are summarized in Table 2.

Table 2 Excavation and secant pile wall characteristics for the case studies

Table 2 Excavation and secant pile wall characteristics for the case studies

From: Deformation Behaviour of Secant Pile Walls in Layered Soil–Rock Profiles: Lessons Learned from Deep Excavations in Copenhagen

Case study	EBR	ØVK	HOL	NEL	MOP	GÅB	SLU
Excavation width B [m]	21.1	21.1	20.4	20.4	20.4	19.2	19.2
Excavation length L [m]	63.0	115.0	70.8	116.0	70.0	57.0	65.0
Excavation depth $H_{e,final}$ [m]	19.2	19.2	22.7	22.7	18.9	23.5	24.6
Secant pile wall length H_{wall} [m]	24.5	24.5	26.6	26.6	22.0	26.6	28.5
Soil layer thickness h_{soil} [m]	9.2	10.2	9.3	5.5	11.3	5.5	9.8

Different wall supporting systems were adopted among the case studies due to differences in ground and loading conditions (see Fig. 2). The number of supports is hereafter used to organize the cases in groups and to present and discuss results correspondingly. This grouping allows also to evaluate the performance of excavations with different system stiffness. Group 1 consists of EBR and ØVK, where one row of anchors + one level of struts were installed. Group 2 comprises of the HOL, NEL, and MOP (two row of anchors + one

level of struts), while the third group consists of SLU and GÅB (three row of anchors + one level of struts). It should be mentioned that all supports at MOP were installed within the soil layer, hence at shallower depths compared to the other two case studies (see Fig. 2), and this results in outlying behaviour in the observed performance.

The characteristics of the ground anchors (free and fixed length, prestressed force, and installed inclination) are presented in Table 3. The horizontal spacing of the anchors is the same among the case studies and equal to 1.8 m. Ground water control during construction was carried out by pumping and re-infiltration within injection wells that were located inside and outside the excavation, respectively. Pumping wells ensured that ground water level was kept at least 1 m below the excavation level and re-infiltration wells that water table outside the excavation was not lowered. The re-infiltration rate was approximately 95% to 100% for all the case studies, except for the EBR and ØVK, where it was decreased in order not to exceed the design assumptions. The excess pumped water was discharged to the harbour. The high re-infiltration rate was deliberately set by Copenhagen's municipality to control the settlement development in the inner city and prevent migration of contaminants.

Table 3 Anchor and strut characteristics

Table 3 Anchor and strut characteristics

From: Deformation Behaviour of Secant Pile Walls in Layered Soil–Rock Profiles: Lessons Learned from Deep Excavations in Copenhagen

	Case study	EBR	ØVK	HOL	NEL	MOP	GÅB	SLU
Anchor 1	Pre-stress force [kN]	1000	1000	720	630	600	500	800
	L_{free} [m]	10.0	12.0	11.0	12.0	10.5	13.8	13.5
	$L_{grouted}$ [m]	8.5	8.0	9.0	6.0	8.0	5.0	6.5
	α [°]	35.0	35.0	32.0	30.0	60.0	30.0	30.0
	Installation depth [m]	5.1	4.5	3.9	2.2	1.7	1.5	5.1
Anchor 2	Pre-stress force [kN]	–	–	630	630	550	700	800
	L_{free} [m]	–	–	10.0	9.0	10.0	8.0	8.0
	$L_{grouted}$ [m]	–	–	8.0	6.0	8.0	5.0	7.0
	α [°]	–	–	30.0	25.0	35.0	20.0	20.0
	Installation depth [m]	–	–	11.1	10.7	5.5	7.0	10.6
Anchor 3	Pre-stress force [kN]	–	–	–	–	–	700	800
	L_{free} [m]	–	–	–	–	–	8.0	8.0
	$L_{grouted}$ [m]	–	–	–	–	–	5.0	7.0
	α [°]	–	–	–	–	–	20.0	20.0
	Installation depth [m]	–	–	–	–	–	10.7	13.4
Strut	Cross section	CHS 1016 × 20 mm, Steel S355						
	Installation depth [m]	12.8	12.8	16.8	17.0	8.1	16.0	17.6

The main construction stages followed at SLU are presented in Table 4 as an indicative example of the construction process at all case studies.

Table 4 Construction stages at SLU station

Table 4 Construction stages at SLU station

From: Deformation Behaviour of Secant Pile Walls in Layered Soil–Rock Profiles: Lessons Learned from Deep Excavations in Copenhagen

Stage	Construction Event	Starting Date	End Date
1	Construction of primary secant piles	26-11-2018	14-06-2019
2	Construction of secondary secant piles	14-01-2019	28-06-2019
4	Excavation until depth (d) of 5.20 m		11-06-2019
5	Installation and pre-stress of the first anchor (d = 5.10 m)	10-06-2019	26-06-2019
6	Excavation until d = 10.90 m		23-07-2019
7	Installation and pre-stress of the second anchor (d = 10.40 m)	01-08-2019	08-08-2019
8	Excavation until d = 14.0 m		22-08-2019
9	Installation and pre-stress of the third anchor (d = 13.60 m)	23-08-2019	04-09-2019
10	Excavation until d = 17.60 m		04-09-2019
11	Activation of strut (d = 17.60 m)	20-09-2019	27-09-2019
12	Excavation until d = 24.61 m		18-10-2019

The construction was comprehensively instrumented to ensure the safety of the adjacent existing structures and evaluate the performance of the deep excavation itself. A monitoring database system, called Kronos, was established, and used for storing field measurements from the Copenhagen metro network (Rabensteiner et al. 2015). Figure 4 shows the plan views and inclinometer locations for the seven deep excavations analyzed. The monitoring items are: a) lateral secant pile wall deflections surveyed by seven-nine inclinometers that were installed on both the longitudinal and transverse sides of the excavation. Inclinometers were fixed to the steel reinforcement cages and equipped with In Place Inclinometer sensors with a maximum vertical spacing of 3 m; b) axial forces of anchors and steel struts, which were measured by load cells that were installed on anchor heads and struts, respectively; c) ground surface settlements along the longitudinal direction behind the excavation, which were measured by levelling points installed on the ground surface and d) ground water level inside and outside the excavation pits acquired by standpipe piezometers.

Fig. 4

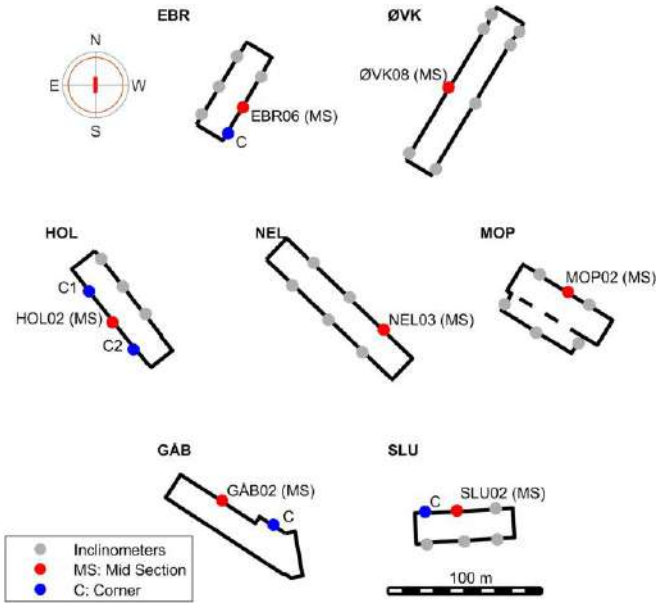

Plan views of the seven deep metro excavations showing the location of the inclinometers situated in the central section (MS) and the ones used to evaluate three dimensional (3D) effects

As shown in Table 5, several inclinometers did not present reliable deflected shapes as the reported values lacked continuity or did not display the expected inward bending. Although all inclinometers were assessed, only those providing reliable information based on obtained deflected shapes and site conditions were used in subsequent analysis. In particular, the inclinometers marked in red in Fig. 4, situated in the mid-section of the excavation, were deemed representative of the plane strain conditions and thus selected for the analysis. However, for the NEL deep excavation, none of the mid-section inclinometers provided reliable measurements. Therefore, NEL 03 was utilized, as its distance from the corner was sufficient to avoid the influence of corner effects. Meanwhile, those marked in blue were included in the evaluation of 3D effects. It is noteworthy that only inclinometers situated on the same side as the reliable mid-section inclinometer were utilized to avoid potential bias in the evaluation process (i.e., different loading conditions on the two sides of the excavation pit).

Table 5 Reliability of inclinometers of the seven deep excavations

Table 5 Reliability of inclinometers of the seven deep excavations

From: Deformation Behaviour of Secant Pile Walls in Layered Soil–Rock Profiles: Lessons Learned from Deep Excavations in Copenhagen

Station	Inclinometer/Location	Comment
EBR	Center of excavation (East side)	No reliable deflected shape
ØVK	–	Consistent measurements on 2 sides of the excavation
	4 inclinometers (North side)	Different structural system (two rows of anchors + one level of struts) than the rest of the station
HOL	–	Different conditions on the 2 sides due to adjacent structure in the West side
NEL	Center of excavation (East side)	No reliable deflected shape
	Center of excavation (West side)	Located close to the staircases (No soil on the active side)
MOP	–	Different conditions on the 2 sides of the excavation
GÅB	Center of Southeast side	No reliable deflected shape (Land reclamation)
SLU	Center of South side	No reliable deflected shape

4 Analysis of Monitoring Data

4.1 Force, Water Levels and Settlement Measurements

Alongside the analysis of wall deflection measurements, the remaining monitoring parameters were also examined. Specifically, the time series of anchor and strut forces were inspected throughout the entire construction period. A comparison of monitored and designed forces was made, especially for anchors with prestressed forces, revealing no significant deviations.

Table 6 presents the strut forces measured at the relevant construction stages, as shown in Figs. 5, 6 and 7. Additionally, the table includes the COV and the 5% and 95% quantiles measured over the investigation period, as the strut forces fluctuate within a day primarily due to temperature variations. Water level measurements were also analyzed, and insignificant deviations were observed within a 24-h duration. The normalized water head difference ($\Delta H_w/H_e$) for all the case studies during the various construction stages is reported in Table S2. Additionally, settlement measurements obtained from leveling points installed in the surrounding area of the excavation pit were analyzed, attempting to associate them with lateral wall deflections. However, their installation distance from the excavation was relatively large (approximately 20 m) and outside the primary influence zone (i.e. the area surrounding the excavation site where the ground experiences the most substantial changes or effects due to the excavation process), preventing valuable insights into ground behaviour. As a result, the measured settlements did not exceed 3 mm in magnitude in any of the examined case studies, which is very close to the measurement precision. Consistently, there was no significant impact on any of the surroundings.

Table 6 Strut forces measured from load cells for the relevant construction stages. The notation of construction stages are in line with the notation used in Figs. 5, 6 and 7

Table 6 Strut forces measured from load cells for the relevant construction stages. The notation of construction stages are in line with the notation used in Figs. 5, 6 and 7

From: Deformation Behaviour of Secant Pile Walls in Layered Soil–Rock Profiles: Lessons Learned from Deep Excavations in Copenhagen

Stage	Strut installation			Final excavation stage		
Case study	Mean [kN]	COV [-]	Quantiles [5%, 95%]	Mean [kN]	COV [-]	Quantiles [5%, 95%]
EBR	–	–	–	2757	0.14	[2237,3524]
ØVK	–	–	–	3468	0.06	[3254,3919]
HOL	354	0.02	[348,359]	3276	0.04	[3111,3488]
NEL	541	0.63	[183,855]	2689	0.29	[1796,4215]
MOP	801	0.36	[499,684]	908	0.07	[823,1016]
GÅB	–	–	–	2085	0.14	[1654,2512]
SLU	–	–	–	3663	0.04	[3476,3854]

Fig. 5

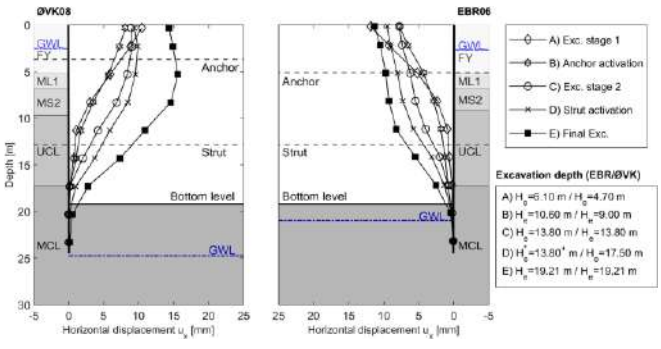

Lateral deflections measured on ØVK and EBR shafts (Group 1) by inclinometers representative of the plane strain conditions (ØVK08 (left) and EBR06 (right)) for different construction stages. * Excavation depth cannot be accurately defined

Fig. 6

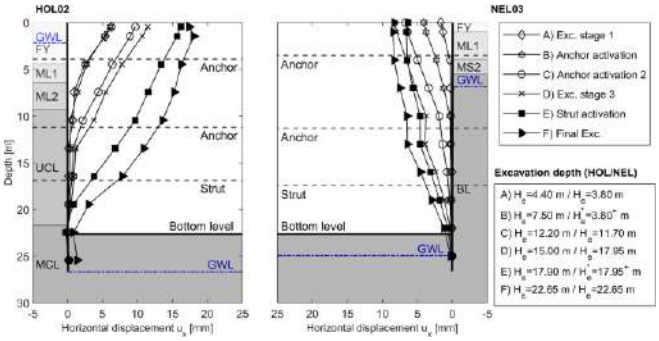

Lateral deflections measured on HOL and NEL shafts (Group 2) by inclinometers representative of the plane strain conditions (HOL02 (left) and NEL03 (right)) for different construction stages. * Excavation depth cannot be accurately defined

Fig. 7

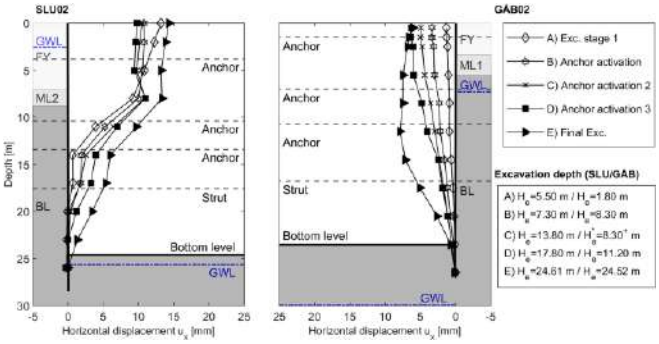

Lateral deflections measured on SLU and GÅB shafts (Group 3) by inclinometers representative of the plane strain conditions (SLU02 (left) and GÅB02 (right)) for different construction stages. * Excavation depth cannot be accurately defined

4.2 Wall Deflected Shapes

The lateral wall deflections measured by inclinometers located in the mid-section of the excavations for each group, which are considered to be representative of the plane strain conditions during the main construction stages, are presented in Figs. 5,6 and 7 for the three groups, respectively. In Group 1, a cantilever movement of the secant pile walls was observed in both cases until the anchor installation. Inward bending in the walls became more evident during the second excavation stage, transitioning from an initial cantilever deflection to a characteristic typical of braced excavations. The maximum wall deflection moved deeper as the excavation progressed. Although the ground conditions were similar at EBR and ØVK, larger deflections were measured consistently at ØVK compared to the EBR, which might be associated with the higher water head difference and the larger spacing between vertical supports at ØVK.

In Group 2, the secant pile walls exhibited a cantilever type deflected shape until the third excavation stage, and the walls began to bend slightly following the installation of the struts. Unlike Group 1, the secant walls in both cases developed the maximum deflection at the top of the wall/ground surface. This can be attributed to the higher system stiffness of the walls, as an additional row of anchors was installed, and a higher percentage of the excavations were within the limestone, especially for NEL. The latter has a clear effect on the magnitude of the observed deflections, as greater deflections were measured at HOL, which might also be associated with the larger water head difference.

The deflected shape of the secant pile walls of Group 3 is similar to that in Group 2, which further supports the argument that the higher system stiffness governs the deflected shape. Although lateral wall deflections at SLU were larger than those at GÅB, this difference can be attributed to the thicker fill layer encountered at SLU. However, the incremental increase in wall deflections in both case studies was of a similar magnitude. Note that the deflected shape at MOP is omitted due to the inherent differences in support conditions, due to the shallow presence of struts, which makes direct comparison impossible.

4.3 Maximum Lateral Wall Deflections

4.3.1 Cantilever Stage

To better investigate the wall displacements, Fig. 8 plots the maximum wall deflection observed at the cantilever stage for all the case studies, corresponding to inclinometers in the mid-section. Wall performances measured from inclinometers facing each other were in agreement, except for SLU and EBR where only one of the two inclinometers provided reliable results. Additionally, wall deflection measurements at MOP are not shown in Fig. 8, as they were not available at this stage. At the unsupported stage, the normalized wall deflections were found to vary in magnitude, ranging from 0.05 to 0.25%, which falls within the lower range of values reported by Long (2001) for cantilever walls in stiff ground conditions with comparable wall stiffnesses. Data points from unsupported excavations in stiff ground conditions reported in CIRIA C760 are also displayed in Fig. 8. CIRIA C760 (Gaba et al. (2017)) recommends an upper bound limit corresponding to 0.25% H_e, which is supported by the observations in this study. Additionally, Fig. 8 shows data from Long et al. (2012), derived from case studies in Dublin with similar ground conditions to those of the investigated sites, where a good agreement in wall deflections between the two sets of cases was observed.

To investigate the variation in the alignment of the data points in Fig. 8, two different analytical approaches were applied. The first approach follows a bilayer model, similar to the methodology used by Long (2001) in constructing its database. In this approach, the data points were plotted with respect to the ratio of the soil thickness to the wall length (Fig. 9a). The second approach takes into account the stiffness of each soil layer. The equivalent ground stiffness was determined based on Eq. 2 and is illustrated in Fig. 9b. Comparison between Fig. 9a and b shows that despite a noticeable trend of increasing normalized wall deflections with an increasing ratio of soil thickness to wall length, the scatter is significant when considering a bilayer model. In contrast, when the equivalent soil stiffness is used in Fig. 9b, the data shows a linear decrease in normalized deflection with increasing equivalent soil stiffness. Both analyses include data from Long et al. (2012), where the relevant details were available. However, it was challenging to perform the latter analysis comprehensively, as values of ground stiffness were not consistently reported for all the case studies in the literature. Despite the greater uncertainty in defining the equivalent soil stiffness for these cases, the overall agreement is strong. To define the bounds of the equivalent soil stiffness ($E_{s,eq}$) for the cases from Long et al. (2012), the reported ranges of stiffness, primarily derived from SPT (Standard Penetration Test) results, were utilized.

Fig. 8

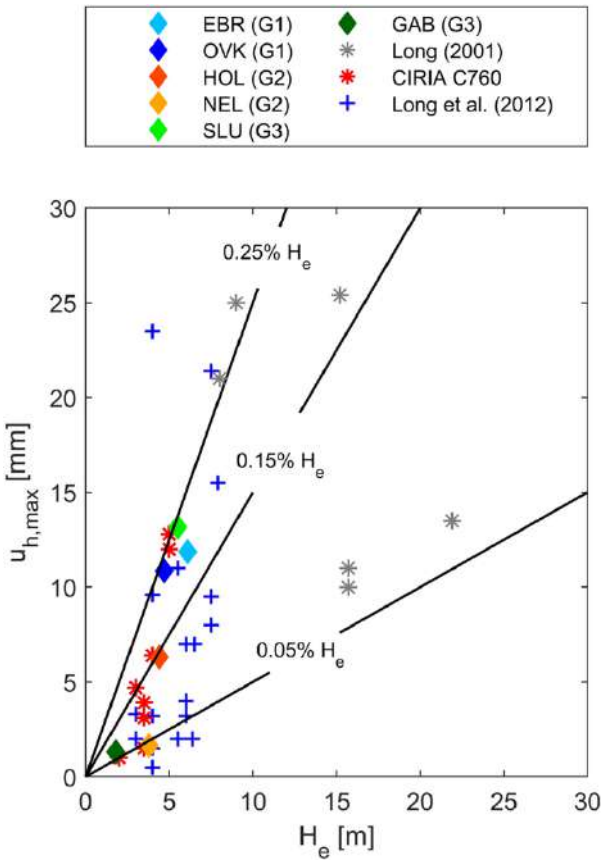

Maximum lateral deflection in unsupported plane strain conditions as a function of excavation depth

Fig. 9

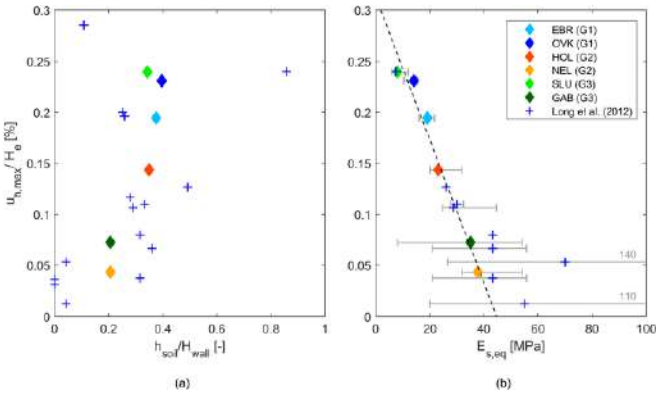

Normalized maximum lateral deflection with respect to the excavation depth in plane strain conditions vs (**a**) ratio of the soil thickness to the wall length h_{soil}/H_{wall}, and (**b**) equivalent soil stiffness $E_{s,eq}$ for all the case studies for the unsupported case

4.3.2 Supported Stages

Similar to the unsupported stage, the maximum wall deflections measured at the subsequent construction stages with respect to the excavation depth are shown in Fig. 10a–c for the three groups, correspondingly. A drop in lateral wall deflections after the prestress of the anchors was observed in all cases, which is a function of the prestress force. It should be highlighted that the total movements measured at the cantilever stage at EBR, SLU, and ØVK were 0.9, 0.9, and 0.65 of the total movements measured at the final excavation stage, respectively. In the rest of the stations, the corresponding ratio ranged between 0.20 and 0.35, which is a function of the equivalent soil stiffness. A linear development

of maximum wall deflections with excavation is observed in all groups. However, different rates of increase (RI) of maximum lateral deflections were observed for the different case studies. By comparing the rate of increase within each of the three groups defined previously shows that in Group 1, the RI at ØVK is much higher ($RI_{ØVK}$ = 0.66–0.74 mm/m) than at EBR (RI_{EBR} = 0.38–0.40 mm/m), even though the two systems have similar stiffness. This observation could potentially be attributed to the larger water head difference that occurred at ØVK station and the slightly larger vertical prop spacing.

Fig. 10

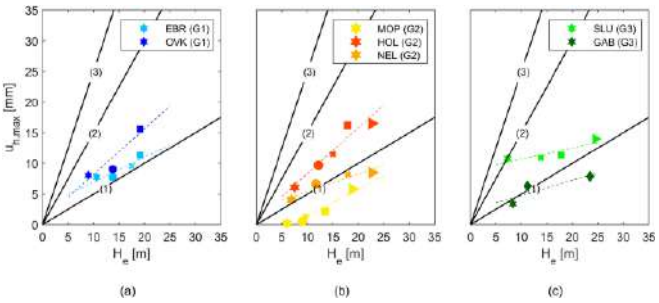

Maximum lateral deflections with respect to the excavation depth in plane strain conditions for the three different groups, (**a**): Group 1, (**b**): Group 2 and (**c**): Group 3 for all the construction stages after the installation of the top anchor. **Group 1**: one row of anchors + one level of struts, **Group 2**: two rows of anchors + one level of struts and **Group 3**: three rows of anchors + one level of struts. (1): $u_{h,max} = 0.05\%H_e$, (2): $u_{h,max} = 0.15\%H_e$, and (3): $u_{h,max} = 0.25\%H_e$

As far as Group 2 is concerned, the highest rate of increase was observed at HOL (RI_{HOL} = 0.70–0.80 mm/m), while the lowest at NEL (RI_{NEL} = 0.24–0.32 mm/m), which is mainly attributed to the higher equivalent stiffness at NEL compared to the other two case studies. A slightly lower rate is observed at MOP during the first excavation stages, which is attributed to struts being installed at shallower depth. Thereafter the rate increases and is comparable to HOL. The installation of the struts at shallow depth seems to have a clear effect on the developed maximum deflections as the values measured in this case study were the smallest observed. Finally, RI measured for the case studies of Group 3 are of similar magnitude (RI_{SLU} = 0.199 mm/m and $RI_{GÅB}$ = 0.244 mm/m), even though the wall deflections at SLU were relatively higher than the ones measured at GÅB. This is mainly attributed to the fact that both excavations are within the Bryozoan limestone unit after the installation of the second anchor and therefore, similar development of wall deflections is anticipated.

Across groups there is no particular trend either on RI or on maximum wall deflections, apart from Group 3 where consistently low RI values are recorded so that it is concluded that the differences in the support systems alone cannot explain the development and accumulation rates of deformations for the secant pile walls of these excavations.

Upon analyzing the influence of system stiffness, k_s, on the normalized maximum deflection, Fig. 11 shows that data from this study exhibit a wide range in k_s. Nonetheless the normalized deflections are small and with only a slight decrease with increasing system stiffness. Figure 11 also includes the data from Yoo (2001) and their upper bound equation, as well as data from Table 2 in Long (2001) that focused on cases with the dredge line in stiff material, like in this study, and data from Long et al. (2012). The data from the present case studies is noticeably situated within the lower range of reported data from both Yoo (2001) and Long (2001). However, details of the geotechnical properties of the soil layers are not provided by Yoo's (2001), making it unclear whether the data pertains to dredge levels in stiff ground conditions.

Fig. 11

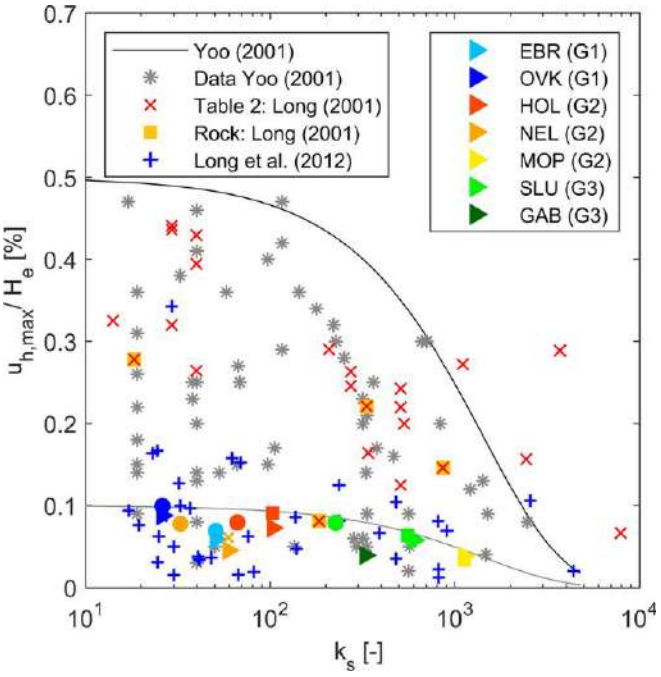

Normalized maximum lateral deflection with respect to the system stiffness (●After activation of 2 anchors, ▶ Final excavation stage)

Long's data (2001) have a higher proportion of soft to stiff soils and lower SPT values in the soft soil units, compared to the conditions encountered in the present study, which are associated with presumably lower equivalent soil stiffness. In particular, the undrained shear strength of the soft soils in Long's (2001) database ranges from 5 to 50 kPa and the stiff soils from 50 to 200 kPa, which is significantly lower than in the present study, where all data shown in Fig. 11 correspond to construction stages with rock at dredge level. Four cases are emphasized with yellow squares in Fig. 11, where the dredge line is situated on rock, like the case studies in this work. These plot on the lower bound of Long's data likely because of higher equivalent soil stiffness. The single point that positions around those from this work concerns a diaphragm wall with higher stiffness, where wall deflections in the unsupported stage would not be significantly influenced by ground stiffness. Because specifics on the stiffness of soft and stiff layers are absent in Yoo (2001), it is difficult to further clarify the observed scatter. Nevertheless, the data clearly indicate that ground stiffness influences wall deflections in accordance with numerous other studies in the literature. This is particularly notable in walls of lower stiffness during initial stages. Yoo (2001) confirmed this when presenting the normalized maximum deflection as a function of the ground stiffness ratio ($E_{s,eq}/(\gamma H_e)$), from results of numerical analyses of deep excavations in soil overlying rock. A set of functions was found that depended on the soil system k_s. However, when the ground stiffness ratio exceeded 450, wall deflections tended to approach a plateau value. Indeed, the data in this study presented in Fig. 12 follow one trend line despite the extensive range of system stiffness values (see Fig. 11). The trend shows a very good coefficient of determination, while the scatter of the estimated elastic modulus is taken into consideration. The error bars indicate the confidence interval (± 95%) obtained based on the probabilistic analysis. This confirms that the system stiffness has no significant impact on deflections when the ground stiffness ratio is high. It is important to note that data from Long et

al. (2012) could not be incorporated into this plot, either due to insufficient stiffness data for inclusion in the analysis or, in cases where stiffness data were available, the ground stiffness ratio was significantly lower compared to that of the investigated case studies.

Fig. 12

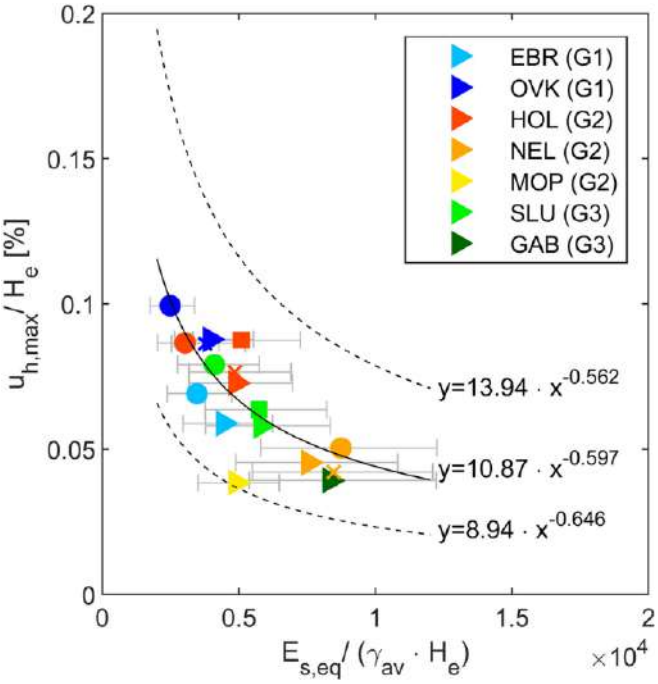

Normalized maximum lateral deflection with respect to the normalized equivalent soil stiffness (✸After anchor activation, ● After activation of 2 anchors, ▶ Final excavation stage). Coefficient of determination $R^2 = 0.868$

Finally, an attempt to evaluate the combined effect of all important parameters was made. The water head difference and the dimensions of the excavation pits were investigated in combination with the system stiffness, which incorporates information of the ground stiffness, the wall bending stiffness and the vertical spacing of the props. The horizontal spacing of the props was not considered as they were the same among the different cases studies. Similarly, the safety factor against bottom heave, that was taken into account in the studies from Clough and O'Rourke (1990) and Bryson and Zapata-Medina (2012) was disregarded in the present study since it was found that this factor does not play a crucial role in walls embedded in weathered or intact rock. Initially, a non-linear regression analysis was carried out to define the coefficients of the predictive response R, which expresses the product of the abovementioned factors, as it is shown in Eq. 3. The calculated coefficients α_1, β_1, γ_1 and δ_1 are presented in the axis title of Fig. 13 and the root square mean error was found to be 0.01%. It is noticed that the coefficient related to the equivalent stiffness attains the highest value, indicating that it is the dominant factor in this predictive equation. As for Fig. 12, the transformation model depicted in Fig. 13 is applicable only for a ground stiffness ratio greater than 2500, specifically in excavations where the dredge line is within stiff ground conditions. If the ground stiffness ratio falls below 500, Yoo (2001) observed that the parameter k_s seems to assume significance, thereby indicating an expected variation in the exponent of k_s. Cautious use of the established transformation model is necessary when employing walls of lower stiffness, such as sheet pile walls. These walls are more likely to experience increased deflection during the unsupported stage, potentially resulting in greater normalized wall deflections than those predicted by the transformation model.

$$R = \left(\frac{E_{s,eq}}{\gamma_{av} \cdot H_e}\right)^{\alpha_1} \cdot (k_s)^{\beta_1} \cdot \left(\frac{\Delta H_w}{H_e}\right)^{\gamma_1} \cdot \left(\frac{L}{B}\right)^{\delta_1} \pm \varepsilon\ (\%) \quad (3)$$

Fig. 13

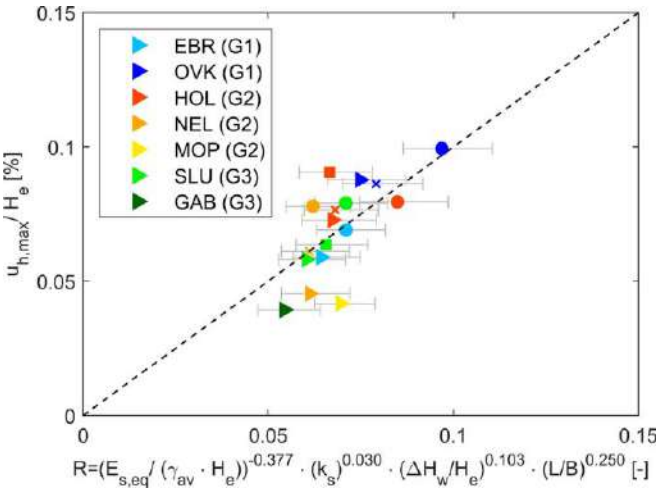

Normalized maximum lateral deflection with respect to the relative stiffness ratio R (✸After anchor activation, ● After activation of 2 anchors, ▶ Final excavation stage). Coefficient of determination $R^2 = 0.964$

4.4 3D Effects

To assess the presence of 3D effects in the examined case studies, wall deflection measurements were taken from all inclinometers not situated in the center of the excavation pit but displaying reliable wall deflection shapes. Ou et al. (1996) introduced a parameter called the plane strain ratio (PSR) to predict 3D effects on lateral wall deflections. PSR is a function of the dimensions of the excavation pit and the distance of the inclinometer from the corner, and it can be estimated graphically. PSR was estimated graphically according to Ou et al. (1996) and then compared with the PSR measured from the inclinometers. The results are shown in Fig. 14, where it can be seen that the predicted and estimated PSR values are in agreement ($R^2 = 0.994$), which suggests 3D effects are not ground conditions specific. The PSR of the datapoints shown in Fig. 14 was estimated based on maximum wall deflections at the final excavation stage measured by an inclinometer considered to be representative of plane strain conditions and by an inclinometer closer to the corners (C) in the same side of the former inclinometer so as to avoid introducing any bias in the assessment (i.e., different loading conditions in the two sides of the excavation pit). Measurements from ØVK are not included in this analysis, as a different wall supporting system (two rows of anchors + one level of struts) was used closer to the edges of the excavation. 3D effects were clearly observed at HOL, SLU, GÅB, NEL and EBR at all construction stages.

5 Conclusions

Via a long-term comprehensive instrumentation program, the performance of seven deep metro excavations constructed with the bottom-up method in stiff over-consolidated deposits and weak rocks in Copenhagen was extensively investigated. A key factor in the analysis was the consideration of the equivalent stiffness of the soil profile taking into account the statistical variation of the elastic modulus for all layers in the examined stratigraphist. The examination and discussion of the primary factors impacting the performance of deep excavations (specifically, observed wall deflections) were conducted by comparing them with published field data, both under similar ground conditions and in contrasting scenarios. Based on the analyses of the field monitoring data, the following major conclusions can be drawn.

Fig. 14

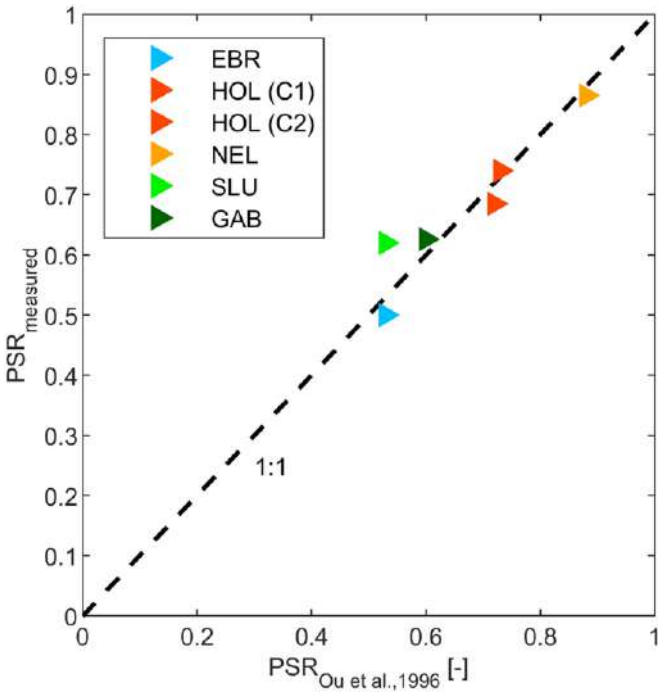

PSR measured by the inclinometers vs PSR estimated graphically according to Ou et al. (1996). Coefficient of determination $R^2 = 0.994$

- In stiff ground conditions of soil overlying rock profiles, i.e. ground stiffness ratio greater than 2500, the system stiffness is less significant, and the developed deflections are primarily governed by ground stiffness, which aligns with the findings published by Yoo (2001).

- Specifically at the cantilever stage a clear linear correlation between normalized maximum deflection and equivalent ground stiffness is demonstrated.

- In the subsequent construction phases, the correlation of normalized deflections with equivalent ground stiffness deviates from linearity following the installation of the props. For cases with large number of support levels a significantly lower rate of increase of deformations was observed.

- Two correlations with good coefficient of determination have been established that allow for the estimation of the maximum wall deflection for supported wall systems in stratigraphist with ground stiffness ratio greater than 2500. These are expected to reduce some of the conservatism of using upper bound trends in stiff ground conditions.

- Three-dimensional (3D) effects observed at most of the present cases during all construction stages were correctly quantified by PSR (Ou et al. 1996), highlighting that this method remains applicable to layered stiff ground conditions. This method can serve as a reference for determining the optimal placement of inclinometers in future constructions.

- The installation of props at shallower depths, particularly above the rock layer, can substantially restrict the observed deflections compared to a more even distribution of the supports along the excavation depth.

The results of this study highlight the importance of detailed site characterization with particular focus on stiffness estimation of different soil layers for reliable predictions of secant pile wall deflections. Moreover, these predictions can support more sustainable design and construction of deep excavation projects in stiff ground conditions as they do not pertain to upper bounds. Note that only for the cantilever stage the upper bound suggested in the literature compared well with the presented data herein. Otherwise in supported stages the upper bound predicts five times larger deflections than the recorded. It is worth noting that the exact construction surcharge behind the wall during the stations' construction remains unknown, which should be taken into account for further refinement in future investigations.

Geotechnical and Geological Engineering, Volume 43, article number 119, (2025), Open access

Download PDF

https://link.springer.com/article/10.1007/s10706-025-03076-4

AI Digs Deep, Engineers Go Deeper: How AI is Radically Transforming Geotechnical Engineering

Dr. Reginald Hammah, Director of Rocscience in Africa at Rocscience

Beneath every building or dam, in every mining or tunnelling project, lies a realm of uncertainty – an underground world that has confounded engineers for generations. What if the mysteries of soil and rock masses could be unravelled or better accommodated? In today's era, AI is not just automating mundane calculations. It is reimagining the very heart of geotechnical design and analysis, turning age-old detective work into a creative partnership between human ingenuity and machine intelligence.

We are on the cusp of a future where engineers can speak naturally to AI and simulation software in their natural engineering language, unlocking faster, more innovative solutions to problems that once took weeks or months to solve. The story of geotechnical engineering is about to be rewritten. Join us as we dig deeper to see how AI is radically transforming the ground beneath our feet.

Engineering Analysis vs. Engineering Design and the Foundations for AI Transformation

What lies beneath the surface is a mystery that plagues all geotechnical engineering projects. Every project starts with unanswered questions on the underground.

All geotechnical projects, whether in the civil or mining industry, start with two foundational practices: analysis and design. Think of analysis as the detective – it digs through the dirt, numbers, and forces to reveal the truth about the ground. Design is the visionary – it imagines what could stand safely. One breaks things down, the other builds them up. Together, they turn uncertainty into the solid ground our world depends on.

The main difference between engineering analysis and engineering design is how each one is used to solve problems. Engineering analysis takes complex systems apart to reveal how they function. An engineer takes a structure or system and figures out what happens when different loads act on it. The goal is to predict if the structure will stand up to the job. In geotechnical engineering, analysis, for example, helps determine whether soil will support a building, whether a slope might collapse, or how much the ground will settle under load.

Engineering design, on the other hand, is about developing solutions to meet a need. It is a creative process in which engineers think about what should be built and how best to build it. They decide what the project will look like, which materials to use, and make sure the end product is safe, reliable, and cost-effective.

Design is about making choices, solving problems, and sometimes trying something new. It often means creating several options, picking the best one, and improving it step by step. Good design also requires judgment and experience, especially when things are uncertain or there are no clear answers.

In short, analysis helps answer "How will this work?" while design asks, "What should we build, and why?" Both are needed – they work together. You cannot design something well without analyzing how it will behave, and you cannot perform a good analysis without having a design or idea to test. Together, they lead to safe, creative, and practical engineering.

When engineers work on a project, they usually start with design ideas. After that, they use analysis (including computer models) to check if these ideas will actually work in real life. They repeat this process over and over: design, analyze, make changes, and test again. They keep cycling between design and analysis until they find the solution that is 'best.'

How AI and Natural Engineering Language (NEL) Will Transform Engineering Design and Analysis

AI is transforming geotechnical engineering in significant ways. Today, AI helps engineers quickly make sense of large amounts of field and test data. For example, it can help determine underground conditions at a new building site, predict how the ground will behave, identify the best foundation type, and assess risks by identifying patterns that would take people much longer to notice. AI smartly sorts through lots of numbers and records to help experts make better decisions, faster.

For AI to be especially useful to everyday geotechnical engineering, it needs to understand the specific language and details that experts use in the field. That is where ideas like Natural Engineering Language (NEL) come in – it helps the AI "speak" like an engineer, making teamwork smoother and more effective. It will combine with advanced AI and simulation models to take engineering practice a step further.

NEL, a term coined by Professor Youssef Hashash, means a form of domain-specific yet intuitive communication that allows engineers to express technical intentions, designs, and problem-solving logic to software in a human-like way. It bridges natural human language and formal programming syntax, enabling software tools and AI models to interpret, reason about, and execute engineering tasks with minimal translation effort.

NEL will let engineers "talk" to computers in everyday technical language, rather than tricky programming code or conventional software user interfaces and workflows (with their learning curves). For example, you could simply write, "Design a wall that will hold up a 6-meter slope in soft soil and handle earthquakes," and AI will understand what you want and help build the relevant models and solve the problem.

This shift will make it much easier for engineers to try out new ideas, customize designs, and look up similar projects. It will save time and open the door to more creative thinking. However, this shift shows that instead of replacing engineers, AI with NEL will be more like a helpful teammate. It can quickly suggest options, spot clever solutions from past experience, and handle the math and rules so that human engineers can focus on the big picture – choosing the best idea, making improvements, and weighing the risks.

In this new era, designing will feel more like a conversation between engineers and AI. The AI can act as an intelligent assistant, offering suggestions, checking code, and helping perform or guide heavy calculations.

Perspectives on AI in Design

Rocscience strongly believes (and many experts agree) that AI is a tool that will help engineers do their jobs better and not a technology that will completely take over or replace them. AI will let engineers create safer, smarter, and more dependable solutions by working faster and handling more information. Still, the experience and judgment of a professional engineer are always needed, especially when things are not straightforward. Even as computers and AI handle more routine work, human engineers will still use their judgment to make final decisions, review results, and fix problems. This recognition is significant because real-world situations are often messy and unpredictable.

The best way for AI and humans to work together is for the computer to handle number crunching and error checking, while people ensure that designs are sensible and safe.

Challenges and Considerations

While the potential benefits of AI in geotechnical engineering are immense, there are (and will be) key challenges, including the following:

1. Interpretation and Understanding

From experience with large language models (LLMs) such as ChatGPT, we know that AI models can sometimes get confused by unclear words or instructions, or by terms that mean different things in different contexts. In geotechnical engineering, computers need to truly understand what engineers want. If the information provided is unclear or incomplete, the AI should ask questions rather than guess or make mistakes. This challenge is one area in which Rocscience will seek to make significant contributions.

2. Validation and Checking

AI can suggest designs that may look good on screen but might not work in the real world. Only trained engineers can verify that these designs are safe and suitable for a site's actual ground conditions. Human review is always needed for essential decisions; AI should be a tool, not the final decision-maker.

3. Reliability and Mistakes

Sometimes, AI can produce answers that sound convincing but are actually wrong! In engineering, these kinds of mistakes can be serious or even dangerous. That is why it is vital to have systems in place to catch errors and ensure that everything meets safety standards before use.

4. Working With Engineering Judgment

Geotechnical engineering depends on the know-how gained from years of experience. AI needs to work alongside human experts and use their wisdom as backup. This recognition is especially true for tricky or unusual problems. AI should be programmed with clever shortcuts and tips learned by engineers over the years, but it must still recognize when a problem exceeds its capabilities and ask for help.

5. Data Quality and Knowledge

AI algorithms can only be as good as the data they learn from. For geotechnical work, this means having extensive, reliable information from previous projects, soil tests, and field experience. It is essential to keep this data up to date and to include knowledge from diverse sources, sites, and construction methods so that AI "knows" what is necessary and can continue to improve over time.

The Path Forward

We believe that using AI and NEL in geotechnical design will develop in these steps:

Near-term (2025-2027):

- AI tools will help with basic calculations, checking codes, and writing reports.
- Engineers will use plain NEL to explore within design databases and past projects, and perform limited interactions with existing software.
- Computers will automatically create early design options for simple projects.

Medium-term (2027-2030):

- Engineers will work together with AI, telling it what they want, and the AI will then suggest several reasonable solutions.
- AI will combine design ideas with performance tests in repeating cycles to keep improving results.
- AI will also help engineers explore creative or unusual design ideas.

Long-term (after 2030):

- Everything in the design process will work together smoothly, with engineers and the AI teaming up at every step by using NEL.
- These systems will learn from experience, making their design suggestions better over time.
- Powerful design tools will be available to more people, thanks to simple, user-friendly language interfaces.

RSInsight and the New Engineering Paradigm

Rocscience's RSInsight is an AI chatbot that is already helping with this latest transformation. It is the first step toward engineers simply telling the software what they are trying to achieve, and for AI and the software to figure out how to do it.

RSInsight uses AI to understand what engineers are asking and can search through multiple documentation sources to find the correct answers. It remembers what you said in previous conversations, so you can have ongoing technical discussions without having to start over each time.

Very soon, however, RSInsight will do much more than just answer questions. Engineers will be able to NEL to ask it to run analyses. For example, an engineer can say "Calculate the safety factor for this slope with these soil types," and the AI will provide complete, ready-to-use engineering workflows. Instead of engineers having to tell the software every single step (click here, enter this number, run this command), they will explain what they want, and the software will execute.

Rocscience's AI platform will soon automatically generate or modify models and create professional reports based on specified inputs and results. RSInsight will learn from your project documents, past work, and team notes to give you advice tailored to your specific situation. It will also seamlessly connect with other Rocscience software tools to access project data and drive actions across the entire software ecosystem.

RSInsight is helping create a new future for geotechnical engineering. Engineers will no longer need to invest significant time in learning software and entering data. Instead, they can dedicate their efforts to solving their real-world engineering problems while the AI handles all the technical details.

Concluding Remarks: A New Engineering Paradigm

Using AI, especially Large Language Models powered by NEL, is more than just making things faster. It is changing the whole way engineers conduct their work.

AI will take over many manual, repetitive, or complex simulation tasks, performing them much faster than people can. However, design, which is the creative and thoughtful part where engineers make decisions, will still be done by humans. AI will help by giving more ideas, speeding up the design process, and making expert knowledge easier to access.

NEL is highly empowering because it lets engineers communicate with software in their own professional language. This possibility will help engineers stay in the creative flow without needing to learn complicated computer workflows and coding.

Geotechnical engineers have never been just number crunchers. They will guide AI tools to explore design ideas, set goals, review options, and use their judgment to pick the best solutions. AI will handle the "how" of analysis. Humans will focus on the "why" of design.

This transformation will help engineering education and practice focus more on skills such as big-picture thinking, creativity, teamwork with AI, ethics, and solving complex problems. Engineers and software developers who learn to communicate with AI using Natural Engineering Language will lead the way forward.

(ROCSCIENCE, Nov 25, 2025, https://www.rocscience.com/learning/ai-digs-deep-engineers-go-deeper-how-ai-is-radically-transforming-geotechnical-engineering)

Advancements in Wireless & Bluetooth-Enabled Pile Testers

In today's fast-paced construction environments, speed, safety, and accuracy are essential—especially in deep foundation work, where pile integrity testing is critical for **structural reliability.**

Wireless-enabled pile integrity testers that leverage Bluetooth technology have transformed on-site testing practices. Leading manufacturers have integrated Bluetooth connectivity into their Pile Echo Tester (PET) systems, redefining how testing is conducted in the field.

This article explores how Bluetooth PIT testers are revolutionizing pile testing, the benefits they offer, and why forward-thinking contractors and equipment buyers are adopting them worldwide.

The Evolution of Pile Testing Technology

Traditionally, pile testing used wired systems, which limited mobility and required careful handling of sensitive cables and components. While reliable, these systems lacked agility and durability especially in challenging or cluttered job sites.

As construction technology advanced, users demanded faster data acquisition, real-time feedback, improved safety, and seamless integration with mobile devices. Bluetooth-enabled pile testers have emerged to meet these needs by delivering wireless convenience without compromising field robustness.

What Is the PET Bluetooth System?

The PET Bluetooth system is a wireless version of the traditional Pulse-Echo testing device. It uses a low-strain integrity testing method, where a hammer tap on the pile's head sends a stress wave downward. The wave reflects from the pile toe or from internal defects and is captured by a sensor.

The wireless model connects via Bluetooth to Android devices, eliminating the need for USB cables or laptops. Test results are instantly viewable on tablets or smartphones using the dedicated PET app.

Real Benefits on Job Sites

The PET Bluetooth system streamlines pile testing, boosting efficiency, accuracy, and onsite productivity.

1. Improved Mobility and Safety

Job sites are often chaotic and hazardous. Cables can easily get tangled or damaged, and operators must navigate uneven or high-traffic areas. The Bluetooth system removes these issues by:

- Eliminating trip hazards
- Reducing the number of accessories to manage
- Minimizing risks from dragging cables or accidental drops

This enhancement is especially valuable on large or complex sites where many piles must be tested quickly across varied terrain.

2. Faster Setup and Testing

Traditional wired PIT systems require laptops, cable connections, and configuration before testing. The PET Bluetooth system streamlines this process:

- Power on the device
- Connect via the Android app
- Begin testing immediately

This reduces setup time significantly, increasing productivity. Under optimal conditions, a single technician can test a large number of piles quickly.

3. Data Transfer and Reporting On-the-Go

With cloud integration and Android compatibility, test data can be:

- Stored locally on the device
- Synced automatically with central databases
- Shared instantly with engineers or project managers
- Data can be linked to the GPS location and a picture of the pile and its surroundings

This real-time data transfer streamlines quality assurance workflows, shortens response times, and supports better project decisions.

4. Adaptability to Various Work Environments

The PET Bluetooth system suits diverse market needs. Its mobile-first design enables compact, rugged, and affordable operation, providing flexibility for job sites with varying documentation and regulatory requirements.

5. Case-Based Feedback and Learning

The PET app includes integrated feedback from prior test cases, enabling users to reference other piles on site and historical data to understand waveforms better and diagnose pile issues with greater confidence. This feature reduces dependency on expert interpretation while empowering trained operators with clearer insights.

Addressing Common Concerns

Concerns about wireless reliability and data security are common, but the **PET system** uses industrial-grade standard Bluetooth protocols combined with secure firmware designed to function even in noisy physical or electronic environments. The connection remains stable within 10 meters, allowing testers to move around while maintaining data visibility.

Furthermore, data auto-saving and backup features ensure no test results are lost even if device batteries fail or connections temporarily drop. Even erased impacts are not actually erased; they are removed from the averaging function.

Why Contractors Are Making the Switch

For contractors, time is money. Faster, more accurate pile testing means faster project schedules and fewer costly errors.

Wireless testers reduce overhead by:

- Allowing one operator to manage testing processes
- Minimizing wear and tear on laptops and field devices
- Eliminating downtime caused by cable damage or outdated drivers

These benefits translate into higher profit margins, more reliable timelines, and fewer disputes related to pile quality.

PET Bluetooth vs Traditional PIT Testers

FeaturePET	Bluetooth Traditional	Wired PIT
Connection Type	Wireless (Bluetooth)	USB or serial cable
Device Compatibility	Android smartphones/tablets	Laptops or old, outdated VGA system
Portability	Highly portable	Less portable
Setup Time	Less than 1 minute	5 to 10 minutes
Data Sharing	Cloud/email ready	Manual transfer required
Safety	No cables, safer	Cables pose trip hazards
Field Durability	Rugged, IP68-rated design	Varies by brand
Up time	More reliable and is less likely to break in need for servicing	Cables and Connectors are the most common fault/break on PIT equipment

This comparison highlights the tangible operational advantages of wireless PIT testers, especially for fast-paced, large-scale projects.

Looking Ahead: The Future of Wireless Testing

Emerging developments in Bluetooth-enabled PIT testing include integration with:

- AI-driven waveform analysis for automatic anomaly detection
- Augmented reality overlays displaying pile results on site layouts
- Voice-command testing flows to reduce hands-on time
- BIM software integration to feed test data directly into project models

Manufacturers are committed to ongoing innovation, with regular software updates extending device capabilities long after purchase.

Final Thoughts

Wireless and Bluetooth-enabled pile testers are no longer optional extras but are rapidly becoming industry standards. They provide faster, safer testing alongside smarter workflows and improved project outcomes.

Contractors and equipment buyers still using older wired PIT tools should consider upgrading to Bluetooth-enabled systems to benefit their teams and improve operational efficiency. For more information and support, visit **Piletest Support**.

(Gadi Lahat / PILETEST, Oct 30, 2025, https://www.piletest.com/post/bluetooth-pit-testers-benefits)

Υπόγεια Αθήνα. Η αθέατη πόλη κάτω από την πόλη

Αικ. Γ. Δασκαλοπούλου

Introduction

Beneath the bustling streets of modern Athens lies another city, silent, hidden, and ancient.

A labyrinth of forgotten tunnels, wells, and sanctuaries stretches below the surface, bearing witness to thousands of years of human presence. From the waterworks of Peisistratus and the sacred spring of Kallirrhoe to Roman aqueducts and Byzantine crypts, underground Athens tells the untold story of a city that never ceased to reinvent itself, layer upon layer, century after century.]

Κάτω από τους δρόμους της Αθήνας απλώνεται ένας άλλος κόσμος. Σκοτεινός, υγρός και σιωπηλός, μα γεμάτος ιστορία και μυστήριο. Είναι η υπόγεια Αθήνα, μια αληθινή πόλη κάτω από την πόλη, χτισμένη στρώμα-στρώμα μέσα στους αιώνες. Εκεί, όπου το φως δεν φθάνει, ζουν ακόμα τα ίχνη όλων όσων πέρασαν. Αρχαίων τεχνιτών, Ρωμαίων μηχανικών, βυζαντινών μοναχών και σύγχρονων εργατών.

Οι πρώτες υπόγειες κατασκευές

Πολύ πριν από τους Ρωμαίους, ήδη στην αρχαϊκή Αθήνα του Πεισίστρατου, οι άνθρωποι είχαν αρχίσει να σκάβουν τη γη για να φέρουν το νερό και να οργανώσουν την πόλη τους. Το περίφημο Υδραγωγείο του Πεισίστρατου, έργο του 6ου αιώνος π.κ.ε., ήταν μια υπόγεια σήραγγα μήκους πολλών χιλιομέτρων, που διοχέτευε νερό από τις πηγές του Υμηττού ως το κέντρο του άστεως. Σε βάθος έως και 14 μέτρων, κεραμικοί σωλήνες και φρεάτια συντηρούσαν το πολύτιμο δίκτυο ύδρευσης μιας πόλης που τότε γεννιόταν.

Στην ίδια εποχή ανήκουν και τα πρώτα υπόγεια αποχετευτικά έργα. Κανάλια λαξευμένα στον βράχο, που συγκέντρωναν τα νερά της Ακρόπολης και τα διοχέτευαν προς τον Ιλισσό. Στους πρόποδες του Ιερού Βράχου βρισκόταν η Κλεψύδρα, η ιερή πηγή των Αθηναίων, που τροφοδοτούνταν από υπόγεια ρέματα. Εκεί υπήρχε δεξαμενή με σήραγγα που εξασφάλιζε μόνιμη παροχή νερού, ακόμη και σε περιόδους πολιορκίας.

Κάτω από την ίδια την Ακρόπολη υπάρχουν φρεάτια και λαξευτοί διάδρομοι που οδηγούσαν σε βοηθητικούς χώρους ή υπόγειες κρύπτες. Δεν αποκλείεται να υπήρχαν και υπόγειες εγκαταστάσεις στον Παρθενώνα για την αποθήκευση υλικών ή ιερών αντικειμένων, αν και οι αρχαιολογικές αποδείξεις παραμένουν ελλιπείς. Ωστόσο, η τεχνογνωσία των Αθηναίων της κλασικής εποχής σε υπόγεια έργα θεωρείται δεδομένη. Η πόλη διέθετε σύστημα υδροδότησης, αποχέτευσης και δεξαμενών που προηγήθηκε αιώνες των ρωμαϊκών έργων.

Η συνέχεια μέσα στους αιώνες

Στους ρωμαϊκούς χρόνους, το έργο του Αδριανού ήρθε να συμπληρώσει και να εκσυγχρονίσει το αρχαίο δίκτυο. Το Αδριάνειο Υδραγωγείο, που ξεκινούσε από τις πηγές της Πάρνηθας και έφθανε έως το Κολωνάκι, χρησιμοποιήθηκε για περισσότερα από 1.800 χρόνια. Ακόμη και σήμερα, τμήματά του λειτουργούν ως μέρος του συστήματος ύδρευσης της Αθήνας.

Κάτω από εκκλησίες και μοναστήρια δημιουργήθηκαν κρύπτες και υπόγειοι χώροι λατρείας. Στη Ρωσική Εκκλησία της Φιλελλήνων, οι ανασκαφές έφεραν στο φως ρωμαϊκά λουτρά και αρχαίες κατασκευές που έγιναν το υπόβαθρο του ναού. Οι παλιές αφηγήσεις μιλούν για στοές που ξεκινούν από εκεί και φτάνουν ως τα ανάκτορα ή ακόμη και στην Ακρόπολη, θρύλοι που κρατούν ζωντανή τη γοητεία του αθέατου.

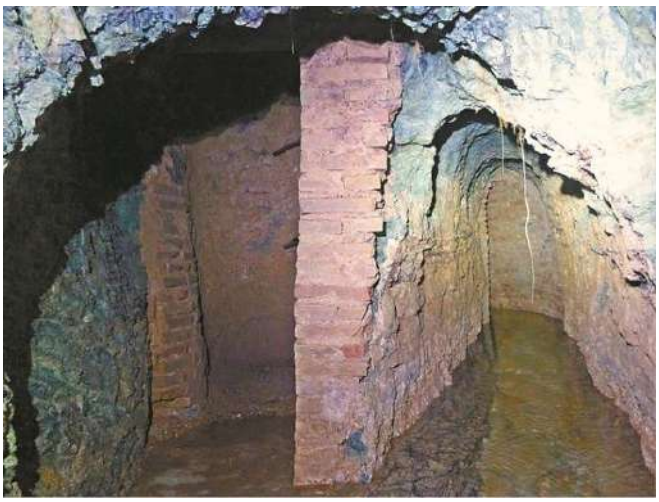

Το Πεισιστράτειο Υδραγωγείο των Αθηνών, κάτω από τα πόδια μας

και η δεξαμενή του Αδριανού, στο Κολωνάκι.

Τα μυστικά του μετρό

Η πιο μεγάλη αποκάλυψη της υπόγειας Αθήνας ήρθε τον 20ό αιώνα, με τα έργα του μετρό. Κάθε σκάμμα ανέσυρε ιστορία. Αρχαίους δρόμους, εργαστήρια, ταφές, γλυπτά, υδραγωγεία και ολόκληρα κομμάτια της αρχαίας πόλης. Πολλά από αυτά εκτίθενται σήμερα σε ειδικές προθήκες στους σταθμούς του Συντάγματος, του Μοναστηρακίου, της Ακρόπολης και του Κεραμεικού.

Τα έργα αυτά απέδειξαν ότι η Αθήνα είναι μια «πολυώροφη» πόλη, όπου κάτω από το παρόν της ζει το παρελθόν της. Οι σήραγγες του μετρό διασταυρώθηκαν με παλιές στοές και δεξαμενές και, σε κάποιες περιπτώσεις, αποκαλύφθηκαν κρυμμένοι χώροι που δεν είχαν καταγραφεί ποτέ.

Οι θρύλοι και η αλήθεια

Οι παλιές διηγήσεις για στοές που οδηγούν στα βουνά, επί παραδείγματι στη σπηλιά του Νταβέλη στην Πεντέλη, για μυστικά δωμάτια γεμάτα αγάλματα του Φειδία ή για κατακόμβες κάτω από τον Παρθενώνα είναι σίγουρα συναρπαστικές, αλλά δεν μπορούν να επιβεβαιωθούν από τη γράφουσα, καθώς δεν υπάρχουν αξιόπιστα στοιχεία.

Ωστόσο, πίσω από κάθε μύθο υπάρχει ένας πυρήνας αλήθειας. Η Αθήνα πάντα έσκαβε τη γη για να επιβιώσει. Το υπέδαφος της πόλης είναι γεμάτο απομεινάρια έργων που κάποτε έδωσαν ζωή στο άστυ και αυτά τα ίχνη είναι που τροφοδοτούν τη φαντασία των ανθρώπων, εδώ και αιώνες.

Η πόλη κάτω από την πόλη

Η υπόγεια Αθήνα είναι ένα ζωντανό αρχείο. Εκεί κάτω, στις υγρές πέτρες και στα σκοτεινά περάσματα, βρίσκονται οι φλέβες μιας πόλης που ποτέ δεν έπαψε να υπάρχει. Από τα φρεάτια του Πεισίστρατου έως τις σήραγγες του μετρό, η ιστορία της Αθήνας δεν γράφεται μόνο στο φως, αλλά και στο σκοτάδι.

Αν σταθείς σήμερα στην πλατεία Συντάγματος και σκεφτείς τι υπάρχει από κάτω, θα νιώσεις ένα ρίγος. Η πόλη αυτή δεν τελειώνει. Κάτω από τα βήματά μας ζει η σκιά της και μαζί της, η ψυχή της.

Βιβλιογραφία και πηγές

1. Μανιάτης, Ν. – Το Αδριάνειο Υδραγωγείο της Αθήνας, Εκδόσεις Μίλητος, Αθήνα 2004.

2. Καραπαναγιώτου, Λ. – Υδροδοσία και Υδραγωγεία της Αρχαίας Αθήνας, Εκδόσεις Καπόν, Αθήνα 2012.

3. Δευτεραίος, Π. – Η Υπόγεια Αθήνα: Στοές, Κρύπτες και Καταφύγια, Εκδόσεις Ιστορική Αναζήτηση, Αθήνα 2018.

4. Λάζος, Χρ. – Υπόγεια έργα και σήραγγες στον αρχαίο κόσμο, Εκδόσεις Δίαυλος, Αθήνα 1995.

5. Μπακοπούλου, Ε. – Η Κλεψύδρα και τα νερά της Ακρόπολης, Αρχαιολογική Εταιρεία, Αθήνα 2007.

6. LIFO – «Η υπόγεια Αθήνα: η αθέατη και αληθινή πόλη κάτω απ’ την πόλη», 2023.

7. ΕΜΕΤΡΟ – Ανασκαφές Μετρό Αθήνας: Αρχαιολογικά Ευρήματα ανά Σταθμό, Αθήνα 2010.

Από το Διαδικτυον

Ancient Greek Civilization - Αρχαία Ελλάς (facebook)

AI rapidly predicts aftershock risk of earthquakes

An international research team has used AI-powered tools to accurately predict aftershocks following earthquakes.

Developed by a team from Edinburgh University, British Geological Survey and University of Padua in Italy, the machine learning tools were trained using earthquake data from seismic hotspots including California, New Zealand, Italy, Japan and Greece. The technology was applied to earthquakes of magnitude four or higher and tasked with predicting how many aftershocks would occur in the 24 hours following the initial tremor.

According to the researchers, the newly developed AI model performed similarly to the Epidemic-Type Aftershock Sequence (ETAS) model, a commonly used tool in earthquake-prone countries such as Italy, New Zealand and the US. But while both forecasting systems produced similar results, the AI platform delivered its results almost instantly, whereas the ETAS can take several hours to make its computationally demanding predictions. The work is published in the journal *Earth, Planets and Space*.

"This study shows that machine learning models can produce aftershock forecasts within seconds, showing comparable quality to that of ETAS forecasts," said study lead Foteini Dervisi, a PhD student at Edinburgh University's School of GeoSciences and the British Geological Survey.

"Their speed and low computational cost offer major benefits for operational use: coupled with the near real-time development of machine learning-based high-resolution earthquake catalogues, these models will enhance our ability to monitor and understand seismic crises as they evolve."

By training the AI tools on records of past earthquakes from regions with different tectonic landscapes, the research team said their models could be used to forecast aftershock risk across most parts of the world that experience regular seismic activity. What's more, the speed with which aftershock predictions are delivered could help authorities with decision-making about public safety measures and resource allocation in disaster-hit areas.

The study was supported by the European Union's Horizon 2020 research and innovation programme under the Marie Skłodowska-Curie SPIN Innovative Training Network.

(THE ENGINEER, 25 Nov 2025, https://www.theengineer.co.uk/content/news/ai-tools-rapidly-map-aftershock-risk-of-earthquakes)

Towards a deep learning approach for short-term data-driven spatiotemporal seismicity rate forecasting

Foteini Dervisi, Margarita Segou, Piero Poli, Brian Baptie, Ian Main & Andrew Curtis

Abstract

Recent advances in earthquake monitoring have led to the development of methods for the automatic generation of high-resolution catalogues. These catalogues are created at considerably reduced processing times and contain significantly larger volumes of data concerning seismic activity compared to standard catalogues created by human analysts. Disciplinary statistics and physics-based earthquake forecasting models have shown improved performance when rich catalogues are used. The use of high-resolution catalogues paired with machine learning algorithms, which have recently evolved due to the rise in the availability of data and computational power, is therefore a promising approach to uncovering underlying patterns and hidden laws within earthquake sequences. This study focuses on the development of short-term data-driven spatiotemporal seismicity forecasting models with the help of deep learning and tests the hypothesis that deep neural networks can uncover complex patterns within earthquake catalogues. The performance of the forecasting models is assessed using metrics from the data science and earthquake forecasting communities. The results show that deep learning algorithms are a promising solution for generating short-term seismicity forecasts, provided that they are trained on a representative dataset that accurately captures the properties of earthquake sequences. Comparisons of machine learning-based forecasting models with an epidemic-type aftershock sequence benchmark show that both types of models outperform the persistence null hypothesis commonly used as a benchmark in forecasting the behaviour of other types of non-linear systems. Machine learning forecasting models achieve similar performance to that of an epidemic-type aftershock sequence benchmark on the Southern California and Italy test datasets at significantly reduced processing times - a major advantage in applications to short-term operational earthquake forecasting.

Graphical Abstract

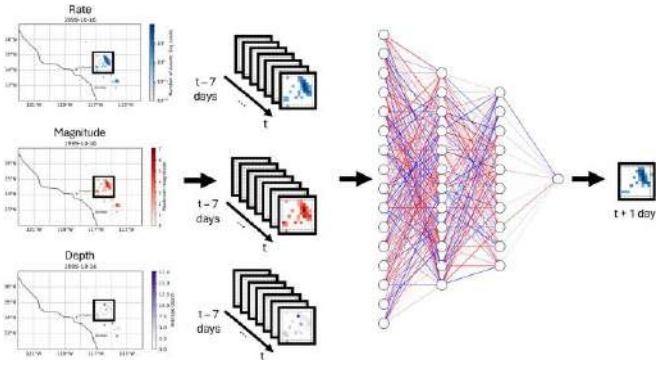

(Dervisi, F., Segou, M., Poli, P. *et al.* Towards a deep learning approach for short-term data-driven spatiotemporal seismicity rate forecasting. *Earth Planets Space* **77**, 185 (2025). https://doi.org/10.1186/s40623-025-02241)

(Earth, Planets and Space, 25 November 2025, Volume 77, article number 185, https://link.springer.com/article/10.1186/s40623-025-02241-6#citeas)

AFG - Active Faults Greece: a comprehensive geomorphology-based 1:25,000 fault database

John G. Begg, Vasiliki Mouslopoulou, David Heron & Andy Nicol

Abstract

Greece is Europe's most seismically active country, as it is being deformed by an active subduction-system and one of the world's fastest-spreading continental rifts. Onshore active faults pose seismic-hazard that cannot be reliably assessed in the absence of a comprehensive map of potential earthquake sources. Here, we use high-resolution Digital Elevation Models (DEMs), in conjunction with hillshades and slope-models, to map and characterise faults in Greece at a scale of 1:25000. The Active Faults Greece (AFG) database records 3815 fault-traces assigned to 892 interpreted faults. Of these traces, 53% were mapped here for the first time, with their geometries and slip-sense constrained by displacement of landscape features. AFG includes >2000 active and 1632 probably-active traces, while 35 traces result from historic surface-ruptures. Many faults (57%) exhibit strong depositional-control (DC) on sedimentation patterns, with active faults featuring approximately equal numbers of sharp (32%), moderate (29%) and rounded (29%) scarps. AFG is the first fault database in Greece generated using nationwide interpretation of geomorphology, with applications in paleoseismology, seismic-hazard-assessment, mineral-resources exploration and resilience-planning.

Background & Summary

Seismic hazard in tectonically active regions like Greece is strongly influenced by the distribution, geometry and activity of crustal faults. Accurate mapping of fault traces is a prerequisite for estimating credible earthquake magnitudes on individual faults and developing a national seismic hazard model. Historical earthquakes that have ruptured the ground-surface globally provide information on the dimensions, slip patterns and timing of future events[1,2,3,4]. These earthquakes afford an empirical basis for estimating the likelihood of rupture termination at fault irregularities (e.g., steps and bends)[5], and for assessing the conditions that favour co-seismic transfer of slip between faults (e.g.[6,7]). Historical surface-rupturing earthquakes in Greece have also highlighted the occurrence of temporally clustered slip on nearby faults (i.e., 1981 M6.4-6.7 Alkyonides Earthquake Sequence[8]), of multi-fault ruptures (i.e., the 1978 Thessaloniki Earthquake[9]), and of earthquakes that ruptured concealed faults or faults with subtle geomorphological expression (e.g. the 2008 M6.7 Ilia-Achaia Earthquake[10] and/or the 2021 Tyrnavos Earthquake Sequence[11]). Multi-fault ruptures have the potential to produce larger and less frequent earthquakes, with greater total slip than events restricted to individual faults (i.e.[12,13,14]), while rupture of concealed and/or sub-resolution faults can be expected for all fault systems[15], and may have important repercussions for seismic hazard, as was the case for the 1987 Edgecumbe earthquake[16] and the doublet of Christchurch earthquakes in New Zealand[17]. Thus, where possible, subtle and/or concealed traces should be incorporated into fault maps and seismic hazard models.

Despite experiencing hundreds of historical moderate to large-magnitude damaging earthquakes (i.e.[18,19]), to date Greece lacks a landscape-based active fault map of national coverage. Three active fault databases which are publicly available (GreDaSS, NOAFaults, HeDBAF)[20,21,22], have been developed or are being developed from a selection of existing literature and unpublished data. Here, we build a new open-access homogeneous database of continental active faults in Greece: The **Active Faults Greece** (**AFG**) database. AFG represents a development in active-fault mapping for Greece, both in terms of its coverage and methodological consistency. It includes all previously known active faults with appropriate referencing, revisited here using geomorphic criteria on high-resolution DEMs, as well as numerous newly identified structures, and effectively doubles the number of fault-traces of existing national compilations.

AFG comprises active faults, probably active faults, and faults with uncertain Quaternary activity, all constrained by interpretation of geomorphic features in the landscape. These features include fault scarps, displaced terraces, alluvial fans, ridge crests, facetted spurs, linear valleys and range fronts, which serve as diagnostic indicators of neotectonic activity and help establish relative rates of fault activity. This approach enhances the interpretability, reliability, and future adaptability of the database, especially in regions where paleoseismic or geophysical data are limited. The value of this approach derives from its national extent, uniformity of compilation methods and a consistent philosophy of geomorphic attribution. Central to this active-fault compilation was to redraft all previously described faults and map new faults using landscape features, observed on high-resolution DEMs (2 or 5 m grids) of national extent, during a process of careful and systematic scanning. As a result, we remapped the surface traces of 1783 previously recognised fault-traces (in many cases significantly modifying previously reported fault-trace locations, geometries and lengths) and introduced 2031 new fault-traces. Our database displays active-fault geometries, activity and geomorphic expression at 1:25,000 scale, always with reference to previously published work. Our mapping philosophy emphasizes a unified and reproducible methodology that integrates high-resolution topographic data (e.g., DEMs, satellite imagery, hillshades and slope maps), remote sensing imagery, field observations, and, where applicable, sub-surface datasets (e.g. trenching & seismic-reflection lines). This strategy was designed to address ambiguities and inconsistencies between existing Greek fault databases, which often differ in scope, purpose, and inclusion criteria.

Beyond its scientific rigor, AFG serves broader goals: it offers a resource for understanding and managing Greece's earthquake risk. AFG provides a foundation for national and regional seismic hazard models, supports earthquake preparedness and resilience planning, and offers a reproducible model for other nations seeking to systematize active fault data collection and presentation. Last, the 2023 Mw 7.8 and 7.7 Kahramanmaraş earthquakes in southeastern Turkey — triggered by a cascade of fault ruptures[13,23], including previously quiescent segments—underscore the urgent need for active-fault datasets that not only reflect known seismicity and 'easily identifiable' faults on the landscape but also anticipate potential sources of future events on subtle or quiescence segments.

Methods

Faults form within the Earth's brittle crust and, the largest of them, are capable of generating M > 6 earthquakes, with the seismic energy released causing ground shaking over distances up to hundreds of kilometres from their epicentre. Fault-surfaces are commonly buried beneath the ground surface and are generally visible only in outcrops (i.e.[24]), and/or through the use of geophysical tools[25]. Fault ruptures during large-magnitude (>M6) earthquakes often, however, propagate to the ground-surface and displace topography (e.g. fan surfaces, spurs, ridge-crests and streams), with displacements ranging from a few cm's to several metres (i.e.[26,27,28]). It is these fault traces that comprise the core of the AFG in onshore Greece.

In the following, we first present our methodological approach to mapping individual fault-traces using a number of specific geomorphic criteria (see '*Fault trace mapping*' section) and subsequently discuss the individual steps taken to characterise and attribute each AFG trace. Collectively, the AFG contains 3815 normal, reverse and strike-slip fault

traces (see '*Classification of fault type*'), with each trace represented on the landscape as earthquake fault-scarp, topographic fault-scarp or flexure (Fig. 1). Fault traces are subsequently merged into individual faults and, where possible, fault systems (see section '*Fault Hierarchy: from fault traces, to faults and fault systems*') (Fig. 2a,b). By tailoring the definition of active faulting for Greece (see discussion below), fault traces are subsequently classified as historically active, active, probably active or of uncertain activity. Last, following specific geomorphic criteria, active fault traces are classified as sharp, moderate, rounded or poor (see section '*A geomorphic classification in AFG*'). The flow-chart in Fig. 2a summarizes the methodology developed in AFG and discussed in detail below.

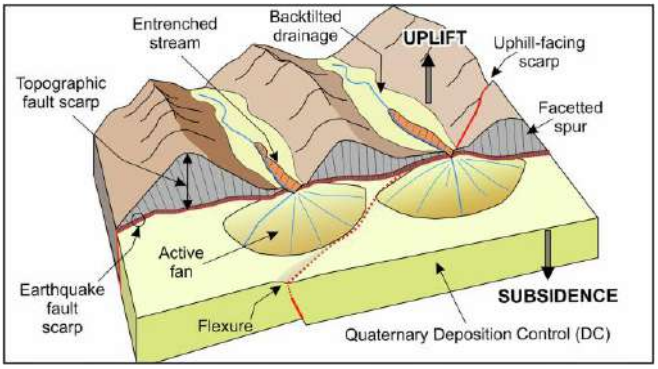

Fig. 1 Summary of landscape features used in AFG. Schematic diagram illustrating the main geomorphic features used to trace the surface expression of active faults in AFG (such as earthquake fault-scarps, topographic fault-scarps, uphill-facing scarps, flexures, etc) atop a schematic Quaternary depocenter (DC).

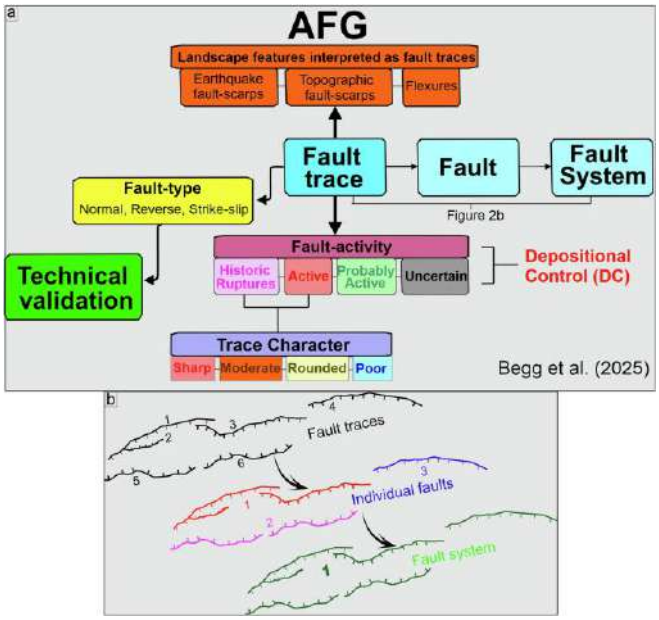

Fig. 2 (**a**) Flow chart summarizing the AFG structure. (**b**) diagram illustrating schematically the upscaling in AFG from individual fault traces to faults and, where applicable, fault systems.

Fault trace mapping

The AFG is of Greek national onshore coverage and has been compiled at 1:25,000 scale. Because it is geomorphologically-based, it is restricted to fault traces with surface expression (with the single exception of a concealed fault that ruptured historically and was identified through its aftershock sequence10,29). Linear landscape features such as ridge-crest damage, ridge-crest displacement, valley alignment, air-gaps along ridgelines, or drainage displacements were used as proxy indicators for faulting30. Initial systematic geomorphological scans of DEMs, hillshades and slope-maps allowed identification of lineaments that warrant further investigation. To assess the tectonic origin of these lineaments we tested them against the following geomorphic criteria, with the requirement that at least one is honoured (Fig. 1a):

a) Measurable displacement of materials traversed by traces or lineaments.
b) Prescence of fault facets or facetted spurs.
c) Stream-channel displacement or changes in channel-incision across the inferred trace.
d) Linear range fronts adjacent to areas of active deposition.
e) Elongate slope changes that cut geomorphic features and cross geological units.
f) Elongate lineaments clearly distinct from basement texture and/or cross-cutting bedrock fabric.
g) Significant displacement or truncation of ridge-lines.

Here, the term displacement refers to any type of displacement (vertical, horizontal, or oblique), and the above criteria apply to dip-slip (normal or reverse), strike-slip (left or right-lateral) and/or oblique-slip faults. Following verification that these features represented fault traces, digitisation and attribution of geometric fields (dip direction and orientation) followed. All assembly and processing of data included in AFG were completed using the open-access software QGIS31. Tiles of 2 m digital elevation models (DEMs) from the Greek Cadastre Agency were merged prior to fault mapping, and hillshades from varying azimuths of illumination and inclination angles were generated and used as overlays on colour-ramped DEMs. Derivative slopemaps were also used as overlays and proved particularly useful in identifying low, linear traces across gently sloping landscapes (e.g. Figure 3). Existing published literature describing and mapping active faults in Greece was assembled and all relevant maps were georeferenced. Each fault was checked against published georeferenced maps to determine whether it had previously been identified. Where previously identified (even approximately), appropriate citation was included. Thus, an empty shapefile, with a coordinate reference system of WGS 84 (EPSG:4326), was progressively populated with digitised and attributed lines during a complete and systematic scanning of the entire country. Google Earth was used, where possible, to corroborate the presence of faults using satellite imagery.

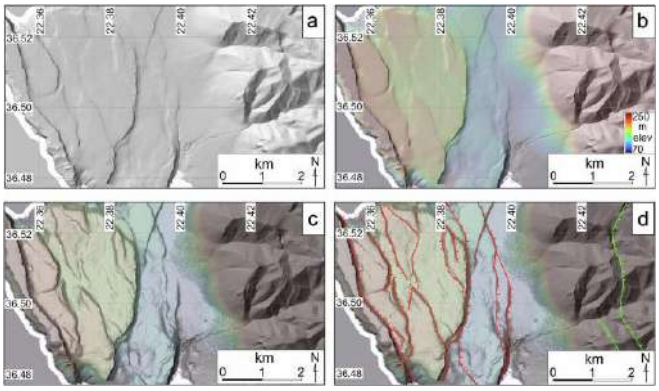

Fig. 3 Enhanced fault mapping through digital elevation raster images. Figure demonstrating the methodology followed to map fault traces using digital elevation models and various derivative raster images. Here, an area immediately NW of Gerolimenas in south Peloponnese is (**a**) lit from 315° at 40°; (**b**) illustrated with slightly transparent hillshade (70% transparency) underlain by the colour-ramped DEM; (**c**) is shown as colour ramped DEM and hillshade overlain by slightly transparent (70%) slopemap; and (**d**) populated by fault traces mapped using collectively the above data.

It should be noted that there are several places where fault traces are discontinuous in geomorphic expression over distances of a kilometre or more (i.e. where Holocene deposition obscures pre-existing scarps) and thus the trace cannot be mapped at 1:25,000 scale within these intervals. In these cases, fault-traces are located as accurately as possible within the context of the landscape between mappable traces. Further, where lineaments are parallel to bedrock fabric, including bedding, they have commonly not been interpreted as fault traces in AFG. Last, short traces (length <100 m) with little or no displacement, particularly when extending proximal to other larger features (i.e. fault-splays at tips or fault junctions), have not been mapped exhaustively. Thus, while the suite of AFG traces identified from the DEMs is not exhaustive, those present are believed to represent all major faults and fault systems in onshore Greece that outcrop at the ground surface.

Classification of fault type

Observed displacements of landscape features underpinned assignation of a 'fault type' for each AFG trace (normal, reverse or strike-slip). Dip-slip on landscape features can be readily observed where fault scarps are formed and record vertical displacement. Almost all traces in AFG are attributed to being elements of normal faults or fault systems (Table 1). Assessing whether there has been oblique or strike-slip movement on a fault is more difficult and requires careful examination of the landscape to identify lateral displacements of unambiguous piercing points (e.g., ridge-crests and spurs, or streams). For a fault with long-term downthrow on the hanging-wall resulting in active deposition, strike-slip displacement may be difficult to observe in the landscape. However, laterally offset fans and stream courses should demonstrate strike-slip displacement. Despite careful examination for indicators of significant lateral displacements, only 20 strike-slip traces were recorded (Table 1), suggesting that strike-slip displacement is unlikely to be an important deformation mechanism at the ground surface in onshore Greece.

Table 1 Table summarizing the characteristics of the fault traces included in the AFG database.

Fault Trace Attributes		
Total number of fault traces	3815	
Total number of faults	892	
Total number of fault systems	237	
Faults by Activity		
Active faults	2090	55%
Probably active faults	1626	43%
Historic fault-trace ruptures	35	1%
Uncertain faults	64	2%
New and Previously Mapped Fault Traces/Faults		
New fault traces	2031	53%
Previously mapped fault traces	1783	47%
Fault Traces by Type		
Normal	3798	>99%
Reverse	2	<1%
Strike-slip (dextral or sinistral)	20	<1%
Fault Length		
Minimum fault length (km)	0.5	
Maximum fault length (km)	161.5	
Average fault length (km)	16.6	
Median (m)	11.5	
Geomorphic Characteristics of Active faults		
Sharp fault traces	708	34%
Moderate fault traces	595	28%
Rounded fault traces	590	28%
Poor fault traces	198	9%
Faults characterised	**2091**	
Depositional Influence		
Depositional control (DC)	2167	57%
Non Depositional Control (na)	1651	43%

Earthquake fault-scarps, topographic fault-scarps and flexures

The 3815 AFG traces mapped using the DEMs include earthquake fault-scarps, topographic fault-scarps and flexures (Fig. 1a). Fault-scarps represent surface displacements along active faults produced either by single surface-rupturing earthquakes (co-seismic fault scarp) or, more commonly, due to several (<10) large-magnitude earthquakes on individual faults[32,33]. Earthquake fault-scarps are sharp and often linear or gently curved discontinuities commonly of <20 m height. In limestone bedrock these scarps are defined by the outcropping fault surfaces, which typically dip at 60–70°. Fault-scarps due to historic surface-rupturing earthquakes in Greece range in dip-slip from 10 cm to 4 m (*i.e.*[34,35,36]). In contrast, topographic fault-scarps are larger topographic lineaments that represent 100 m to kilometer-scale displacements accrued on faults over 100's of thousand to millions of years due to many (10s to 1000s) large-magnitude earthquakes[32,37] (Fig. 1a). Flexures recorded from the DEMs may also result from a series of rupture events that, in this case, failed to penetrate to the ground surface (Fig. 1a). Here, the location of the buried fault may be deduced from an approximately linear fold developed in the existing landscape[30,38]. The majority of active faults recorded in AFG are earthquake and/or topographic fault-scarps (Fig. 1a).

Fault hierarchy: from fault-traces to faults and fault systems

Active faults commonly include numerous individual fault traces. Although fault traces may or may not be linked in map-view, they usually merge at depth to form a common slip surface that represent a single coherent active fault (*i.e.*[38,39]). This is often the case in AFG, where neighbouring normal fault-traces are interpreted to represent a single fault at depth (Fig. 1b). In such cases, we upscale, using a

different attribute-field, these line observations from 'trace' to 'fault' (Table 1; Fig. 2a,b). We have used one or more criteria to determine which fault traces are part of an individual fault. These criteria are: i) fault traces are approximately co-linear with a common dip direction, ii) fault traces are formed along a single continuous range-front, and iii) fault traces are closely spaced (<3 km horizontal separation). Similarly, where individual faults are located proximal to one another and appear to accommodate displacements interdependently40, we have upscaled the 'fault' interpretation to 'fault system', introducing a new field in the attribute table (Table 2; Fig. 2a,b).

Table 2 Summary of fault trace attributes in AFG. GIS field attributes are also illustrated.

Fault Attributes Table					GIS Field Attributes				
Category	**No.**	**Attribute**	**Required**	**Description**	**Field type**	**Type name**	**Length**	**Precision**	**Derivation, restricted values**
ID	1	TraceId	Obligatory	Each fault-trace mapped is given a unique identification number, distinguishing it from other traces. Each trace starts and ends where its geomorphic expression is no longer recognized. Individual traces start/end at natural breaks in geometry.	Decimal (double)	Real	19	0	Unique
Nomenclature	2	FaultNo	Obligatory	Fault number is a unique number associated with each fault.	Integer (32 bit)	Integer	7	0	Manually assigned
	3	Fault-Name	Obligatory	Fault name is based on the first publication (definition) date or, if new, introduced here for first time.	text	String	80	0	Manually assigned
	4	FaultSyst	Optional	Name of the fault system to which the trace belongs, based on structural relationships between faults.	text	String	80	0	Manually assigned
Geometry	5	Type	Obligatory	Fault type: normal, reverse, or strike-slip (dextral, sinistral). Minor obliquity is ignored. Ticks on the downthrown side indicate normal faulting, triangles thrust and arrows strike-slip faulting.	text	String	25	0	normal, reverse, dextral strike-slip, sinistral strike-slip
	6	DipDir	Obligatory	Dip direction inferred from downthrown sector. Not registered if strike-slip with no dip component.	text	String	7	0	XXX, where X = N, E, S, or W
	7	Orient	Obligatory	Average fault strike direction, given as a sector of the E hemisphere.	text	String	4	0	XXX, where X = N, E, S, or W
	8	TraceL_m	Obligatory	Length of the individual fault trace (in metres), estimated by QGIS.	Decimal (double)	Real	10	1	Calculated from shapefile geometry
	9	FaultL_km	Obligatory	Length of individaul faults (in kilometres), estimated manually.	Decimal (double)	Real	4	1	Assigned, Measured manually

Fault Attributes Table					GIS Field Attributes				
Category	No.	Attribute	Required	Description	Field type	Type name	Length	Precision	Derivation, restricted values
Activity	10	Activity	Obligatory	Interpreted relative activity: "historically active", "active", "probably active", or "uncertain". Colour-coding: purple, red, green, black (respectively).	text	String	30	0	historically active, active, probably active, uncertain
Geomorphic Expression	11	TraceChar	Obligatory (for active faults only)	Describes geomorphic expression of active traces: "sharp", "moderate", "rounded", or "poor". Colour-coding: red, orange, yellow, blue (respectively).	text	String	10	0	sharp, moderate, rounded or poor
	12	QuatDep	Obligatory (for active faults only)	Indicates whether a fault trace defines a range-front or shows signs of Holocene depositional control. Values: DC (depositional control), or na (not applicable).	text	String	10	0	DC, na
Supplementary Information	13	Literature	Obligatory	Reference to relevant publications (citations provided separately).	text	String	254	0	free text
	14	Comm	Optional	General comments on historic ruptures, geomorphic characteristics, etc.	text	String	100	0	free text

Adopting a definition of "Active faulting" for Greece

Approaches to 'active faulting'

The term "active fault" indicates fault rupture in the relatively recent geological past and also acknowledges the possibility of future rupture (*i.e.*41,42). Historically, the term "active fault" has been applied using geological, seismological and historical criteria identifying a fault as a potential source of seismic hazard. Formal definitions of "active faults" contain constraints on temporal activity, which may be dictated by the state of knowledge of geological marker horizons. A commonly used definition for the term "active fault" includes those that have ruptured the ground surface at least once during the last 125,000 years (*i.e.*43,44). One advantage of adopting 125,000 years as the boundary between "active" and "inactive" faults is that, in many areas, deposits or surfaces of this age are widespread and easily identifiable (using marginal marine benches or deposits, sea level curves and paleontological, palynological, and/or paleoclimatological data). However, the 125,000 year age limit for active faults may exclude some slow-moving seismogenic faults with long recurrence intervals and destructive potential (e.g. faults in the Basin and Range, USA). Internationally, alternative shorter time-period definitions are also used. In California for example, the legal definition of an "active fault" is one with a proven rupture history during the last 11,000 years (Holocene; https://www.law.cornell.edu/regulations/california/14-CCR-3601). Such refinement is possible where a comprehensive paleoseismological database of fault ruptures has accumulated. This is not the case in Greece.

'Active faulting' in Greece

Greece is situated on the upper-plate of a convergent plate-boundary along which the African Plate is subducting beneath the Eurasian Plate45 (Fig. 4). Arc-shaped plate-convergence marks extensive offshore thrust faulting (i.e. along the Hellenic Trough) and widespread normal faulting landward, towards mainland Greece and the islands35,37,45,46. This deformation style is, however, superimposed by two further deformational processes that operate simultaneously, that of the Hellenic slab-rollback and the westward extrusion of the Anatolian Plate with increasing velocities from East (Anatolia) to south-west (southern Aegean), resulting in extensive normal and oblique-slip faulting throughout continental Greece47,48,49 (Fig. 4).

In an effort to identify chronological markers and establish relative chronology of faulting on the landscape of Greece, some workers have used rupture younger than the last glacial maximum (LGM = ~18 thousand years) in separating "faults with post-glacial activity" from older faults. This concept, originally proposed in Greece by Armijo *et al*.46, reflects the conceptual initiation of a period of landscape stability (post-LGM) following elevated climate-induced landscape instability during the last glacial period, has been tested and used by many studies in Greece and the circa-Mediterranean subsequently (*i.e.*35,37,50,51,52,53,54,55,56). In parts of Greece, such as Crete and the Peloponnese, these "post-glacial traces" in limestone substrates are represented by clearly mappable elongate ribbons of bedrock exposure, visible as pale, bare or poorly vegetated scarps traversing the landscape.

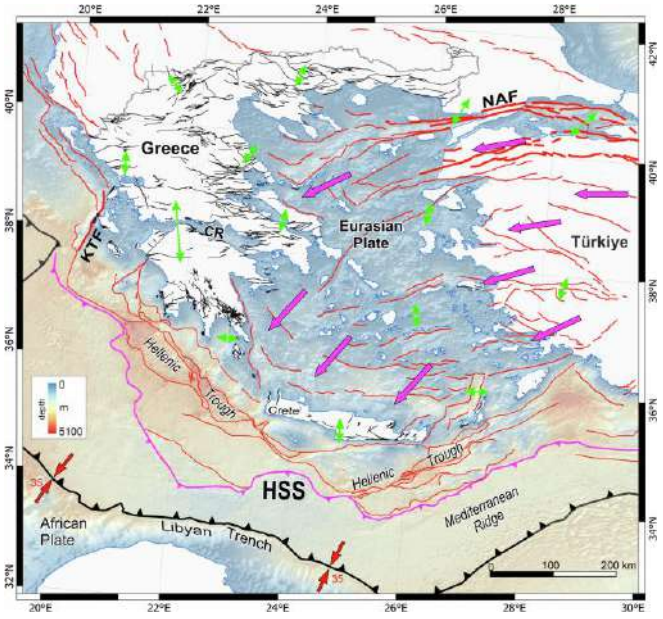

Fig. 4 Map summarising the geotectonic setting of Greece and indicating the main tectonic features and kinematics[23,45,47]. Faults in onshore Greece are active traces from this study. Faults offshore Greece and onshore neighbouring countries are summarized from citations[23,45,49,64]. Purple arrows indicate average horizontal GNSS velocities with respect to stable Eurasia while green indicate extension directions[47]. Red arrows represent the orientation of the plate-convergence while numbers the relative rate. HSS = Hellenic Subduction System, KFS = Kefalonia Fault System, NAF = North Anatolian Fault, CR = Corinth Rift.Offshore digital elevation model is from EMODnet (https://doi.org/10.12770/ff3aff8a-cff1-44a3-a2c8-1910bf109f85).

As a mountainous country with varying basement lithologies there are, however, many parts of the Greek landscape that lack youthful chronological markers. Much of the country has been terrestrial for at least the last 5 million years and thick sequences (>2 km) of alluvial and/or terrestrial deposits are present in many places. Fault-traces restricted to mountainous areas are commonly preserved only as lineaments in the landscape (i.e. topographic fault-scarps) and/or as fault damage zones in bedrock. The longevity of a fault-scarp or fault-line scarp in bedrock depends on the resistance to erosion of the rock itself, as well as the local erosional regime[28]. In some lithologies and erosional circumstances, fault traces may last for hundreds of thousands of years, while in others they will disappear within decades to hundreds of years. Furthermore, the expression of an old inactive fault in the landscape may be exaggerated by differential erosion where contrasting lithologies are present on either side. To better understand the persistence of fault scarps in varying materials and our ability to detect them using available data, we assessed the geomorphic expression of the fault traces associated with each historical surface-rupturing earthquake in Greece. In many cases, we found that surface ruptures recorded in the literature for large earthquakes in the last 2500 years are difficult to identify in the available DEMs and satellite imagery.

In the absence of comprehensive and accurate, nation-wide, youthful geochronological markers a philosophical decision was required on how inclusive the database should be. The decision influences whether all active or potentially active faults are included within the database, or merely the largest and most obvious active faults. To avoid the possibility of omitting significant seismic sources, we have chosen to be inclusive, and extend the time-window of 'active faulting' to include the Quaternary (i.e., since 2.58 Ma). This definition was adopted because faulted Quaternary *alluvial fans,* that retain their original fan morphology, and *lowland basins* provide widespread chronostratigraphic markers in Greece (note that although these a*lluvial fans* are considered Quaternary in age, most likely they are considerably younger). In AFG, fault-traces displacing these fans are designated as 'active' (Fig. 5a). Fans adjacent to *lowland basins* commonly exhibit gently undulating surface morphology and likely represent areas of late Quaternary deposition (probably < 70,000 years, the start of the last glacial period of landscape modification). Where these surfaces are displaced by faults, there is little doubt that they should be regarded as 'active', even using the commonly accepted criterion of 125,000 years. *Lowland basins* are normally sites of deposition, so existing surfaces are necessarily young (in many cases they are inferred to be Holocene in age). Fault traces preserved across these surfaces are considered "active", while many traces buried by ongoing deposition may also be "active". Our geomorphological mapping is unable to locate these concealed active faults, although in some cases their existence can be inferred by along-strike projection of fault traces into the basin. Further, all traces characterized as 'sharp' (see following section) are potential indicators for late-Pleistocene and/or Holocene activity and should also be considered as "active".

Thus, within the AFG active faults are those that have ruptured the surface during the Quaternary, leaving remnants of geomorphic expression (note that some may not qualify as "active" using strict application of definitions described above). These faults warrant further investigation (e.g., constrain the timing of their last rupture and/or their paleoearthquake history, earthquake recurrence interval, earthquake magnitude, etc) to better understand the hazard they represent. For the purposes of seismic hazard assessment, in the interests of inclusivity, named faults that have active fault traces should be regarded as active unless otherwise proven. Of the 892 faults in the database, 54% have active traces and thus should be regarded as active as defined within this database; the other 46% may be optionally treated differently within the seismic hazard assessment, or excluded from the assessment altogether.

A classification of fault activity in AFG

Assigning fault activity involved checking for scarps across Quaternary deposits, or for facets on bedrock spurs, where lineaments are present at the margin of basinal deposits. Here, where either a scarp in Quaternary sediments or fault facets were identified, the fault was described as "*active*". Where younger materials are not displaced, a trace may be defined as "active" when: a) it is located directly along-strike from a demonstrably active trace; b) there is a clear structural connection with demonstrably active traces; and/or c) when there is a clearly 'sharp' trace (i.e., earthquake fault-scarp) identified somewhere along its length (Fig. 5a). Fault traces that do not displace young sediments, do not meet the above criteria or whose extent is limited to land underlain by bedrock, are characterised as "*probably active*" (Fig. 5b). Future investigation of individual fault traces designated as "probably active" in our dataset may change their attribution to "*active*" (or vice versa). Fault traces that we attribute as "*uncertain*" represent features that do not meet any of the above criteria and, further, there is uncertainty whether they represent stratigraphy and not faulting (i.e., represent an erosional expression of contrasting lithologies) or whether they are relict older faults or folds that are no longer active. While there is no intention to include inactive faults in the AFG, it remains possible that the dataset contains some of these older faults.

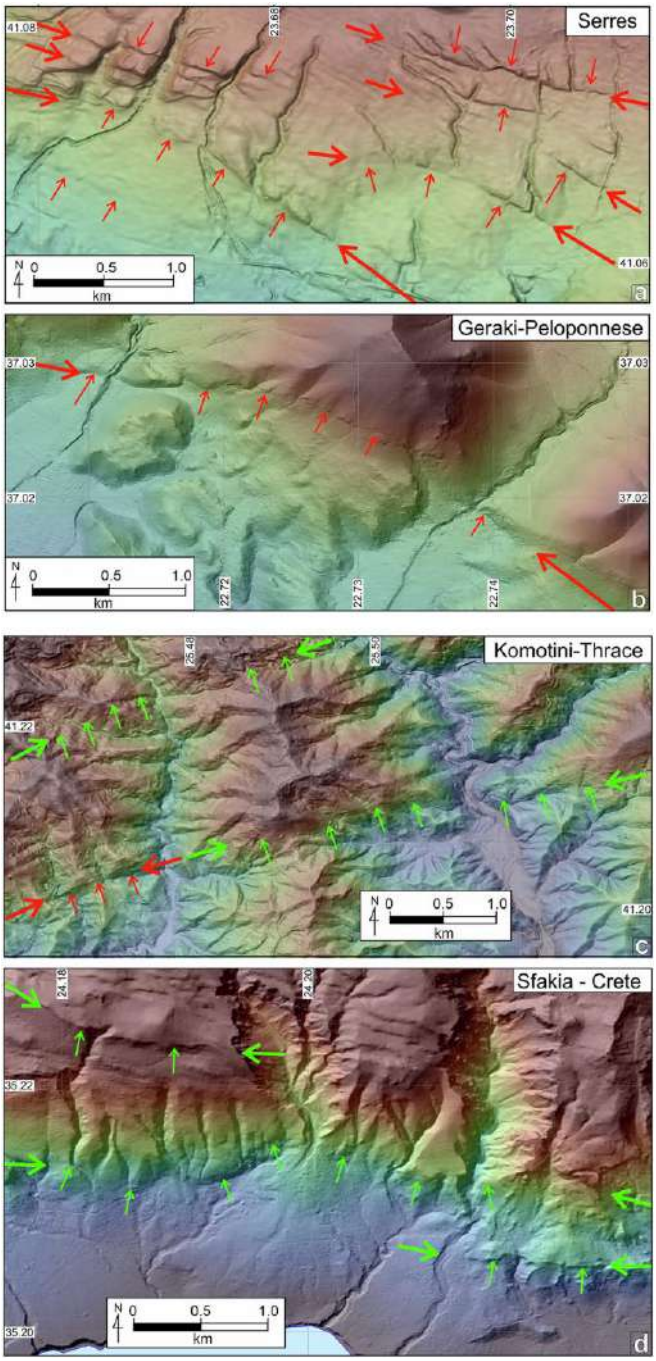

Fig. 5 Examples of "*active*" and "probably active" fault traces in the landscape. (**a**) Multiple sharp active traces of the Serres Fault crossing a Quaternary fan in the Serres area (2.5 km NE from Chryso). Note that fault traces displace fans, that retain their depositional morphology. (**b**) The West Parnon Fault displaces youthful alluvial deposits where it crosses two small streams 4 km NE of Geraki in the central Peloponnese. Active faults in (a) and (b) are marked close to the edge of the figure with heavy red arrows; traces are indicated using lighter arrows at right angles along their length. (**c**) The Kavala-Xanthi-Komotini Fault System in Thrace (northeast Greece), includes active and probably active fault traces. The western trace in this image, about 14 km northeast of Komotini, has a sharp geomorphic expression and is clearly active; its northeast extension lacks this character, nevertheless, facetted spurs, an abrupt change in land elevation and river entrenchment strongly indicate the presence of a fault. Another trace of similar strike about 1.8 km to the north, is also attributed as probably active. (**d**) Traces of the Sfakia-Sella Fault System in southwest Crete (Sfakia region) features prominent triangular facets and a clear topographic signature without, however, a clear continuous active trace with identifiable post-glacial scarps. The coordinate system used is WGS 84, EPSG: 4326.

A geomorphic classification of active fault traces

To assign confidence level on our fault trace mapping, we have introduced a qualitative geomorphic trace descriptor. This geomorphic classification was only undertaken for faults attributed "*active*" or "*historically active*" (the latter where discernible). Where historically active traces are not resolvable, they are attributed as "not applicable" (na). We have assigned to active and historically active faults the primarily qualitative geomorphic descriptor of "sharp", "moderate", "rounded" or "poor" to reflect geomorphic expression in the landscape. The "sharpness" of expression of fault traces in natural situations is a continuum and the qualitative descriptors are necessarily imprecise, with overlap between these terms. Examples of each geomorphic descriptor are illustrated in Fig. 6. Where a trace is "sharp" anywhere along its length, the entire trace is considered "sharp". The same rule is applied to other options in this field (i.e., in the progressive sequence from "sharp", "moderate", "rounded" to "poor"). In terms of its use as an indicator for accuracy of line location, we estimate that "sharp" and "moderate" traces are located within 100 metres of the fault itself. "Rounded" and "poor" traces have a less certain location, which we estimate to range from 100 to 1000 meters. Further, some inference for timing of rupture may be gained from the geomorphic expression of fault traces. The classifications provided may be used as qualitative estimates for the timing of the last rupture. Faults attributed as "sharp" may be interpreted as having ruptured within the Holocene, for example, while those with "rounded" attribution probably last ruptured substantially earlier (e.g., 100 kyr to 1 Myr ago). Although clearly, a "sharp" scarp will remain longer in the landscape on competent erosion-resistant rocks than in soft sediments, a qualitative use of this geomorphic descriptor field may help identify sites suitable for future paleoseismological studies. In summary, these descriptors can be viewed as indicators of the 'confidence level' with which each trace is represented on the landscape.

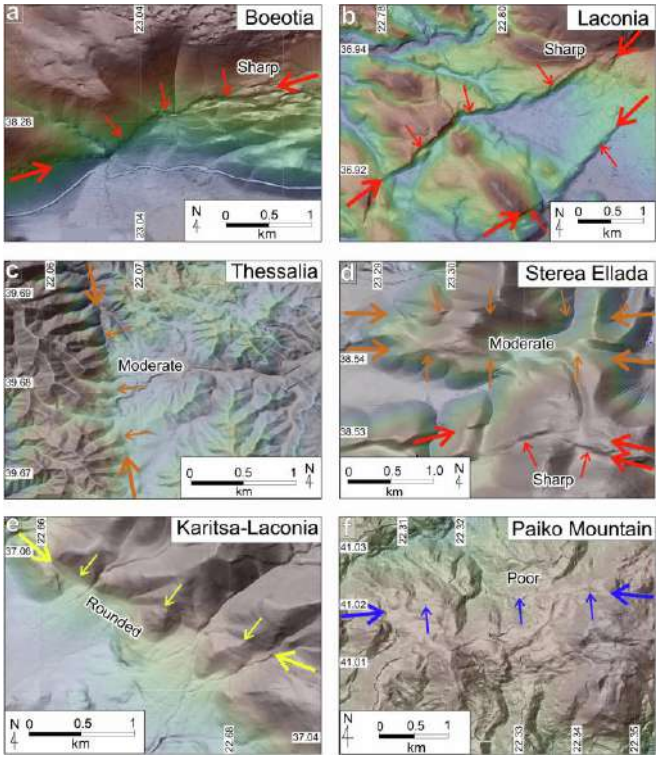

Fig. 6 Examples of varying geomorphic expressions of active faults. Maps illustrate typical examples of "*sharp*" (**a,b**), "*moderate*" (**c,d**), "*rounded*" (**e**) and "*poor*" (**f**) traces of active faults in AFG. Heavy arrows along the strike of traces identify the fault, while lighter arrows at right angles mark the location of the fault trace. Arrows are colour-coded according to the geomorphic expression of the trace (red = sharp, orange = moderate, yellow = rounded, blue = poor). (**a**) Traces of the Neochori-Leontari Fault about 5.5 km southwest of Neochori (Boeotia Prefecture) with a sharp geomorphic expression on the landscape; (**b**) Active traces of the Apidea Fault System in Lakonia (Eastern Peloponnese) sharply displace Quaternary fans and streams; (**c**) trace of the Farkadona-Kalyvia Fault System approx. 1.6 km southwest of Megalo Eleftherochori in Thessalia traverse dissected hill country, exhibiting facetted spurs but a rounded geomorphic expression; (**d**) Traces of the active Lokris and northern Orchomenos fault systems in central Greece (Sterea Ellada), displacing ridge-crests that have "*moderate*" geomorphic expressions (orange arrows), while the traces of the southern Orchomenos Fault are markedly clearer and are characterised as "*sharp*" (red arrows); (**e**) The active trace with "rounded" geomorphic expression of the Karitsa Fault System in south Peloponnese (Laconia - 5.4 km northeast of Agioi Anargyri). The fault traces displace ridge systems and active fans, and bound entrenched streams; (**f**) The "*poor*" geomorphic expression of the Belles Fault System in Paiko Mountain Range in Macedonia: although its traces appear to clearly displace a series of ridges, its landscape expression is limited and difficult to locate between displaced features. Coordinate system: WGS 84, EPSG: 4326.

To complement the geomorphic analysis, we have also assessed whether fault traces exert control on local sediment deposition (depositional control – DC) (Tables 1, 2; Fig. 1). Where a trace defines a range-front between hill/mountain and Quaternary depocenters or shows indications of Holocene depositional control (interpreted as likely to be an association between fault development and deposition), it is attributed as DC (Fig. 1). As we have done for the sharpness descriptor, any fault-trace with evidence indicating DC anywhere along its length, is attributed DC in its entirety. On the other hand, where there is either no recent deposition along the length of the fault trace or no unequivocal indication of fault-controlled deposition the trace is characterised as 'na' = 'not applicable' (Table 2).

A geomorphological caution - Landscape modification

The long human occupation of Greece (>5000 yrs) has implications for active fault preservation. Significant historic (<1500 years) and pre-historic (1500 to 5000 years BP) anthropic landscape modification is recorded in many parts of Greece[57,58]. Such modification has changed the original surface expression of faults, particularly of lowland faults (in intensively cultivated areas), across much of the country. Because active fault ruptures are commonly small in displacement, they are particularly prone to anthropic modification. The impacts of anthropic modification include soil development and soil loss leading to degradation of fault scarps on flat or gently sloping landscapes, terrace-building and other constructions that disguise the presence of faults, and consequent blurring or obliteration of geomorphology useful in defining faults as 'active'. Local studies, mostly for the purposes of archaeology[57,58], provide a local basis for understanding the impact and chronology for potential soil development and thus fault scarp modification.

Data Records

The dataset is available at GFZ Data Services[59] in the format of an ESRI shapefile, Google Earth kmz and Excel formats. The associated reference list AFG is presented in the Supplementary Information of this article in Word format. Further, the AFG may be viewed and queried on an ArcGIS webserver that is publicly available through the GFZ Data Services[59].

Fault attributes

All fault traces were mapped using 2 m and 5 m DEMs and derivative attributes were generated as described above. The database includes a total of 3815 trace records, assigned to 892 individual faults and 236 fault systems (Table 1), with each individual trace containing 14 attributes (Table 2; the GIS field attributes are also included). The AFG attribute table, assigns obligatory and optional fields for each trace, including descriptors of ID, name, geometry, type, activity, geomorphic expression, and reference to previous work with associated comments. The following fields are present in the ESRI shapefile, and below are grouped to illustrate the overall structure of the attribution (Fig. 2a; Table 2).

1) ***TraceId:*** Obligatory field. Each fault-trace mapped is given a unique identification number (Unique ID), distinguishing it from other traces; each starts and ends close to where its geomorphic expression can no longer be recognised; individual traces start and end at or near a natural break in their geometry.

Name

2) ***FaultNo:*** Obligatory field. Fault number provides a unique ID for each interpreted fault (that, in many cases, comprises multiple fault traces; see Fig. 2b).

3) ***FaultName:*** Obligatory field. Fault name, where present, determined by first publication (definition) date. Where previously unnamed, a name is selected from a nearby village or town.

4) ***Fault_Syst:*** Optional field. Fault system name; fault system for grouped individual faults, allocated based on perceived structural relationships between traces and faults.

Geometry

5) ***Type:*** Obligatory field. Fault type includes normal, reverse or strike-slip (dextral or sinistral); minor components of obliquity are ignored.

6) ***DipDir:*** Obligatory field. Dip direction of the fault-trace plane, interpreted from the defined downthrown sector. The only case where no dip direction may be registered is where a fault is considered strike-slip, with no significant dip slip component.

7) ***Orient:*** Obligatory field. Generalised average fault-trace strike expressed as a sector of the E hemisphere.

8) ***TraceL_m:*** Obligatory field. Individual fault trace length estimates (in metres) calculated automatically by QGIS software.

9) ***FaultL_km:*** Obligatory field. Individual fault length estimates (in kilometres), measured manually for each fault.

Assessment of activity

10) ***Activity:*** Obligatory field. Interpretation of relative activity based on historic and geomorphic characteristics; field options include "*historically active*", "*active*", "*probably active*" or "*uncertain*". Colour-coding: purple, red, green, black (respectively).

Geomorphic expression

11) ***TraceChar:*** Obligatory only for "active" faults. Qualitative descriptor of the geomorphic expression of active fault

traces; where applied, options are either "*sharp*", "*moderate*", "*rounded*" or "*poor*". Colour-coding: red, orange, yellow, blue (respectively).

12) ***QuatDep:*** Obligatory field only for "active" faults. Records fault traces defining a range-front between hill/mountains and Quaternary depocentres or shows indications of Holocene depositional control; depositional control – DC; na = not applicable (either due to no Holocene deposition along the length of the trace or no unequivocal indication of fault control of deposition). Any fault with evidence for DC anywhere along its length is attributed DC in its entirety.

Supplementary Information

13) ***Literature:*** Obligatory field. Reference to relevant publications (full citations are listed in an accompanying Word file).

14) ***Comm:*** Optional field. General comments noting historic ruptures, or specific geomorphic or other characteristics of the fault-trace.

Fault distributions and trends

The vast majority of the AFG traces (>99%) are normal faults, with only two trace entries of reverse faults and 20 of strike-slip faults, which make up one reverse and six strike-slip faults, respectively (Table 1 and Supplementary Table S1). Although strike-slip displacements are difficult to detect in Greece's landscape, in Fig. 7 we present clear evidence for horizontal displacements on two individual faults: (1) The Petousi Fault System in Epirus (western Greece), where sinistral displacement of ridge-crests and valley margins are recorded (Figs. 7a) and (2) The Karkinagri Fault at the south Ikaria Island that exhibits consistently sinistral offset of spurs and drainage channels (Fig. 7b). In contrast, the large right-lateral strike-slip faults of Ilia-Achaia (Peloponnese) and Strymon (Macedonia) could not be identified at the ground surface, and their location was approximately positioned using the aftershock sequence of the 2008 M6.4 earthquake10,29 and geodetic observations60. Only two trace-records, part of the same fault on Zakynthos, are attributed to thrust mechanisms (Supplementary Table S1); a correlative fault ~10 km to the south, is interpreted as a thrust in offshore seismic-reflection profiles61. Figures 8, 9 illustrate the AFG queried as per fault activity and geomorphic expression, respectively. In Fig. 8 "*active*" fault traces appear red, "*probably active*" fault traces green, and "*uncertain*" fault traces are illustrated black, while "*historic ruptures*" are shown in purple. Here, "*active*" and "*probably active*" faults dominate, with the "*active*" faults being slightly more abundant than the "*probably active*" (55% vs. 43%). Figure 9 suggests that "sharp" (red), "moderate" (orange) and "rounded" (yellow) traces appear to be approximately equally distributed throughout the active faults of Greece (Fig. 9, Table 1), with the location of the sharp traces potentially indicating sites for future paleoseismic trench excavations. Of the discernable historical fault ruptures, half are characterised as sharp, the other half as rounded (Supplementary Table S1).

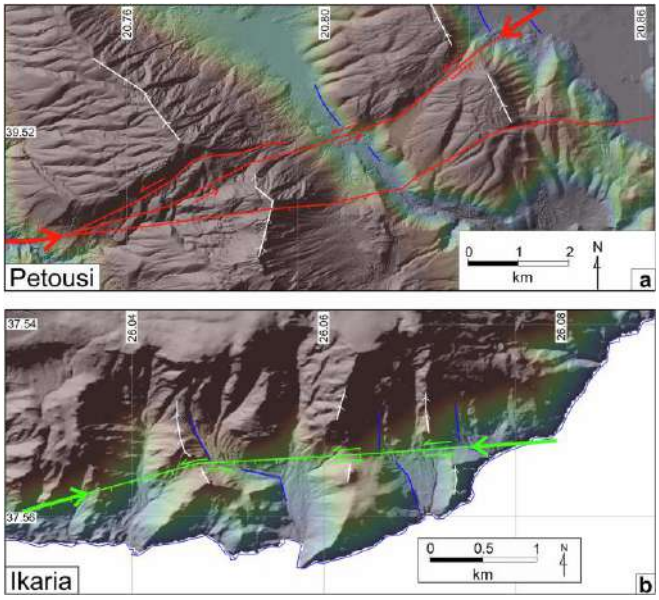

Fig. 7 Example of possible strike-slip displacements. (**a**) An apparent sinistral displacement of ridge-crests (white lines with ticks) and valley margins (blue lines) is present across active traces of the Pertouli-Souli Fault System between the villages of Tseritsana and Episkopiko (Kalamas Prefecture). It is likely that these displaced landscape features result from an earlier phase of fault activity (i.e. there is no clear lateral displacement of younger landscape features). (**b**) On southwestern Ikaria Island, between Karkinagri and Trapalo, a probably active trace displaces left-laterally ridge-crests and stream-beds (indicated by white and blue lines, respectively). Active faults in (**a,b**) are marked close to the edge of the figure with heavy red arrows. The coordinate system used is WGS 84, EPSG: 4326.

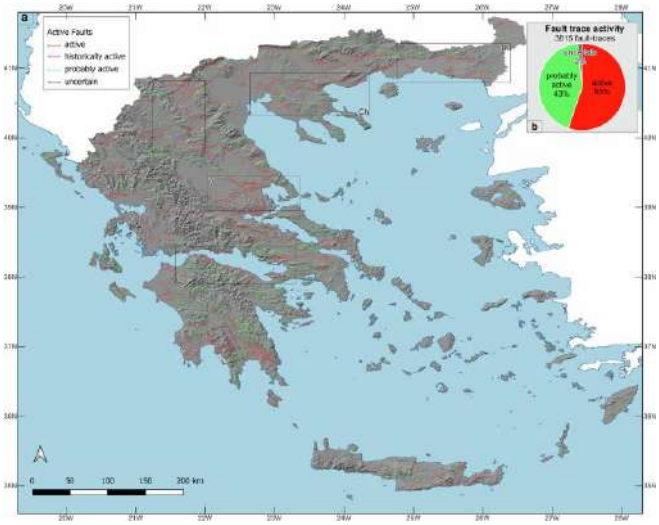

Fig. 8 (a) The AFG database. Red lines illustrate "*active*" fault traces, green lines "*probably active*" traces, black lines denote "*uncertain*" faults while magenta lines indicate "*historic ruptures*" (for a complete list see Table S1 in the SI). (**b**) Chart illustrating the contribution (%) of each type of fault activity in AFG. The hillshade on the basemap was created using 30 m Shuttle Radar Topography Mission (SRTM GL1) Global elevation data available from Open Topography (https://portal.opentopography.org). Six black boxes indicate the regions sampled for the analysis presented in Fig. 11a: G = Grevena, Th = Thrace, V = Volos, Ch = Chalkidiki, C = Corinth, L = Laconia. For high-resolution version of this figure see https://datapub.gfz.de/download/10.5880.FIDGEO.2025.047-VEnuis/.

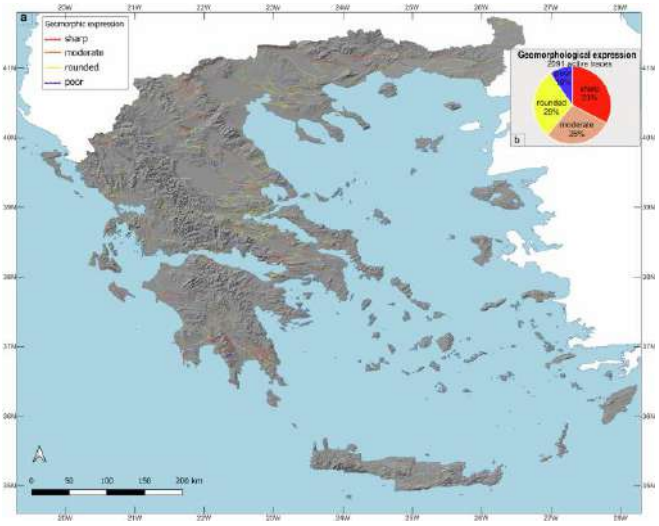

Fig. 9 (a) Geomorphic expressions in AFG. Figure illustrating active fault traces characterized by their geomorphic expression as sharp (red), moderate (orange), rounded (orange) and poor (blue). (b) Chart illustrating the trace character contribution (%) in the distribution of active faults. The hillshade on the basemap was created using 30 m Shuttle Radar Topography Mission (SRTM GL1) Global elevation data available from Open Topography (https://portal.opentopography.org). For high-resolution version of this figure see https://datapub.gfz.de/download/10.5880.FIDGEO.2025.047-VEnuis/.

Technical Validation

Normal faulting in Greece largely reflects active multi-directional extension, with a predominance in NW-SE and N-S extension (Figs. 4, 8–10). Specifically, the dominant strike of the "*active*" fault traces is NE-SW, representing however only 18% of the total active fault-trace length population (because these fault traces are short), whereas for the "*probably active*" fault traces the dominant strike is E-W, amounting to 30% of the total fault lengths (Fig. 10a). The dominant strike of historic ruptures is also NE-SW (rotated slightly more eastward than the "*active*" fault traces), accounting for about 45% of the historic rupture lengths. Fault traces listed with "*uncertain*" activity represent only 2% of the database and are found largely on Kefalonia, Peloponnese and some islands (Kythira, Rhodes, Amorgos and Chios). "Uncertain" faults are typically shorter than most "active" or "probably active" traces, with 14 of these traces showing some indication of depositional control (i.e. they may be active). The dominant strike of "uncertain" faults is NW-SE (i.e. approx. perpendicular to the dominant trend of the "active" and "probably active" faults), representing about 25% of the "uncertain" trace-length population. Fault-dip directions for normal fault traces in the AFG mainly dip to the south, while historic ruptures form an outlier (compared to active faults) as they mostly dip to the north (although responding to the same N-S extensional field as the active faults) (Fig. 10b).

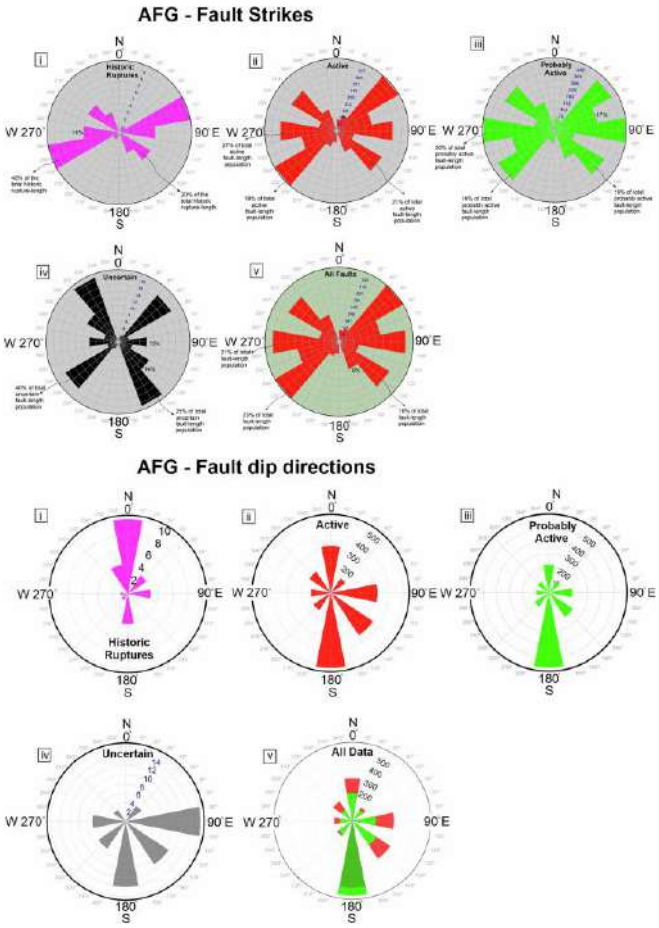

Fig. 10 Principal fault geometries. (**a**) Rose diagrams illustrating the prevailing fault-trace strikes in AFG as per different fault activity (i-iv) and collectively for the entire dataset (v). (**b**) Rose diagrams illustrating the prevailing fault-dip directions in AFG as per different fault activity (i-iv) and collectively for the entire dataset (v).

To test whether the geometry and kinematics of the active fault traces included in AFG agree with fault attributes that derive from different methodologies, we compare the mean extension direction from six regions in AFG (Corinth, Chalkidiki, Laconia, Volos and Thrace; Fig. 8), with the extension direction that derives in each region from independent geodetic and seismological datasets and historical ruptures (Fig. 11a). Specifically, assuming pure normal faulting, we have calculated, using the trend of the mapped AFG fault traces, the extension direction in each selected region and compared it with extension directions that derive from geodetic measurements47, inversion of earthquake moment tensors48 and that of historic ruptures (this study). Comparison shows that in all six cases there is a good agreement (within ±20°) between the mean extension direction in AFG database and that calculated over significantly shorter timescales (i.e. 'earthquake timescales'), here represented by historic ruptures (red datapoints), geodetic (blue datapoints) and seismological data (black datapoints) (Fig. 11a). The vertical separation of each datapoint from the '1:1'line denotes the uncertainty between the mean trend of the AFG traces and each sampled 'short-term' dataset whereas the vertical separation of the datapoints in each region reflects uncertainties arising from using various datasets (note that in all six cases deviations are ≤30° and mostly ≤20°). This is also reinforced by the mean trend of the historical ruptures which is comparable to the dominant trend of the active fault traces. These comparisons provide a first-order validation of our fault mapping and cannot work in regions of Greece where normal faulting is multi-directional (i.e. southeast Peloponnese; Fig. 8).

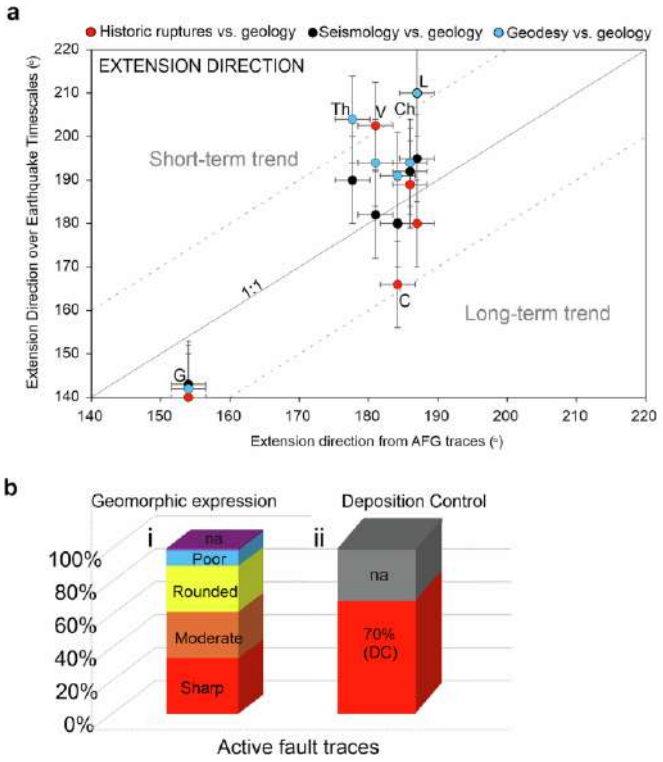

Fig. 11 Validation of fault geometries and fault-trace character. (**a**) Mean extension direction of the AFG traces included in each of the six regions sampled (see Fig. 8 for location), plotted against the mean extension direction (for the same regions) of historic ruptures (red), geodetic measurements (blue) and inversion of seismological data (black). Dashed lines represent ~20° uncertainty. G = Grevena, Th = Thrace, V = Volos, Ch = Chalkidiki, C = Corinth, L = Laconia. (**b**) Histograms illustrating the percentage of sharp and moderate traces (62%) in the active fault AFG population (i) and the percentage (70%) of 'deposition control' (DC) for the entire AFG (ii).

To further validate the mapped AFG traces we have tested the geomorphology of the "*active*" fault traces (red in Fig. 8) against a series of qualitative geomorphic attributes introduced in Table 2. Our fault mapping may be rationalised if most '*active*' faults exhibit "*sharp*" or "*moderately sharp*" traces with "*deposition controlled*" activity (DC). Indeed, analysis suggests (Fig. 11b) that the majority (62%) of the mapped AFG traces are well imprinted on the landscape while 71% of them are characterised by deposition control (DC). Fault lengths in AFG range from 500 m to >150 km, with the average fault length at 16.6 km and the majority (80%) shorter than 25 km (Fig. 12a). The "active" and "probably active" fault-trace length populations indicate power-law scaling, in agreement with other global and local fault compilations[62,63], while the historic ruptures are truncated due to limited sampling resolution (Fig. 12b). Further, we have georeferenced and compared our traces with all previously published faults. Comparison reveals a good agreement between the two independently derived fault datasets and, in most cases, AFG improves the location of previously published faults (often by several km's) because its traces are tailored to specific geomorphological markers (Figs. 5–7).

In summary, the AFG is a database designed to provide the best available data for those seeking to work further on faults in Greece. While only a subset of traces (c. 45%) has been field-checked, the database is based on geomorphological data that can be independently checked by potential users. We have confidence that the geomorphic features we have used to identify fault traces (e.g. displaced surfaces, linear slope changes, offset ridges and streams) are reliable indicators. Historical ruptures provide validation for some of the faults but future large-magnitude earthquakes in onshore Greece will provide the ultimate test for some of our proposed fault traces and their attribution.

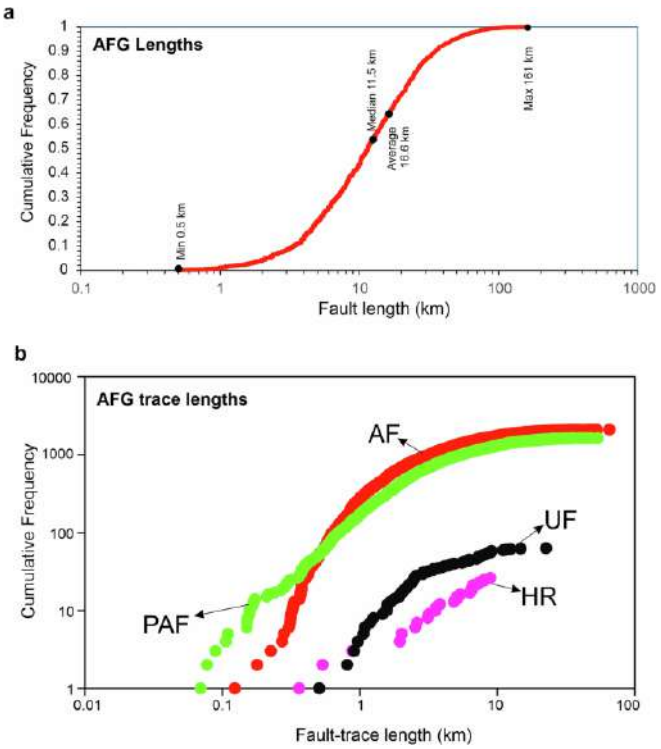

Fig. 12 Fault lengths and fault trace lengths in AFG. (**a**) Normalised cumulative distribution of AFG fault lengths. Min-max, median and average values are indicated. (**b**) Log-log plot of cumulative frequency of fault-trace lengths colour-coded as per Fig. 10. AF = "*Active Faults*", PAF = "*Probably Active Faults*", UF = "*Uncertain Faults*" and HR = "*Historic Ruptures*".

Usage Notes

Because AFG aims to be a long-term community-based project, it can be viewed and queried through an online web-map server[59], from where data and metadata may be extracted in the form of shapefiles or kmz files. The AFG metadata (including a comprehensive reference list) are attached to the shapefile and also stored at the GFZ Data Services website[59] (https://doi.org/10.5880/fidgeo.2025.047). Restrictions apply to the availability of the Digital Elevation Models (DEMs) used to map the fault traces. These data belong to the Greek Cadastre Agency and may be accessed upon request to the agency.

Data availability

The AFG dataset is available at the GFZ Data Services website[59] (https://doi.org/10.5880/fidgeo.2025.047). Note that the AFG may be viewed and queried on an ArcGIS webserver that is also publicly through the GFZ Data Services website[59].

Code availability

For producing the fault maps in Figs. 3–9 we used the open-source software QGIS (2020): Version 3.16 [https://www.qgis.org/]. Hillshades presented in Figs. 5–7 are from DEMs provided by the Greek Cadastre and are available upon request. The hillshade on the basemap in Figs. 8, 9 was created using 30 m Shuttle Radar Topography Mission (SRTM GL1) Global elevation data, available from Open Topography (https://portal.opentopography.org). The dataset is freely available at

https://doi.org/10.5880/fidgeo.2025.047 under a Creative Commons Licence in ESRI shapefile, kml and Excel formats.

References

1. Wells, D. L. & Coppersmith, K. J. New empirical relationships among magnitude, rupture length, rupture width, rupture area and surface displacement. *Bull. Seismol. Soc. Am.* 84, 974–1002 (1994). Article Google Scholar

2. Wesnousky, S. G. Displacement and geometrical characteristics of earthquake surface ruptures: issues and implications for seismic hazard analysis and the process of earthquake rupture. *Bull. Seismol. Soc. Am.* 98, 1609–1633 (2008). Article Google Scholar

3. Biasi, G. P., Weldon, R. J. & Dawson, T. Distribution of slip in ruptures. *US Geol. Surv. Open-File Rep.* 2013–1165, 41 (2013). Google Scholar

4. Mouslopoulou, V., Nicol, A., Howell, A. & Griffin, J. D. Comparison of paleoearthquake elapsed-times and mean interevent-times for a global dataset of active faults: implications for future earthquakes and seismic hazard. *J. Geophys. Res. Solid Earth* 130, e2024JB030036 (2025). Article ADS Google Scholar

5. Biasi, G. P. & Wesnousky, S. G. Steps and gaps in ground ruptures: empirical bounds on rupture propagation. *Bull. Seismol. Soc. Am.* 106, 1110–1124 (2016). Article Google Scholar

6. Mouslopoulou, V. *et al*. Breaking a subduction-termination from top-to-bottom: the 2016 Kaikōura earthquake, New Zealand. *Earth Planet. Sci. Lett.* 506, 221–230 (2019). Article ADS CAS Google Scholar

7. Shaw, B. E. Beyond backslip: improvements of earthquake simulators from new hybrid loading conditions. *Bull. Seismol. Soc. Am.* 109, 2159–2167 (2019). Article Google Scholar

8. Jackson, J. A. *et al*. Seismicity, normal faulting, and the geomorphological development of the Gulf of Corinth: the Corinth earthquakes of February and March 1981. *Earth Planet. Sci. Lett.* 57, 377–397 (1982). Article ADS Google Scholar

9. Tranos, M. D., Papadimitriou, E. E. & Kilias, A. A. Thessaloniki–Gerakarou Fault Zone (TGFZ): the western extension of the 1978 Thessaloniki earthquake fault (Northern Greece) and seismic hazard assessment. *J. Struct. Geol.* 25, 2109–2123 (2003). Article ADS Google Scholar

10. Konstantinou, K. I., Melis, N. S., Lee, S. J., Evangelidis, C. P. & Boukouras, K. Rupture process and aftershock relocation of the 8 June 2008 Mw 6.4 earthquake in Northwest Peloponnese, Western Greece. *Bull. Seismol. Soc. Am.* 99, 3374–3389 (2009). Article Google Scholar

11. Mouslopoulou, V. *et al*. A deeper look into the 2021 Tyrnavos Earthquake Sequence (TES) reveals coseismic breaching of an unrecognized large-scale fault relay zone in continental Greece. *Tectonics* 41, e2022TC007453 (2022). Article ADS Google Scholar

12. Wang, T. *et al*. The 2016 Kaikoura earthquake: simultaneous rupture of the subduction interface and overlying faults. *Earth Planet. Sci. Lett.* **478**, 44–51 (2017). Google Scholar

13. Jia, Z. *et al*. The complex dynamics of the 2023 Kahramanmaraş, Turkey, Mw 7.8–7.7 earthquake doublet. *Science* **381**, 985–990 (2023). Article ADS CAS PubMed Google Scholar

14. Howell, A. *et al*. Comparison of ground-shaking hazard for segmented versus multi-fault earthquake-rupture models in Aotearoa New Zealand. *Seismol. Res. Lett.* **95**, 186–200 (2024). Article Google Scholar

15. Nicol, A., Van Dissen, R., Stirling, M. & Gerstenberger, M. Completeness of the paleoseismic active fault record in New Zealand. *Seismol. Res. Lett.* 86(6), 1299–1310 (2016). Article Google Scholar

16. Beanland, S., Berryman, K. R. & Blick, G. H. Geological investigations of the 1987 Edgecumbe earthquake, New Zealand. *N. Z. J. Geol. Geophys.* 32, 73–91 (1989). Article Google Scholar

17. Gledhill, K., Ristau, J., Reyners, M., Fry, B. & Holden, C. The Darfield (Canterbury, New Zealand) Mw 7.1 earthquake of September 2010: a preliminary seismological report. *Seismol. Res. Lett.* 82, 378–386 (2011). Article Google Scholar

18. Ambraseys, N. N. *Earthquakes in the Mediterranean and Middle East: A Multidisciplinary Study of Seismicity up to 1900* (Cambridge Univ. Press, 2009).

19. Papazachos, B.C.; Papazachou, C. The Earthquakes of Greece; Ziti Publication: Thessaloniki, Greece, p. 304 (1997).

20. Caputo, R. & GreDaSS, W. G. *The Greek Database of Seismogenic Sources (GreDaSS), version 3.0.0: A compilation of potential seismogenic sources (Mw > 5.5) in the broader Aegean Region*. https://doi.org/10.15160/unife/gredass/0300 (2025).

21. Ganas, A., Oikonomou, I. A. & Tsimi, C. NOAfaults: a digital database for active faults in Greece. *Bull. Geol. Soc. Greece* 47, 518–530 (2013). Article Google Scholar

22. Galanakis, D. *et al*. The Hellenic DataBase of Active Faults (HeDBAF): a new, national geodatabase of active faults for the broader Greek territory. EGU General Assembly Conf. Abstracts EGU25-9230 (2025).

23. Zabcı, C., Şengör, A. M. C. Neotectonics of the Anatolian *Scholle*. In: Hamimi, Z. *et al*. *Seismotectonics of the East Mediterranean-Red Sea region. Advances in Science, Technology & Innovation*. Springer, Cham. https://doi.org/10.1007/978-3-031-80928-6_2 (2025).

24. Delogkos, E., Manzocchi, T., Childs, C., Camanni, G. & Roche, V. The 3D structure of a normal fault from multiple outcrop observations. *J. Struct. Geol.* 136, 104009 (2020). Article Google Scholar

25. Tanner, D. C. *et al*. Fault detection. In *Understanding Faults* 81–146 (Elsevier, 2020).

26. Lay, T., Kanamori, H. & Ammon, C. J. The Great Sumatra-Andaman Earthquake of 26 December 2004. *Science* 308, 1127–1133 (2005). Article ADS CAS PubMed Google Scholar

27. Rodgers, D. W. & Little, T. A. World's largest coseismic strike-slip offset: the 1855 rupture of the Wairarapa Fault, New Zealand, and implications for displacement/length scaling of continental earthquakes. *J. Geophys. Res. Solid Earth* 111 (2006).

28. McCalpin, J. P. *Paleoseismology*, 2nd edn, Vol. 95 (Elsevier, 2009).

29. Feng, L., Newman, A. V., Farmer, G. T., Psimoulis, P. & Stiros, S. C. Energetic rupture, coseismic and post-seismic response of the 2008 MW 6.4 Achaia-Elia Earthquake in northwestern Peloponnese, Greece. *Geophys. J. Int.* 183, 103–110 (2010). Article ADS Google Scholar

30. Adam, R. N. *et al*. A systematic approach to mapping tectonic faults and documenting supporting geomorphology. *Geosphere* 21, 227–244 (2025). Article ADS Google Scholar

31. QGIS Development Team. QGIS Geographic Information System. Version 3.16. https://www.qgis.org/ (2020).

32. Nicol, A., Walsh, J. J., Berryman, K. & Nodder, S. Growth of a normal fault by the accumulation of slip over millions of years. *J. Struct. Geol.* 27, 327–342 (2005). Article ADS Google Scholar

33. Mouslopoulou, V. *et al*. Fault-slip accumulation in an active rift over thousands to millions of years and the importance of paleoearthquake sampling. *J. Struct. Geol.* 36, 71–80 (2012). Article ADS Google Scholar

34. Palyvos, N. *et al*. Paleoseismological investigation of the oblique-normal Ekkara ground rupture zone accompanying the M6.7–7.0 earthquake on 30 April 1954 in Thessaly, Greece: archaeological and geochronological constraints on ground rupture recurrence. *J. Geophys. Res.* 115, B06301 (2010). ADS Google Scholar

35. Mouslopoulou, V. *et al*. Normal faulting in the forearc of the Hellenic subduction margin: paleoearthquake history and kinematics of the Spili Fault, Crete, Greece. *J. Struct. Geol.* 66, 298–308 (2014). Article ADS Google Scholar

36. Tsodoulos, I. M. *et al*. Tectonic geomorphology and paleoseismology of the Angelochori fault segment of the Anthemountas extensional detachment fault, Central Macedonia, Greece: paleoseismic evidence from the 1677 CE earthquake. *Geomorphology* 463, 109372 (2024). Article Google Scholar

37. Nicol, A., Mouslopoulou, V., Begg, J. & Oncken, O. Displacement accumulation and sampling of paleoearthquakes on active normal faults of Crete in the eastern Mediterranean. *Geochem. Geophys. Geosyst.* 21, e2020GC009265 (2020). Article ADS Google Scholar

38. Nurminen, F. *et al*. Probability of occurrence and displacement regression of distributed surface rupturing for reverse earthquakes. *Front. Earth Sci.* 8, 581605 (2020). Article Google Scholar

39. Walsh, J. J. & Watterson, J. Geometric and kinematic coherence and scale effects in normal fault systems. In *The Geometry of Normal Faults* (ed. Roberts, A. M.) 193–203 (Geol. Soc. Lond., Spec. Publ. 56, 1991).

40. Nicol, A., Walsh, J. J., Berryman, K. & Villamor, P. Interdependence of fault displacement rates and paleoearthquakes in an active rift. *Geology* 34, 865–868 (2006). Article ADS Google Scholar

41. Slemmons, D. B. & McKinney, R. Definition of "Active Fault". U.S. Army Engineer Waterways Experiment Station, Misc. Paper S-77-8, 22 pp. (1977).

42. Wu, Z. & Hu, M. Definitions, classification schemes for active faults, and their application. *Geosciences* 14, 68 (2024). Article ADS Google Scholar

43. Langridge, R. M. *et al*. The New Zealand active faults database. *N. Z. J. Geol. Geophys.* 59, 86–96 (2016). Article Google Scholar

44. Maldonado, V., Contreras, M. & Melnick, D. A comprehensive database of active and potentially-active continental faults in Chile at 1:25,000 scale. *Sci. Data* 8, 20 (2021). Article PubMed PubMed Central Google Scholar

45. Mouslopoulou, V. *et al*. Hellenic subduction system and upper-plate structures revealed by deep high-resolution seismic-reflection profiles and seafloor bathymetry. *Tectonics* 44, e2025TC008943, https://doi.org/10.1029/2025TC008943 (2025). Article ADS Google Scholar

46. Armijo, R., Lyon-Caen, H. & Papanastassiou, D. East-west extension and Holocene normal-fault scarps in the Hellenic arc. *Geology* 20, 491–494 (1992). Article ADS Google Scholar

47. Chousianitis, K., Sboras, S., Mouslopoulou, V., Chouliaras, G. & Hristopulos, D. T. The upper crustal deformation field of Greece inferred from GPS data and its correlation with earthquake occurrence. *J. Geophys. Res. Solid Earth* 129, e2023JB028004 (2024). Article ADS Google Scholar

48. Konstantinou, K. *et al*. Present-day crustal stress field in Greece inferred from regional-scale damped inversion of earthquake focal mechanisms. *J. Geophys. Res.* 122, 506–523 (2017). Article ADS Google Scholar

49. Sengör, A. M. C.; Zabci, C. The North Anatolian Fault and the North Anatolian Shear Zone. In Landscapes and Landforms of Turkey; Springer International Publishing: Cham, Switzerland, pp. 481–494 (2019).

50. Mitchell, W. *et al*. Displacement history of a limestone normal fault scarp, northern Israel, from cosmogenic 36Cl. *J. Geophys. Res.* 106, 4247–4264 (2001). Article ADS CAS Google Scholar

51. Benedetti, L. *et al*. Post-glacial slip history of the Sparta fault (Greece) determined by 36Cl cosmogenic dating of limestone fault scarps: evidence for non-periodic earthquakes. *Geophys. Res. Lett.* 29, 871–874 (2002). Article Google Scholar

52. Benedetti, L. *et al*. More than 30 large earthquakes broke the Fucino faults (Central Italy) in synchrony in the last 12 ka, as revealed from *in situ* 36Cl exposure dating. *J. Geophys. Res.* 118, 4948–4974 (2013). Article ADS Google Scholar

53. Veliz, V. *et al*. Millennial- to million-year normal-fault interactions on the forearc of a subduction margin, Crete, Greece. *J. Struct. Geol.* 113, 225–241 (2018). Article ADS Google Scholar

54. Veliz, V., Mouslopoulou, V., Nicol, A., Begg, J. & Oncken, O. Normal faulting along the Kythira–Antikythira Strait, southwest Hellenic forearc, Greece. *Front. Earth Sci.* 9, 730806 (2022). Article Google Scholar

55. Mozafari, N. *et al*. Dating of active normal fault scarps in the Büyük Menderes Graben (western Anatolia) and its implications for seismic history. *Quatern. Sci. Rev.* 220, 111–123 (2019). Article ADS Google Scholar

56. Konstantinou, K. I., Mouslopoulou, V. & Saltogianni, V. Seismicity and active faulting around the metropolitan area of Athens, Greece. *Bull. Seismol. Soc. Am.* 110, 1924–1941 (2020). Article Google Scholar

57. van Andel, T. H., Zangger, E. & Demitrack, A. Land use and soil erosion in prehistoric and historical Greece. *J. Field Archaeol.* 17, 379–396 (1990). Article Google Scholar

58. Glais, A., Lespez, L., Vannière, B. & López-Sáez, J.-A. Human-shaped landscape history in NE Greece: a palaeoenvironmental perspective. *J. Archaeol. Sci. Rep.* 15, 405–422 (2017). Google Scholar

59. Begg, G. J., Mouslopoulou, V., Heron, D. & Nicol, A. Active Faults Greece (AFG): a comprehensive geomorphology-based 1:25,000 fault database. *GFZ Data Services* https://doi.org/10.5880/fidgeo.2025.047 (2025).

60. Mouslopoulou, V., Saltogianni, V., Gianniou, M. & Stiros, S. Geodetic evidence for tectonic activity on the Strymon Fault System, northeast Greece. *Tectonophysics* 633, 246–255 (2014). Article Google Scholar

61. Kokkalas, S., Kamberis, E., Xypolias, P., Sotiropoulos, S. & Koukouvelas, I. Coexistence of thin- and thick-skinned tectonics in Zakynthos area (Western Greece): insights from seismic sections and regional seismicity. *Tectonophysics* 597–598, 73–84 (2013). Article ADS Google Scholar

62. Watterson, J., Walsh, J. J., Gillespie, P. A. & Easton, S. Scaling systematics of fault sizes on a large scale range fault map. *Journal of Structural Geology* 18, 199e214 (1996). Article Google Scholar

63. Zygouri, V., Verroios, S., Kokkalas, S., Xypolias, P. & Koukouvelas, I. K. Scaling properties within the Gulf of Corinth, Greece; comparison between offshore and onshore active faults. *Tectonophysics* 453, 193–210 (2008). Article ADS Google Scholar

64. Sakellariou, D. & Tsampouraki-Kraounaki, K. Plio-quaternary extension and strike-slip tectonics in the Aegean. In Duarte, J. C. (Ed.), *Transform plate boundaries and fracture zones* (pp. 339–374). Amsterdam, The Netherlands: Elsevier, https://doi.org/10.1016/B978-0-12-812064-4.00014-1 (2019).

Download references

Acknowledgements

The Greek Cadastre (Ν.Π.Δ.Δ. ΕΛΛΗΝΙΚΟ ΚΤΗΜΑΤΟΛΟΓΙΟ) is sincerely thanked for providing access to the 2 m and 5 m DEMs used for the onshore landscape analysis. The authors have self-funded this work and acknowledge Springer Nature for a full APC waiver. Kirsten Elger is thanked for her help in setting up the GFZ data service. We thank the Associate Editor Alireza Foroozani, the external Editorial Board Member Daniel Melnick, and the reviewers Cengiz Zabcı and Sean Gallen, for their valuable and constructive comments.

Begg, J.G., Mouslopoulou, V., Heron, D. *et al.* AFG - Active Faults Greece: a comprehensive geomorphology-based 1:25,000 fault database. *Sci Data* **12**, 1853 (2025). https://doi.org/10.1038/s41597-025-06283-z

Scientific Data **volume 12**, Article number: 1853 (2025)

Why deeper earthquakes pack more power than shallow ones

Researchers analyzing 11 years of seismic data from Japan found that earthquakes occurring at greater depths release more energy, revealing a direct link between stress release and crustal rock strength.

An SH-60F helicopter assigned to the Chargers of Helicopter Antisubmarine Squadron (HS) 14 from Naval Air Facility Atsugi flies over the port of Sendai to deliver more than 1 500 pounds of food to survivors of an 9.0 magnitude earthquake and a tsunami (2011 Tōhoku earthquake and tsunami). The citizens of Ebina City, Japan, donated the food, and the U.S. Military provided earthquake and tsunami relief support. Credit: U.S. Navy

A team led by Prof. Dr. Armin Dielforder from the University of Greifswald and Dr. Gian Maria Bocchini from Ruhr University Bochum has found that the deeper an earthquake occurs, the more energy it releases. The discovery, published in Communications Earth & Environment, shows that rock strength is the key factor governing how much stress is released when faults rupture.

The researchers examined data from more than 10 000 earthquakes in northeastern Japan, recorded between 2011 and 2022, following the M9.0 Tohoku-Oki megathrust event. They discovered that earthquakes occurring at greater depths in the Earth's crust experience a larger stress drop, meaning a greater release of built-up energy.

This depth dependence is not random. As rocks at depth are subjected to higher pressure, they become more compact and can bear greater stress before breaking. When failure occurs, the release is proportionally larger. These results confirm a long-suspected relationship between rock rigidity and seismic energy.

The analysis suggests that seismic data can serve as a window into the hidden strength of the Earth's crust. By measuring the energy released in earthquakes, scientists can infer how resistant different regions of the crust are to deformation.

Measuring the strength of the deep crust

The team used advanced spectral analyses to estimate how much stress each earthquake released. This value, called the stress drop, reflects the difference between the stress before and after rupture. They combined two methods, single-spectrum fitting corrected for attenuation and spectral-ratio analysis, to improve precision.

To test whether these results matched the physics of the crust, the researchers compared them with computer models that simulate the distribution of stress in the forearc of Japan. These finite-element models calculated the maximum shear stress, known as τ_{max}, throughout the upper 60 km (37 miles) of the lithosphere.

The observed stress drops increased steadily with depth, roughly 0.8 MPa for every 10 km (6 miles). This correlation means that the energy released in an earthquake is proportional to the maximum stress stored in the surrounding rock. Stronger rocks can accumulate more stress before they fail, producing more energetic earthquakes.

The pattern was consistent across two main study regions: one near Iwaki and another near Sendai. The Sendai transect, with slightly higher crustal stress, showed somewhat larger median stress drops. This agreement between field data and model predictions strengthens the case for a physical link between earthquake energy and rock strength.

A decade of seismic observation in Japan

The dataset used in this research was among the most detailed in the world. Japan's dense network of Hi-net borehole seismometers provided continuous, high-quality recordings for more than a decade. The scientists analyzed over 10 000 well-located earthquakes with magnitudes of 2.5 and above, ensuring accurate depth and spectral data.

By examining 11 years of seismicity after the Tohoku-Oki event, they identified a consistent trend: stress drop values increased with depth and remained stable over time. Even as aftershocks diminished and tectonic stresses shifted, the relationship between depth and stress drop held steady.

This stability suggests that the physical properties of the faults did not change significantly. Despite the enormous strain released during the 2011 megathrust earthquake, the surrounding crustal rocks retained their strength. The finding implies that once faults reach a certain equilibrium state, they continue to behave consistently over long periods.

Prof. Dielforder noted that the stress drop values have hardly changed since 2011, suggesting that the solidity of faults remains constant. This consistency helps explain why aftershock sequences often follow predictable decay patterns over time.

How stress is stored and released

In simple terms, earthquakes occur when stress accumulated along a fault exceeds the rock's ability to resist it. This breaking point, or failure stress, depends on the rock's composition, the confining pressure, and the fluid content within its pores. The deeper the rock, the greater the confining pressure, and the stronger it becomes.

The Japanese data revealed that earthquakes at depths up to 60 km (37 miles) released between 10 and 30 percent of the total stress that had built up. This means that not all stored energy is released during a single rupture, allowing faults to reload and fail repeatedly in future events.

The models also showed that maximum shear stress values ranged from about 10 MPa near the surface to as high as 70 MPa in deeper sections of the crust. These stresses are much lower than theoretical estimates based on laboratory friction experiments, indicating that natural faults operate under lower effective friction due to fluids and temperature effects.

By combining seismological data and physical modeling, the study provides a more realistic picture of how stress accumulates and releases inside the Earth. It confirms that crustal strength is a key factor controlling earthquake energy, rather than simply the size of the rupture.

Why this discovery matters

The implications of this research extend far beyond Japan. Subduction zones around the world, from Chile to Alaska,

share similar geological structures. If stress drop is proportional to rock strength in these regions as well, it may be possible to estimate the mechanical state of faults using only seismic data.

This approach could help scientists identify zones of unusually high or low crustal strength, which is key to assessing seismic risk. It might also help explain why some regions produce frequent moderate earthquakes while others accumulate stress for centuries before unleashing catastrophic megathrust events.

Understanding how stress varies with depth also refines models of the earthquake cycle. The finding that fault strength remains stable over time suggests that seismic hazard assessments can incorporate long-term mechanical properties rather than short-term variations.

In a broader sense, this study turns earthquakes into diagnostic tools. By analyzing how much energy they release, scientists can infer how strong the crust is and how close it may be to its next failure point. This insight brings us closer to understanding the physics behind one of Earth's most powerful natural processes.

References:

[1] Earth's Crust Under Stress: Researchers Decipher Energy Release During Earthquakes – University of Greifswald – November 20, 2025

[2] Earthquake stress-drop values delineate spatial variations in maximum shear stress in the Japanese forearc lithosphere – Gian Maria Bocchini et al. – Communications Earth & Environment – October 29, 2025 – https://doi.org/10.1038/s43247-025-02877-y – OPEN ACCESS

(Reet Kaur / THE WATCHERS, November 25, 2025, https://watchers.news/epicenter/why-deeper-earthquakes-pack-more-power-than-shallow-ones)

Τι συνέβη στο ηφαίστειο της Σαντορίνης το 1572 μ.Χ.; «Φωτιά, καπνός και πέτρες», οι κάτοικοι του νησιού αναγκάστηκαν να το εγκαταλείψουν

Από την προφορική παράδοση προκύπτει ότι στη Σαντορίνη έγινε μια έκρηξη κατ' άλλους το 1570 ή το 1573 ή από το 1570 έως το 1573 μ.Χ. Πρόκειται για μια ιστορική έκρηξη για την οποία μέχρι τώρα γνωρίζαμε ελάχιστα. Ένα άγνωστο αλλά αξιόπιστο χειρόγραφο του 1588 μ.Χ. βελτιώνει σημαντικά τις γνώσεις μας για την έκρηξη. Το χειρόγραφο αποτελεί το οδοιπορικό του ταξιδευτή Ιάκωβου Μιλοίτη εκ Πάτμου που δημοσιεύτηκε από τον Σ. Παπαγεωργίου στο περιοδικό Παρνασσός το 1882. Εκεί τεκμηριώνεται ότι η έκρηξη συνέβη το 1572 μέσα στην καλδέρα, μεταξύ της Σαντορίνης και της Παλαιάς Καμμένης. Το χειρόγραφο καθιστά σαφές ότι «φωτιά, καπνός και πέτρες» έβγαιναν ανάμεσα στα δύο νησιά και γεννήθηκε ένα νέο ηφαιστειακό νησί που ονομάστηκε Μικρή Καμμένη. Αυτό το τοπίο επαληθεύεται από χάρτες του 17ου και 18ου αιώνα, ένας εκ των οποίων είναι αρκετά λεπτομερής και δείχνει ότι πάνω στη Μικρή Καμμένη ενεργοποιήθηκαν έξι κρατήρες. Η επιπλέουσα ελαφρόπετρα μεταφέρθηκε από τη θαλασσα μέχρι τη Θεσσαλονίκη και την Κωνσταντινούπολη. Μαθαίνουμε πολλά και για τις συνέπειες της έκρηξης: (1) ο καπνός και η θερμότητα κατέστρεψαν τους αμπελώνες στη Σαντορίνη, άρα η έκρηξη πιθανότατα έγινε την άνοιξη-καλοκαίρι, (2) πιθανώς απελευθερώθηκαν θειούχα αέρια, (3) οι κάτοικοι της Σαντορίνης αναγκάστηκαν να μετακινηθούν στη Νάξο και σε άλλα νησιά. Η διάρκεια της έκρηξης ήταν περίπου ένα έτος, αλλά η φωτιά και ο καπνός εξαφανίστηκαν ξαφνικά. Εκτίμησα ότι ο Ηφαιστειακός Δείκτης Εκρηκτικότητας (VEI) της έκρηξης του 1572 ήταν 3 σε 8βάθμια κλίμακα. Πιο πρόσφατα, κατά το ηφαιστειακό επεισόδιο του 1925-1926, η Μικρή Καμμένη ενοποιήθηκε με τη Νέα Καμμένη, η οποία σήμερα αποτελεί το κύριο ηφαιστειακό νησί μέσα στην καλδέρα της Σαντορίνης.

Η γνώση των ιστορικών εκρήξεων είναι πολύτιμη για την καλύτερη κατανόηση του ηφαιστειακού κύκλου και τη βελτίωση των εκτιμήσεων κινδύνου.

Γεράσιμος Παπαδόπουλος

Το νέο άρθρο μου στο έγκυρο περιοδικό GeoHazards, μας διαφωτίζει σημαντικά. **https://www.mdpi.com/2624-795X/6/4/76**

The 1572 CE Santorini Eruption from Little-Known Historical Documents

Gerassimos A. Papadopoulos

Abstract

The Santorini volcano in the South Aegean Volcanic Arc is of great scientific importance. Knowledge of historical eruptions is valuable for better understanding the volcanic cycle and for improved hazard assessments. One of the little-known historical eruptions occurred either in 1570 or in 1573 or from 1570 to 1573 CE. We bring to light a very little-known but reliable Greek manuscript dated in 1588 CE which improves our knowledge about this eruption. The manuscript documents that the eruption occurred in 1572 and took place within the sea caldera between Santorini and Palaia Kameni. It makes it clear that "fire, smoke, and stones" were coming out between the two islands and a new volcanic island named Mikri Kameni was born. This landscape has been verified by independent maps of the 17th and 18th centuries. The floating pumice was transported by the sea as far as to Thessaloniki and Constantinople. Also, we learn a lot about the consequences of the eruption: (1) smoke and heat destroyed the vineyards and the planting season on Santorini, i.e., spring–summer, (2) it is likely that sulfurous gases were released, and (3) the residents of Santorini were forced to move to nearby islands. The duration of the eruption was ~1 year, but the fire and smoke disappeared suddenly. The Volcanic Explosivity Index of the eruption was estimated to be as high as 3.

1. Introduction

The volcano of Thera (Santorini) in the South Aegean Volcanic Arc, Greece (**Figure 1**a), attracts great scientific interest, which was renewed after the intense seismicity cluster recorded in the area during 2024 and 2025 [**1**,**2**,**3**,**4**,**5**]. After the Plinian Late Bronze Age (LBA) or Minoan (~1613 BCE) caldera-forming eruption, e.g., [**6**,**7**], the volcano activated repeatedly with intra-caldera eruption episodes historically documented in 197 BCE, 19 CE, 46, 726, 1457–1458 (?), 1570 or 1573, 1707–1711, 1866–1870, 1925–1926, 1928, 1939–1941 and 1950 [**6**,**8**]. A well-documented powerful extra-caldera eruption took place in 1650 CE in the Kolumbo submarine volcano, which is situated about 7 km off northeastern Santorini, and constitutes a source of important future hazards [**9**].

Regarding the impact of the previous eruptions, from archaeological observations, it is inferred that the LBA eruption was catastrophic, e.g., [**8**]. It has been historically documented (see review in [**9**]) that the 1650 CE eruption and its associated phenomena, like earthquakes and tsunamis, caused serious damage and human victims. No human victims were reported because of the rest of the historical eruptions. The estimated probability for an eruption to occur in the next 20 or 50 years, starting from 2003, is as high as ~0.25 or ~0.55, respectively [**10**].

Today, the Santorini Island complex consists of Santorini, Therasia and Aspronisi, which are the three islands that remained after the great Minoan eruption (**Figure 1**b). They surround as a ring the submarine caldera, the diameter of which is 11 km in the N–S direction and 7.5 km in the W–E direction [**8**]. Lavas erupted within the caldera during historical times and formed the islands of Palaia (Old) Kameni (the Burned) and Nea (New) Kameni (**Figure 1**b).

Knowledge of historical eruptions is valuable for better understanding the volcano evolution as well as for the volcanic hazard assessment and forecasting. In this context, of particular interest is the eruption that reportedly occurred in 1570 or in 1573. Our knowledge about this eruption, however, remains limited since only a brief historical account is available, thus making doubtful even the year of occurrence. In the present brief report, a little-known manuscript, written about 18 years after the eruption, is presented and examined critically. The information contained in the manuscript enriches our knowledge about the eruption and the evolution of the volcano.

2. Historical Materials and Research Methods

2.1. Earlier Reports on the 1570 or 1573 Eruption

Father Richard (1657) [**13**], a missionary who was in Santorini during the 1650 CE Kolumbo eruption, says: *There is good number of old men on the island who claim that they saw with their own eyes an island neighboring ours formed by fire in the middle of the sea in year 1573 and for that it is called Mikri Kameni,* i.e., *the small burnt island, to distinguish it from the large Kameni, which is another island a little further away and which has three different times received the mediocre size that it now has.* Kircher (1665) [**14**] recalled that Father Richard, during their meeting in Rome, narrated what he heard from old people in Santorini: *The second island [Mikri Kameni], which is close to the other [Palea Kameni], was formed in 1570, with no less terror to Santorini [population], when it lasted for one year, as the Elders testify, who saw it with their eyes. In the middle of this small island, which was one slightly shaped, a large and deep pit is*

seen to this day. The previous accounts are similar, but the first placed the eruption in the year 1573 CE, while the second placed it in 1570 CE. Information about the eruption was repeated by several subsequent authors, e.g., [15,16,17,18]. In modern scientific reviews of the historical eruptions in Santorini, one may find the information that an eruption occurred either in 1570 or in 1573 CE [8,18] or from 1570 CE to 1573 CE [6].

All the previous authors derived information about the erupt-

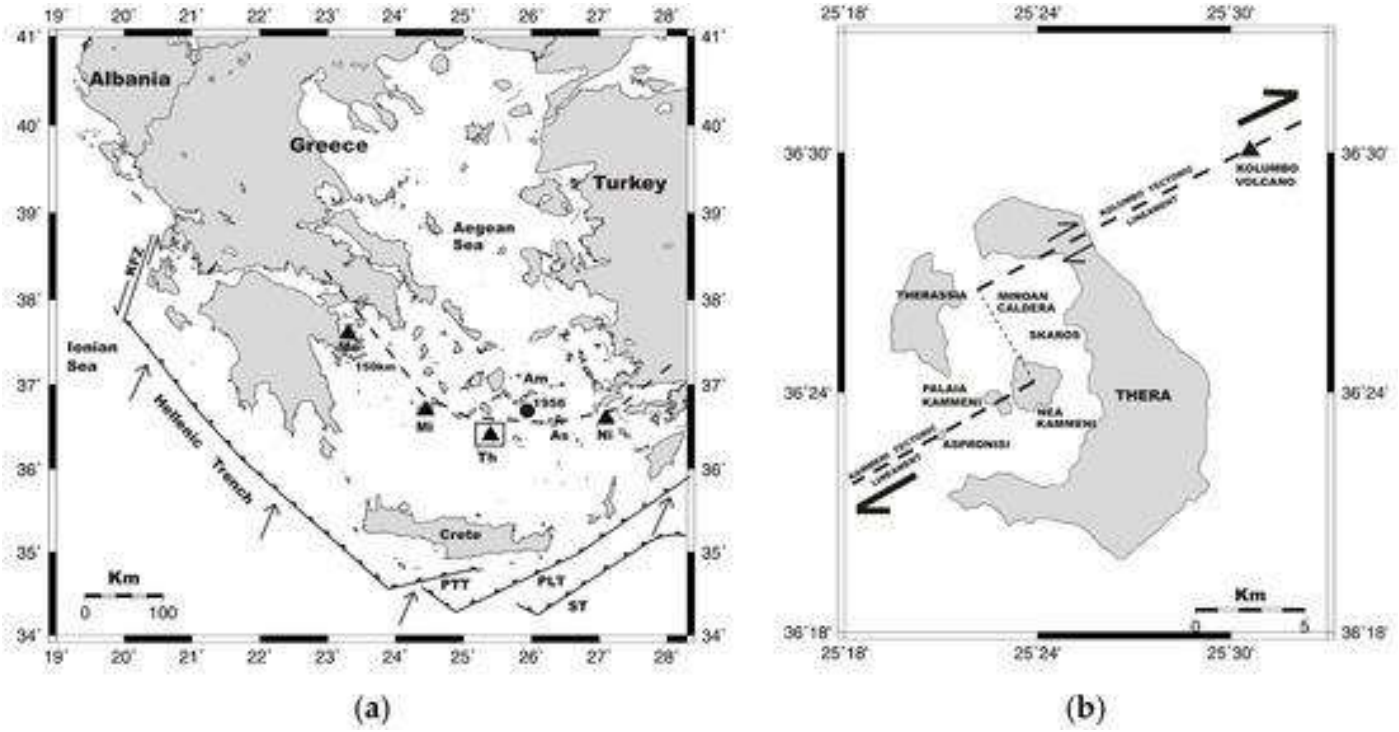

Figure 1. (**a**) Geodynamic setting of the broad Aegean Sea region. The Mediterranean or Nubian lithosphere moves from about SW to NE and subducts beneath the Aegean Sea at the southern Eurasian plate margin along the Hellenic Trench system, e.g., [11]; PTT, PLT and ST represent the Ptolemy, Pliny and Strabo trenches, respectively. Arrows show the directions of lithospheric plate motions. There are five main volcanic centers (triangles) situated along the South Aegean Volcanic Arc above the sesmic isodepth of ~150 km: Methana (Me), Milos (Mi), Thera or Santorini (Th), Nisyros (Ni) and Kolumbo (for the last, see the position in Figure 1b). Box illustrates the study area shown in (**b**). To the northeast of Santorini, the 9 July 1956 large tectonic earthquake of M_w = 7.7 ruptured the submarine trough between the islands of Amorgos (Am) and Astypalaea (As). (**b**) Volcanotectonic sketch map in the area of Santorini volcano (modified from [12]).

tion from the local tradition. The same tradition is also included in a lengthy but valuable manuscript found in the nearby Naxos Island by the medical doctor J. Vouros. Part of the manuscript consists of a metrical description of the 1650 CE eruption written in Greek by a Santorinian eyewitness. The anonymous local author narrated the volcanic episode of 1650 CE up to its very end in December 1650 CE. This implies that the manuscript perhaps was written during the ongoing eruptive phenomena but very likely was completed after 1650 CE. The fragment of the manuscript reads as follows: *In their time [of elder people] an island was born called Kameni; it is said that 80 years have passed since. Our parents experienced the events but neglected to write about them…* This part of the manuscript published by Assopios [19] has so far been the only known documentary source regarding the local memory for an eruption that occurred about 80 years before 1650 CE. Comparing this fragment with the narration by Father Richard [13], one may observe that the latter added a little more information, which very likely was recollected from the memory of the local people.

…

GeoHazards **2025**, *6*(4), 76;
https://doi.org/10.3390/geohazards6040076

Magma pulses beneath Santorini revealed as the true cause of intense 2025 earthquake swarm

A massive swarm of earthquakes that rattled the Aegean Sea between January and March 2025 was not caused by fault movement, as scientists first feared, but by waves of magma slicing through the crust beneath Santorini. The finding, published in Science on November 20, offers a detailed look at how Earth's interior pulses and shifts beneath volcanic regions.

Photograph of Santorini caldera from the air. Credit: kallerna

Over a span of eight weeks, more than 25 000 earthquakes struck between Santorini and Amorgos Islands, with hundreds strong enough to be felt by residents and tourists.

Magnitudes frequently exceeded 4.5, forcing school closures and prompting local authorities to declare a state of emergency. For weeks, scientists debated whether this activity signaled a rising eruption at Santorini or Kolumbo, the nearby underwater volcano.

When researchers from University College London and Aristotle University of Thessaloniki reanalyzed the seismic data, they found that the earthquakes came not from faults slipping but from dikes—thin vertical sheets of magma—cutting horizontally through the crust about 10–15 km (6–9 miles) below ground. These dikes advanced in pulses, slicing through rock in bursts rather than moving smoothly.

Each pulse of magma created local stress shifts, triggering thousands of small quakes that propagated across a 20–30 km (12–19 miles) stretch of crust. The team estimates the intruded magma's volume at roughly 500 million m^3 (17.6 billion $feet^3$), enough to fill 200 000 Olympic swimming pools.

The intrusions shot outward from a magma reservoir connecting Santorini's caldera to Kolumbo volcano. Yet, despite its force, the magma lacked the buoyancy to break through the surface. This discovery reassured volcanologists and local residents that an eruption was never imminent.

Imaging magma movement in unprecedented detail

The study used advanced machine learning to analyze and relocate more than 25 000 earthquakes recorded by regional seismometers. Each quake acted as a "virtual stress meter," allowing scientists to track subtle changes underground. Dr. Stephen Hicks of UCL's Department of Earth Sciences explained that this approach revealed how the crust flexed and cracked as magma surged through it.

By comparing seismic data with GPS satellite measurements, the researchers confirmed that the ground had bulged slightly upward, consistent with magma forcing its way through the crust. These combined data offered one of the most detailed views ever obtained of a magmatic intrusion in real time.

Lead author Anthony Lomax described the magma flow as a "rebounding pump," noting that it oscillated in waves, opening new fractures, closing others, and building pressure before releasing it in bursts. This pattern created a feedback loop where stress changes themselves generated new earthquake swarms.

Eleftheria Papadimitriou of Aristotle University added that such pulsating intrusions might not be unique to Santorini. Similar processes could occur beneath volcanoes around the world, influencing both how crust grows and how eruptions are triggered.

Machine learning reshapes volcanic science

This research marks one of the most sophisticated applications of artificial intelligence in volcanology to date. By training algorithms to identify and precisely relocate earthquake signals, scientists could reconstruct the subsurface magma pathways with remarkable accuracy—resolving features smaller than 100 meters (328 feet) across within a region spanning 50 km (31 miles).

Hicks said that the same approach could soon allow scientists to monitor swarms as they happen, providing early warnings when magma starts moving beneath volcanoes. Because the method relies only on seismic data, it is particularly useful for underwater systems like Kolumbo, where GPS and satellite imaging cannot easily detect ground deformation.

The researchers believe this machine learning framework could distinguish between tectonic and magmatic causes of seismic swarms, improving forecasts and helping authorities respond faster to signs of unrest.

Santorini's restless geological past

Santorini lies within the Hellenic volcanic arc, where the African plate dives beneath the Eurasian plate. This zone has produced some of Europe's most powerful eruptions and earthquakes. Around 1620 BCE, the island's Minoan eruption reshaped the caldera and left behind layers of ash across the eastern Mediterranean.

The 2025 swarm occurred southwest of the fault that ruptured during the 1956 Amorgos earthquake, a magnitude 7.7 event that devastated parts of the region. Although the recent unrest did not lead to an eruption, it highlighted the constant tension within the Aegean crust, where tectonic and volcanic forces interact on a massive scale.

Santorini's history makes it one of the most closely watched volcanic systems in the world. The new findings reaffirm the need for high-resolution monitoring and rapid data analysis to distinguish between harmless intrusions and precursors to eruptions.

Why this discovery matters

The Santorini study changes how scientists think about magma transport. Rather than moving smoothly upward or sideways, magma can rebound within the crust, pushing forward in a series of pulses. Each pulse alters the stress around it, triggering small earthquakes that can cascade into swarms.

Understanding this feedback between magma pressure and crustal stress will improve forecasts not only for volcanic eruptions but also for earthquake hazards in regions where magmatic and tectonic systems overlap.

These results also show that magma intrusions, though hidden deep underground, continuously reshape the planet's surface from below. For the Aegean, it is a reminder that Santorini's spectacular beauty sits above one of Earth's most dynamic geological engines.

References:

[1] Cause of Santorini earthquake swarm uncovered – UCL – November 20, 2025

[2] The 2025 Santorini unrest unveiled: Rebounding magmatic dike intrusion with triggered seismicity – Anthony Lomax et al. – Science – November 20, 2025 – DOI: 10.1126/science.adz8538

(Reet Kaur / THE WATCHERS, Monday, November 24, 2025, https://watchers.news/epicenter/magma-pulses-beneath-santorini-revealed-as-the-true-cause-of-intense-2025-earthquake-swarm)

The 2025 Santorini unrest unveiled: Rebounding magmatic dike intrusion with triggered seismicity

Anthony Lomax, Vasilis Anagnostou, Vasileios Karakostas, Stephen P. Hicks, and Eleftheria Papadimitriou

Editor's summary

Early in 2025, an intense seismic swarm near the volcanic island of Santorini forced thousands of people to evacuate. To understand the cause of the unrest, Lomax *et al*. used data from seismic stations on Santorini and surrounding islands to locate about 25,000 earthquakes over an 8-week period (see the Perspective by Pinel). Their machine learning–derived maps provide an unusually detailed picture of the seismicity, including episodic tremor bursts just a few hours long. Changes in failure stress indicators suggest that the unrest was caused by pump-like intrusions of magma into newly opened dikes 12 kilometers below the seafloor. —Angela Hessler

Structured Abstract

INTRODUCTION

In early 2025, between the islands of Santorini and Amorgos in the Aegean Sea, intense swarm seismicity alarmed the local population, resulting in school closures and disruptions to tourism. Santorini poses a substantial hazard because it is an active stratovolcano and hosted one of the largest known historical eruptions, the massive and devastating Minoan eruption of ~1620 BCE. The swarm seismicity also occurred just southwest of the destructive moment magnitude (M_w) 7.7 Amorgos earthquake rupture of 1956. Whether the 2025 unrest was caused by a magmatic dike intrusion or tectonic fault slip remains controversial. Imaging and explaining this unrest are therefore essential for basic scientific understanding, public information, hazard assessment, and eruption forecasting.

RATIONALE

Magmatic intrusion in Earth can lead to hazardous volcanic eruptions, but the kinematic and dynamic processes involved remain largely hidden from direct observation. Space-time imaging and modeling of the geometry, emplacement, and internal magma flow of dikes, which are essential to understanding volcanic systems and forecasting eruptions and associated earthquakes, rely on seismological and geodetic measures at Earth's surface, resulting in loss of resolution and constraint of dike activity at depth. To overcome these difficulties, we investigated the cause of the 2025 Santorini-Amorgos unrest using precise, machine learning–derived seismicity (~25,000 earthquakes) as virtual, at-depth measures of Coulomb stress change surrounding possible intrusive and fault slip sources.

RESULTS

Our relocated seismicity reveals intense and complex activity extending up to 50 km northeast of Santorini and more than 15 km in depth. Before mid-January 2025, seismicity was sparse and mainly confined to Santorini's caldera, simultaneous with surface uplift and inferred magmatic inflation under the caldera since mid-2024. From 26 January, dense, swarm-like seismicity developed ~20 km northeast of Santorini, followed by rapid expansion of activity to the northeast between 3 and 6 February. Intense, migrating swarm seismicity between 6 and 19 February extended more than 30 km further to the northeast, widening in a fan-shaped cloud. Using this seismicity as a virtual measure for Coulomb stress change imaging, we demonstrated that the source of the unrest was horizontal magmatic dike propagation and not tectonic fault slip. We imaged, in detail, the space-time evolution of the dike along a ~30-km swath as multiscale rebounding waves of dike opening, magma pressure, and breaking of barriers, together with triggered seismicity.

CONCLUSION

Our relocated seismicity and stress imaging resolve a more complex, rebounding feedback mechanism for dike emplacement than previously recognized, advancing understanding of dike physics and volcanic-tectonic-seismogenic feedback mechanisms. The exemplary time and space resolution of Coulomb-seismicity-stress imaging offers a foundation for advancing the physics-based modeling of dikes and for driving machine learning–based, data-driven procedures for tracking intrusions and forecasting eruptions in near real time.

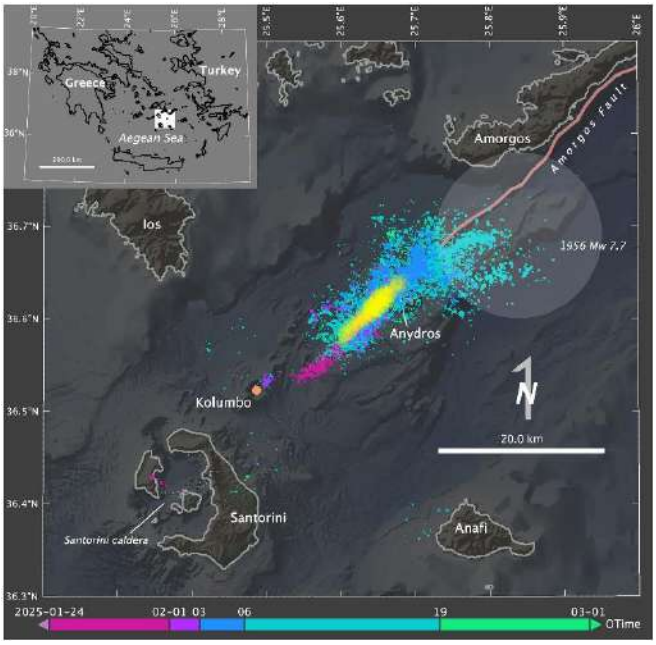

Seismicity and imaged dike.

Machine learning–relocated seismicity for 1 January to 28 February 2025, with symbol size proportional to magnitude and color-coded according to occurrence time (OTime). The yellow patch shows the magmatic dike imaged using the seismicity as virtual measures of stress change due to dike opening. The large gray disk shows the epicentral area of

the M_w 7.7 Amorgos earthquake of 1956. The inset shows the location of the study area (white filled rectangle) in the Aegean Sea.

CREDIT: TOPOGRAPHIC AND BATHYMETRIC BASEMAPS WERE MADE WITH GEOMAPAPP (WWW.GEOMAPAPP.ORG) CC BY FROM W. B. F. RYAN *ET AL*. *GEOCHEM. GEOPHYS. GEOSYST.***10**, 2008GC002332 (2009)

Abstract

Magmatic intrusion in Earth's crust can lead to hazardous volcanic eruptions, but the physical processes involved remain largely hidden from direct observation. We used machine learning–derived seismicity as virtual stress meters at depth to study the disruptive 2025 seismogeodetic unrest in Greece between the Santorini volcano and the epicenter of the devastating moment magnitude 7.7 Amorgos earthquake that occurred in 1956. We show that the cause of unrest was magmatic dike propagation, which we imaged with ~25,000 relocated earthquakes occurring over 2 months. The dike propagated horizontally ~30 kilometers as multiscale rebounding waves of dike opening, magma pressure, and breaking of barriers while triggering intense surrounding seismicity. Our results establish magmatic intrusion as a more complex feedback process than previously recognized and can facilitate physics-based and data-driven modeling and eruption forecasting.

(***Science***, 20 Nov 2025, Vol 390, Issue 6775, DOI: 10.1126/science.adz8538)

A new look at tsunami physics from the Kamchatka M8.8 earthquake

An M8.8 earthquake struck off Russia's Kamchatka Peninsula at 23:47 UTC on July 29, 2025, generating a Pacific-wide tsunami captured for the first time in high resolution by NASA's SWOT satellite.

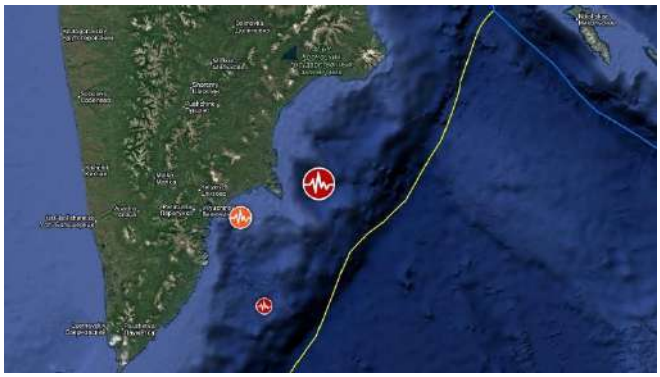

Epicenter of M7.8 earthquake near the east coast of Kamchatka, Russia on September 18, 2025. Credit: TW/SAM, Google

The Surface Water and Ocean Topography satellite captured a 120 km (75 miles) wide swath of sea-surface height variations as the tsunami moved across the northwest Pacific.

This represented the first time a great tsunami generated by a major megathrust earthquake had been observed with such dense spatial coverage. Traditional altimeters only measure a thin line beneath the spacecraft, so their ability to capture tsunami structure has historically been limited.

The SWOT pass revealed a complex wavefield in which the primary wavefront was followed by a series of smaller, lower amplitude waves. These secondary waves showed signs of dispersion and scattering that had rarely been observed in past basin-wide tsunamis.

Ruiz Angulo of the University of Iceland described the effect as acquiring a new pair of glasses, referring to the ability to see patterns that were previously invisible using buoy-based networks.

Before SWOT, researchers relied heavily on DART buoys scattered across the Pacific Ocean. Each buoy can detect tsunamis with millimeter resolution, but they record data at isolated points and cannot visualize the shape of an entire wavefield.

The contrast between continuous swath measurements from SWOT and point-based DART records provided scientists with a unique combination of spatial and temporal insight.

The 2025 event was also the strongest earthquake since the launch of SWOT in 2022, providing the first opportunity to evaluate the satellite's performance during a major subduction-zone earthquake.

As the wave moved beneath the orbiting instrument, the tsunami amplitudes recorded by SWOT aligned closely with those produced by numerical models that included dispersive physics.

A rupture more than 400 km (250 miles) long reveals its true scale

Early models based on seismic and InSAR datasets underestimated the length of the rupture at roughly 300 km (186 miles). When researchers compared that prediction to the tsunami measured by DART buoys, they found mismatches in arrival times.

Waves arrived several minutes early at two stations and more than ten minutes late at a third. This mismatch signaled that the initial rupture model did not fully represent the seafloor deformation that generated the tsunami.

Researchers performed a direct inversion of the DART records, reconstructing initial sea-surface displacement through a grid of Gaussian-shaped uplift elements spaced at roughly 0.3 degrees. The inversion covered a domain larger than the USGS model so that the solution could deviate naturally where needed.

When the inversion was completed, the results showed that the rupture extended at least 400 km (250 miles), with a peak uplift of about 4 m (13 feet) centered near 51 degrees north.

This pattern differed from the earlier USGS finite fault model, which had distributed slip in a narrower band. The inversion showed a broader southern extension and a higher uplift magnitude than previously assumed. However, the inversion lacked significant subsidence, which is expected in a pure thrust earthquake but was underestimated by the Gaussian parameterization. The team addressed this by blending the uplift field from the inversion with the subsidence field from the USGS model.

The combined model reproduced the DART observations with high fidelity. It corrected the timing errors and captured more realistic features of the negative pulse recorded at one of the buoys. This blended deformation pattern became the preferred source model for the 2025 Kamchatka earthquake tsunami.

The new rupture dimensions place the 2025 event alongside the largest megathrust earthquakes of the past century. It reactivated part of the same margin that broke in 1952, yet its rupture occurred farther down dip.

This depth difference reduced the amplitude of the tsunami compared to the catastrophic 1952 event, which produced runups exceeding 15 m (49 feet) along some parts of the Kamchatka coast.

A tsunami that broke the assumption of non-dispersive wave behavior

Tsunamis generated by large subduction earthquakes often contain wavelengths much longer than the ocean depth. Under these conditions, they are commonly treated as non-dispersive waves, meaning they should travel in a stable shape at nearly constant speed.

SWOT observations offered a clear counterexample. Behind the main crest, the satellite detected a sequence of trailing waves with varying amplitudes and spacing.

These secondary waves were not well reproduced by standard shallow water models. The team found that models including dispersive physics produced a better match. They employed a Boussinesq-type solver that incorporated higher-order terms to simulate shorter wavelength interactions. These dispersive models captured the breakup of the primary wavefront and the propagation of lower amplitude features that trailed the main tsunami.

Analysis of synthetic nadir tracks showed how the wave became increasingly disrupted as it moved northward. Between roughly 46 and 49 degrees north, dispersion became noticeable. North of 50 degrees, the wavefront split into multiple pulses due to interactions with the steep bathymetry of the

trench and adjacent slopes. These transitions matched what SWOT observed more closely than nondispersive simulations.

The study concluded that short-wavelength features are probably generated near the source region where bathymetry changes abruptly. These features move away from the trench and require dispersive physics to be captured accurately.

Although the inversion used nondispersive Green's functions, they remained valid for the first-arriving deep water wave. Later features were underrepresented due to the limited resolution of the inversion and the low number of buoys available.

This was one of the most compelling observations made by SWOT. It demonstrated that even tsunamis generated by very large earthquakes can contain a rich spectrum of wave energy, some of which can meaningfully influence coastal waveforms. This finding opens the door to improved hazard modeling that explicitly accounts for dispersive energy transfer across ocean basins.

An earthquake linked to the legacy of the 1952 Kamchatka event

The comparison between the 2025 rupture and the 1952 event reveals insights into the mechanics of the Kuril Kamchatka megathrust. Reconstructions of the 1952 slip pattern, based on historical records and tsunami deposits, indicate that shallow near-trench slip occurred along southern Kamchatka and the northern Kurils. These regions experienced a slip in the range of 9–15 m (29–49 feet).

Given a convergence rate of approximately 8 cm (3 inches) per year, the margin could have accumulated only about 5–6 m (16–20 feet) of slip since 1952. This suggests that the earlier earthquake did not fully release the available strain. The 2025 event likely consumed the residual slip left behind but did not propagate into the shallowest portion of the plate interface.

This depth difference explains why the 2025 tsunami, though recorded across the Pacific Ocean, was far smaller than the destructive 1952 tsunami. Near trench slip displaces more water because it lies closer to the ocean floor surface. A down-dip slip, while powerful, tends to raise and lower the seafloor over a smaller footprint. The 2025 rupture geometry, therefore, moderated the resulting tsunami impact.

For hazard models, the recurrence of two great earthquakes along the same margin in less than a century is a critical signal. Traditional seismic cycle models often assume long recurrence intervals for great earthquakes, but the Kamchatka records show that multiple events can occur on subcentury timescales. This is consistent with other fast-converging margins where incomplete strain release produces a sequence of large events instead of isolated ruptures.

The comparison also shows that megathrusts are capable of diverse rupture behaviors. Even within the same geological segment, the depth distribution of slip controls tsunami strength. This reinforces the need for models that account not just for magnitude but also for rupture geometry and depth when estimating coastal hazard.

A new role for satellite altimetry in tsunami science

The 2025 Kamchatka tsunami provided one of the clearest demonstrations of the scientific value of wide swath satellite altimetry. Prior events such as the 2004 Sumatra tsunami were observed by narrow-track satellites, but the low signal-to-noise ratio and thin spatial coverage limited their utility. SWOT changed this by offering broad and dense measurements across the wavefield.

Although SWOT data typically arrives with a latency of 5 to 10 days, it remains extremely useful for post-event modeling. Assimilating such data into hydrodynamic simulations can refine predictions of coastal impact during extended hazard responses. Even after the initial wave arrival, emergency managers and scientists often need updated models to prepare for later arriving waves or evaluate the risk of secondary events.

The study also showed that satellite altimetry readily complements the DART network. Where DART buoys offer precise timing and amplitude data at a few points, SWOT reveals the large-scale structure of the wavefield. Combined, these datasets form a powerful toolkit for characterizing tsunami sources in the days following a major earthquake.

Future missions with reduced latency or expanded spatial coverage may integrate directly into early warning systems. Even if real-time operations remain challenging, wide swath altimetry will likely become a central component of tsunami science. It offers the ability to observe wave patterns that traditional sensors cannot capture, improving both understanding and forecasting.

Researchers emphasize that the Kamchatka observations represent only the beginning. As SWOT continues to operate, more tsunamis will be recorded across different tectonic settings. Each new event offers an opportunity to refine models, improve inversion techniques, and test hypotheses about wave propagation across complex bathymetry.

References:

[1] SWOT Satellite Altimetry Observations and Source Model for the Tsunami from the 2025 M 8.8 Kamchatka Earthquake – Angel Ruiz-Angulo et al. – GeoScienceWorld – November 26, 2025 – https://doi.org/10.1785/0320250037 – OPEN ACCESS

[2] Tsunami from Massive Kamchatka Earthquake Captured by Satellite – SSA – November 26, 2025

[3] Powerful M8.8 earthquake and tsunami strike Kamchatka Peninsula, sixth strongest earthquake on record – The Watchers – July 30, 2025

(Reet Kaur / THE WATCHERS, Friday, November 28, 2025, https://watchers.news/epicenter/tsunami-physics-kamchatka-2025-m8-8-earthquake)

ΝΕΑ ΑΠΟ ΤΙΣ ΕΛΛΗΝΙΚΕΣ ΚΑΙ ΔΙΕΘΝΕΙΣ ΓΕΩΤΕΧΝΙΚΕΣ ΕΝΩΣΕΙΣ

ΕΛΛΗΝΙΚΗ ΕΠΙΣΤΗΜΟΝΙΚΗ ΕΤΑΙΡΕΙΑ ΕΔΑΦΟΜΗΧΑΝΙΚΗΣ & ΓΕΩΤΕΧΝΙΚΗΣ ΜΗΧΑΝΙΚΗΣ

Συνέντευξη Μ. Μπαρδάνη στη εκπομπή Live Now της Ert News στις 27/11/2025 για τις κατολισθήσεις στη Δυτική Ελλάδα

Στις 27/11/2025 στην εκπομπή Live Now της Ert News με τους δημοσιογράφους Γιώργο Κακούση και Νικολέττα Κρητικού έδωσε συνέντευξη ο Πρόεδρος της Ελληνικής Επιστημονικής Εταιρείας Εδαφομηχανικής και Γεωτεχνικής Μηχανικής Μιχάλης Μπαρδάνης για τις κατολισθήσεις στη Δυτική Ελλάδα κατά τη διάρκεια της κακοκαιρίας «Adel». Η συνέντευξη επικεντρώθηκε στους λόγους εκδήλωσης των κατολισθήσεων και τη δυνατότητα μέτρων πρόληψης. Ο σύνδεσμος για την παρακολούθηση της συνέντευξης βρίσκεται εδώ https://lnkd.in/dHPh9cWf (απόσπασμα από 48:44 έως 54:00)

Η ΕΕΕΕΓΜ εκφράζει τις θερμές της ευχαριστίες προς την Ert News και την κα Βούλα Κουλισοπούλου για την ευγενική πρόσκληση.

SIMSG ISSMGE

International Society for Soil Mechanics and Geotechnical Engineering

ISSMGE News
www.issmge.org/news

CAPG Unveils a New Logo!

ISSMGE IT Administrator / Corporate Associates / 05-11-2025

CAPG is proud to announce the official introduction of our new logo, symbolizing our continued commitment to growth, innovation, and excellence. The new design was selected through a collaborative voting process with our Corporate Associates, reflecting the collective spirit and evolving identity of our organization.

We sincerely thank everyone who contributed to shaping our refreshed identity.

The refreshed logo will be rolled out across all CAPG platforms and communications!

ISSMGE CAPG

Announcing the CAPG LinkedIn Page!

ISSMGE IT Administrator / Corporate Associates / 05-11-2025

We are thrilled to announce that the official **ISSMGE CAPG LinkedIn Page** is now live!

Join us on **ISSMGE CAPG LinkedIn** to stay up to date with the latest news, insights, and initiatives from the Corporate Associates Presidential Group (CAPG) of the International Society for Soil Mechanics and Geotechnical Engineering (ISSMGE).

By following and engaging with our page, you'll become part of a dynamic professional network that bridges research and practice, driving innovation, growth, and collaboration across the geotechnical engineering community.

Your continued support and participation drive our shared mission to advance the industry together.

Follow and like the **ISSMGE CAPG LinkedIn** page today and be part of the conversation shaping the future of geotechnical engineering!

Proceedings of ICSE-12 published in the Online Library of ISSMGE

Shinji Sassa / TC213 / 06-11-2025

The Proceedings of the 12th International Conference on Scour and Erosion (ICSE-12) has just been published in the Online Library of ISSMGE: Online Library | ISSMGE. All papers of ICSE-12 are now freely available and can be found on Scour and Erosion Database at the ISSMGE Online Library.

TC206-220 Monitoring Group 5th Technical Presentation - Monitoring of Earth Structures on the London Underground Network

Ying Chen / TC206 / 06-11-2025

Dear All

You are invited to attend the next **TC206-220 Monitoring Group** meeting, the 5th Technical Presentation.

We are pleased to welcome **Dr Nader Saffari**, Professional Head Earthwork Structures & Geotechnical, Transport for London, who will be presenting a talk titled:

Date: Friday, 12 December 2025

Time: 09:00 10:30 (UK Time)

Presentation Title: **Monitoring of Earth Structures on the LU Network**

Talk Synopsis:

The earth structures on the London Underground (LU) network are over 80 years old with some as old as 150 years old. Most of the cuttings are formed in London Clay and the embankments were generally formed from the excavated material from London Clay cuttings. The original construction of these earth structures was not scientifically undertaken with over-steepened cuttings and poorly compacted embankment fill. Many of them have been showing signs of movement and past instabilities since the early 1990s. Over the last decade the impact of climate change and extreme weather events have become more frequent. This has led to severe flooding and disruption of some rail infrastructure including some injuries and a few fatalities. Therefore, railway infrastructure needs to be carefully managed, and LU has developed and operated a proactive risk-based Earth Structures (ES) asset management regime since the late 1990s which has delivered the key business objectives of improved asset safety, reliability, and availability, whilst delivering efficiency and cost savings. Detailed and deep monitoring of earth structures has provided improvements in the understanding of behaviour of the ES asset base as well as managing the risk of instability. This has allowed decisions to be undertaken with a greater degree of certainty resulting in significant cost savings being realised in the LU ES remediation programme without compromising the safety of the railway.

Dr Saffaris presentation will cover the scope of monitoring activities, data collection and analysis, and how this data is used to manage assets safely and effectively.

Please contract group leader Mr Hock Liong Liew (LindkedIn) for joining the talk.

Observational Method Conference

Ying Chen / TC206 / 24-11-2025

Announcing the Conference on Observational Method in London, UK

We are thrilled to announce the upcoming 1st International Conference on Observational Method, set to take place at #**Imperial College London**, London, UK, on 17th March 2026!

This premier geotechnical event is proudly sponsored by the #**British Geotechnical Association** (**BGA**) and is being developed in collaboration with the #**Construction Indus-try Research and Information Association** (**CIRIA**).

The Conference will bring together leading engineers, researchers, and practitioners to explore the latest advances, case studies, and future directions of the Observational Method in Geotechnical Engineering. You will have opportunity to feedback to the updating CIRIA OM Guide.

Make your calendars and get ready to join this essential industry gathering. Learn more and express your interest at the link below:

https://www.omconference2026.com/event

News
https://www.isrm.net

Proceedings of the 1969 ISRM "International Symposium on the Determination of Stress in Rock Masses" are now available on the ISRM digital library at OnePetro 2025-11-05

The proceedings of the 1969 ISRM "International Symposium on the Determination of Stress in Rock Masses" are now available on the ISRM digital library at OnePetro.

"*Determination of Stresses in Rock Masses*"
1969 May, Lisbon, Portugal
Editor: Manuel Rocha
Organiser: Portuguese National Laboratory for Civil Engineering (LNEC)

CouFrac 2026 - The 5th International Conference on Coupled Processes in Fractured Geological Media: Observation, Modeling, and Application 2025-11-10

CouFrac 2026 - The 5th International Conference on Coupled Processes in Fractured Geological Media: Observation, Modeling, and Application has been approved as an ISRM Specialized Conference.

The conference will take place in Uppsala, Sweden, from 20 to 23 September 2026.

For more information viite the conference website: https://www.coufrac2026.com/

Eurock 2026 — Deadline for Abstract Submission Extended to 15 December 2025-11-17

Due to high interest from authors, the deadline for submitting abstracts for EUROCK 2026 has been extended to 15 December 2025.

For full details, please visit the conference website at https://eurock2026.com/

52nd ISRM Online Lecture will be given by Mr. William Joughin from South Africa - 11 December at 10 A.M. UTC 2025-11-19

The 52nd ISRM Online Lecture will be given by Mr. William Joughin from South Africa. The topic of the lecture will be "Design of concrete plugs for sealing of tunnels to prevent inrush of water and mud". It will be broadcast on December 11 at 10 A.M. UTC and will remain available on the **Online Lecture's page**.

A new ISRM Suggested Method has been published 2025-11-19

Prof. Resat Ulusay, Chair of the ISRM Commission on Testing Methods announced that the *"ISRM SM for determining the tensile strength and elastic constants of rocks by the direct tension test"* has been published in *Rock Mechanics and Rock Engineering (RMRE)*.

It is available to members free of charge in the Suggested Methods page.

Proceedings of the 1971 ISRM International Symposium "Rock Fracture" are now available on the ISRM digital library at OnePetro 2025-11-30

The proceedings of the 1971 ISRM International Symposium "Rock Fracture" are now available on the ISRM digital library at OnePetro.

"Rock Fracture"
1971 September, Nancy, France.
Editor: René Houpert
Organiser: French Committee of Rock Mechanics (CFMR)

News
https://about.ita-aites.org/news

In memoriam Richard Lovat 1928-2025 06 November 2025

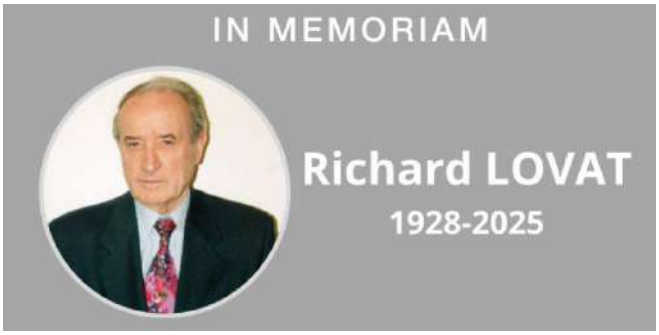

After a long and extraordinary life—much of it dedicated to the early design of TBMs and the development of TBM excavation—it is announced by the Lovat family of the passing of Richard Lovat in Toronto shortly after his 97th birthday.

The family reports that Richard died peacefully in late October with immediate family members at his side.

The Lovat family, a close and private family with roots in Richard's home country Italy and with a proud legacy in his adopted country Canada, requests privacy at this time and asks all who knew Richard, and knew of him, to take a moment to reflect on how he influenced their careers and contributed to an industry as it marches forward, building on the courage and determination of its pioneers.

The Lovat name will forever hold a place in the tunnelling industry history.

2025 WG22 Publication: A sustainable BIM Approach for Lifecycle Management 07 November 2025

New Online Publication: Tunnelling Information Modelling - A sustainable BIM Approach for Lifecycle Management *by Working Group 22 –*

Working Group 22 (WG22) of the ITA-AITES is pleased to announce the online release of its latest document.

Abstract:

Infrastructure projects, particularly tunnels, have significant environmental impacts due to extensive resource use and exposure to natural hazards. To address these challenges, an effective approach integrating environ mental, economic, and social dimensions into the development of underground infrastructure is advisable. This guideline introduces a framework proposed by the ITA-AITES Working Group 22, focused on leveraging Building Information Modelling (BIM) to achieve sustainable practices throughout the lifecycle of tunnelling projects, aligning with the United Nations Sustainable Development Goals (SDGs). The proposed BIM-based framework outlines how sustainable practices can be embedded early in project development, flowing into design, construction, and asset management. The framework considers setting requirements during strategic planning, designing and constructing with low-carbon materials, real-time monitoring of sustainability Key Performance Indicators (KPIs) during construction, and transitioning from Project Information Models (PIM) to Asset Information Models (AIM) for sustainable operation and maintenance using digital twins. The document aims to support all stakeholders involved in various tunnelling projects (new or renovated, conventionally or mechanically excavated). This support focuses on using a BIM methodology to address best practices during the whole lifecycle of a tunnel by: a) Identifying how BIM and digital tools can support stakeholders in making informed decisions about the tunnel lifecycle, b) Facilitating a comprehensive journey of new digital solutions available throughout the lifecycle, c) Providing a pragmatic framework to demonstrate the delivery of sustainability goals and define relevant BIM use cases, d) enabling a data-driven dynamic environ mental impact assessment, e) promoting material reuse, energy efficiency and mitigating overall carbon footprint. This guideline highlights the importance of interoperability to provide a robust basis for the application of BIM in further use cases and to implement other technologies like Artificial Intelligence (AI) and Internet of Things (IoT) in sustainable tunnelling projects.

By Rita Sanfilippo, Masoud Esfandiari, Federico Foria Dan Garbutt, Kathrin Glab, Jurij Karlovsek, Alessandro Menozzi, Galina Paskaleva, Florent Robert.

➡ **Download the guidelines here**

2025 WG22 Publication: Guideline for Mechanised and Conventional Tunnels 10 November 2025

New Online Publication: BIM in Tunnelling: Guideline for Mechanised and Conventional Tunnels *by Working Group 22 –*

Working Group 22 (WG22) of the ITA-AITES is pleased to announce the online release of its latest document.

Abstract:

This guideline has been initiated by the International Tunnelling Association (ITA) Working Group (WG) 22 to sup-port BIM implementation in the tunnelling industry. It pro-vides recommendations which are to be adapted according to the availability of corresponding best practice experiences for all Project parties in order to support the adoption of BIM within a tunnelling Project.

This guideline is intended to be used by all engineers and owners to provide a reference framework for the implementtation of BIM for tunnel Projects. It focuses on the implementtation of BIM for segmentally lined mechanically bored tunnels and conventional tunnels. This guideline primarily covers the implementation of heavy civil elements for a tunnel Project. For more general information concerning BIM and its use in underground construction, the reader is referred to more general guidelines such as The German Tunnelling Committee's (DAUB's) "Building and Operation of Underground Structures – BIM in Tunnelling" or similar documents as provided in Section 16.

Specific recommendations concerning the modelling of non-civil works, e.g., mechanical, electrical, automation, or control systems, or Project-specific internal structures, e.g., concrete infills, plenum walls, duct-banks, smoke ducts, etc. are not provided.

This guideline is not intended to contest Employer's Information Requirements or local best practise. It is only intended to alleviate ambiguity that may exist due to general definitions in the Employer's Information Requirements or provide reference to owners for the development of their Requirements.

It is expected that the BIM's capabilities will continue to expand as new BIM technology is developed. This version of this guideline is, however, based on a review of current international practise of BIM in tunnelling. As such, this document is subject to updates in consequent versions.

By Vojtěch Ernt Gall, Wojciech Mleczko, Florent Robert, Wolfgang Angerer, Jyrki Salmi, Zehao Ye, Jacob Grasmick, Michel Rives, Wolgang Aldrian, Philipp Dohmen, Anne Jacobs, Jelena Ninic, Jurij Karlovsek,

➡ **Download the guidelines here**

Scooped by ITA-AITES #139, 5 November 2025

Tunnel boring machine arrives on site for STM's Blue Line Project | Canada

Investment case for second Mt Vic tunnel "endorsed;" documents to be completed by July | New Zealand

Vietnam's Phu Quoc to build $360M metro line linking airport with APEC conference center

Giant boring machines to start HS2 tunnels from Old Oak Common to Euston 'fairly soon,' says rail minister | UK

Poland's CPK opens tender for underground rail station at airport

Chongqing-Xiamen Railway Tunnel – Drive was completed by TBM | China

Line 19: what is the status of this metro line project in Val-d'Oise? | France

'Moana' bores on for Māngere's $64m wastewater upgrade | New Zealand

Underground gas storage key to global energy security

Optimising ventilation and safety in underground hydropower projects

Scooped by ITA-AITES #140, 19 November 2025

Colombia building what will become longest tunnel in Latin America

Mumbai to spend INR 40,000 crore on new tunnelling projects after Metro 3 success | India

NYC's water tunnel project nears completion after decades | USA

10 longest tunnels used by trains in the world

Europe greenlights record-breaking underwater tunnel, plunging nearly 1,300 feet below the sea | Norway

Minister agrees on train tunnel Costa del Sol | Spain

Contract awarded to study feasibility of 401 tunnel | Canada

Contractors courted for £1.7bn London DLR extension job | UK

Giant caverns complete for Western Harbour TBMs | Australia

Registration Open for WTC 2026 in Montreal | Canada

BRITISH TUNNELLING SOCIETY YOUNG MEMBERS

November Lecture
Connecting Worlds Underground: Digitalisation in Tunnelling

Thursday, 6th November 2025, 18:00 - 19:30 GMT
ICE QH, One Great George Street, London, SW1P 3AA

Event Information

This lecture by Maximilian Lischke will delve into the evolving landscape of digitalisation in tunnelling, emphasizing the importance of human-centered design.

While technologies like digital twins and AI are gaining traction, their impact is limited without addressing operational realities such as fragmented data flows and poor accessibility.

The presentation will showcase how cloud-based IoT platforms and intuitive interfaces can simplify operations, improve clarity, and empower teams.

Attendees will gain insights into integrating OT, IT, and IoT environments to drive smarter planning and execution in tunnelling projects.

The lecture will last 45–60 minutes, followed by a 10–20 minute Q&A session, networking drinks, and informal discussions at the Kendal's Bar with drinks sponsored by Herrenknecht AG.

Speaker

Maximilian Lischke

Maximilian holds a Bachelor of Engineering in Industrial Engineering with a focus on information and communication technologies. Since 2022, he has been part of the Technology & Innovation Digitalisation department at Herrenknecht.

In his current role, he oversees the development and implementation of Herrenknecht. Connected, the company's data management system, and manages digitalization projects worldwide. His work focuses on advancing digital solutions that enhance efficiency, data integration, and connectivity in tunnelling operations.

Zoom Link

INTERNATIONAL GEOSYNTHETICS SOCIETY

www.geosyntheticssociety.org

News

IGS France Celebrates Hit EuroGeo8 November 3, 2025

Hundreds gathered to explore latest industry developments in Europe at the 8th European conference on geosynthetics (EuroGeo8) last month. Hosted this time by the French Chapter Read More »

Say 'Marhaba' To IGS Iraq November 9, 2025

Bid a warm welcome – or 'marhaba' – to the Society's newest members with the launch of IGS Iraq. Led by Professor Mahdi Karkush, President Read More »

10 Questions With... IGS Iraq President Mahdi Karkush November 12, 2025

This fall, the IGS launched its newest Chapter, IGS Iraq, strengthening the Society's reach in the Middle East region. Here, inaugural President Mahdi Karkush gives Read More »

My Engineer Life With... Ness Di Battista November 25, 2025

Have you ever considered the wetting curve of pie dough? From cake mix to waste containment young engineer Ness di Battista shares how geosynthetics engineering Read More »

IGS Diversity Committee Shares Value of 'Collective Care' November 26, 2025

Delegates at the recent EuroGeo8 conference learnt how leading with empathy was key to creating a stronger working environment. Attracting some 130 delegates from the Read More »

Company History: Naue November 30, 2025

This article is part of a Premium Corporate Member spotlight, providing Premium Corporate Members with the opportunity to showcase their history, work and products. It does Read More »

Naue Case Study: GreenLine – Biodegradable geosynthetics November 30, 2025

This article is part of a Premium Corporate Member spotlight, providing Premium Corporate Members with the opportunity to showcase their history, work and products. It does Read More »

An Interview with Naue: Building on Sustainable Ground November 30, 2025

This article is part of a Premium Corporate Member spotlight, providing Premium Corporate Members with the opportunity to showcase their history, work and products. It does Read More »

BGA · THE BRITISH · GEOTECHNICAL ASSOCIATION

News
https://www.britishgeotech.org/news

Call for entries for the 57th Cooling Prize Competition 01.11.2025

The British Geotechnical Association (BGA) is pleased to invite Early Career Ground Engineering Professionals to submit posters for the 57th Cooling Prize Competition on any topic dealing with the engineering behaviour of the ground. Deadline 5 December 2025. Read More

1st BGA Women in Geotechnics Symposium: Inspire an Engineer 06.11.2025

The British Geotechnical Association (BGA), with the generous support of the Association of Geotechnical and Geoenvironmental Specialists (AGS), is excited to announce the launch of Women in Geotechnics (WiGeotech) Afternoon Tea. The event will be held on Monday 2 March 2026 from 14:00 at the Institution of Civil Engineers, Westminster, London. Read More

2025 Fleming Award Shortlist Announced 07.11.2025

The BGA is pleased to announce the shortlisted entries for the 2025 Fleming Award. The finalists will present at the Fleming Award event on 2 December 2025, when a judging panel will select the winner. Read More

ISSMGE Bright Spark Award – Dr Ze Zhou Wang 23.11.2025

Dr. Ze Zhou Wang from the University of Cambridge was recently selected as the recipient and presenter of the ISSMGE Bright Spark Award Lecture at the Third Workshop on the Future of Machine Learning in Geotechnics in Florence this October. Read More

ICSMGE 2026: Uploading of final conference papers – extension of deadline to 14 December 2025 26.11.2025

An extension has been granted to all authors submitted papers for ICSMGE 2026 via the British Geotechnical Association to upload their corrected/final papers on the conference portal latest by 14 December 2025. Read More

The December 2025 issue of Ground Engineering is available on line 27.11.2025

The December 2025 issue of Ground Engineering is available on line. Online access to Ground Engineering (GE) is included in BGA subscriptions. Read More

ΔΙΑΚΡΙΣΕΙΣ ΕΛΛΗΝΩΝ ΓΕΩΤΕΧΝΙΚΩΝ ΜΗΧΑΝΙΚΩΝ

STATIC AND DYNAMIC SOIL – FOUNDATION – STRUCTURE INTERACTION

Prof. em. George Gazetas (NTUA)

Ο Ομότιμος Καθηγητής ΕΜΠ Γιώργος Γκαζέτας προσεκλήθη από το Πανεπιστήμιο του Βουκουρεστίου να παρουσιάση δύο ολοήμερα μαθήματα περί «Αλληλεπιδράσεως Εδάφους-Θεμελίου-Κατασκευής» (6 και 7 Νοεμβρίου, 2025). Η πρώτη ημέρα θα είναι σε επίπεδο μεταπτυχιακών φοιτητών, η δε δεύτερη για επαγγελματίες μηχανικούς.

Panel Discussion "Geohazards & Pipelines: Insights, Mitigation, and Innovation"

Prodromos Psarropoulos

Ο Δρ. Πρόδρομος Ψαρρόπουλος, στα πλαίσια του Pipeline Technology Conference Asia (Kuala Lumpur, Malaysia, 11-13 Νοεμβρίου), προσεκλήθη να συμμετάσχη στην Panel Discussion "Geohazards & Pipelines: Insights, Mitigation, and Innovation" (13 Νοεμβρίου 2025).

Panel Discussion "Geohazards & Pipelines: Insights, Mitigation, and Innovation"

ΠΡΟΣΕΧΕΙΣ ΓΕΩΤΕΧΝΙΚΕΣ ΕΚΔΗΛΩΣΕΙΣ

Για τις παλαιότερες καταχωρήσεις περισσότερες πληροφορίες μπορούν να αναζητηθούν στα προηγούμενα τεύχη του «περιοδικού» και στις παρατιθέμενες ιστοσελίδες.

17th International Conference on Geotechnical Engineering 8th International Symposium on Geohazards, December 4-5, 2025, Lahore, Pakistan, https://17icge-8isg.com

International Conference on Measurement While Drilling (MWD'1), December 9, 19 & 11, 2025, Your Office, www.mwdconferences.com

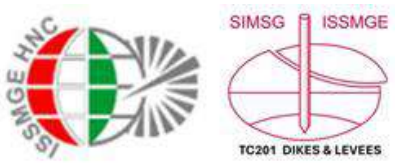

HAS200

4th Unsaturated Soils, Granular Matter And Environmental Engineering Symposium

4th Unsaturated Soil, Granular Matter and Environmental Engineering Symposium In Memory of Professor G. N. Pande
16-01-2026, Hungary , Budapest
https://kti.rkk.uni-obuda.hu/4th-unsaturated-soil-granular-matter-and-environmental-engineering-symposium-in-memory-of-professor-g-n-pande/

The Hungarian National Committee of ISSMGE organises with the support of ISSMGE TC106 and TC201, the Hungarian Academy of Sciences **4th Unsaturated Soil, Granular Matter and Environmental Engineering Symposium in Memory of Professor G. N. Pande** in the 200th anniversary year of the Hungarian Academy of Sciences in January 16, Online. The participation after registration is free.

The organisation is helped by the Rejtő Sándor Faculty of Light Industry and Environmental Engineering, Óbuda University, Budapest, Hungary and the Department of Engineering Geology and Geotechnics, Civil Engineering, BME, Budapest, Hungary.

Past events in similar topic supported by ISSMGE HNC and the Soil Science Institute in Hungary:

1. 1st Unsaturated Soil Symposium, 1999. BME, Budapest, Hungary
2. 2nd Unsaturated Soil Symposium, 2003. 2-5 of November. Ráckeve, Hungary
3. 3rd Unsaturated Soil Symposium, May 5, 2015. RISSAC, Budapest, Hungary
4. 1st Middle European Conference on Landfill Technology2008, at the Hungarian Academy of Science, Budapest, Hungary
5. The Granular Matter Section JETC 2017, BME, Budapest, Hungary
6. June 12, 2018. Workshop on Granular Matter at the Hungarian Academy of Sciences
7. Workshop series on ISC6, September 2021, Hungarian Academy of Science
8. Workshop on Granular Matter, Hungarian Academy of Science, 2023. 24-25th August

The participation is free of charge, but you need to register ***through this link***. The Teams join link will be sent out to the registered e-mail address.

The final programme is available via ***this link***.

The Fifth International Conference on Rock Dynamics and Applications (RocDyn-5), 15-17 Jan 2026, Singapore https://rocdyn.com

SEAGC-AGSSEA CONFERENCE 2026 Advancing Geotechnics for a Resilient and Sustainable Future: Mitigating Multi-hazards amidst Changing Climate, 28÷30 January 2026, Taguig City, Philippines https://seagc2026.pssmge.org

The 5th International Symposium on Slope Risk and Resilience
February 5-9, 2026, Hong Kong, China
https://issrr2026.aconf.org/index.html

Rapid climate change and the increasing frequency of extreme meteorological events are exacerbating slope instability across a broad range of geomorphological settings, from high-mountain regions to coastal low-relief hills and submarine environments. These climate-driven geohazards present substantial threats to human settlements and critical infrastructure, with particularly acute implications for densely populated megacities. Addressing these challenges necessitates a fundamental transition from conventional methodologies toward intelligent, resilience-centered frameworks for slope disaster risk reduction.

The 5th International Symposium on Slope Risk and Resilience will provide as a vital platform for global experts to share cutting-edge research, discuss AI-powered mitigation strategies, and collaborate on innovative solutions for slope resilience. Following successful editions in Shanghai (2018), Edinburgh (2020), Sendai (2022), and Toronto (2024), this symposium will focus on translating scientific insights into

practical actions—strengthening slope resilience in an era of climate change and supporting sustainable, safe urban development.

Conference Topics

- ♦ Climate Change and Slope Instability
- ♦ Slope Failure Mechanisms
- ♦ Intelligent Landslide Early Warning
- ♦ Landslide Risk Assessment
- ♦ Sustainable Slope Design and Resilience
- ♦ Landslide Mitigation Strategies
- ♦ Microscale to Macroscale Geomechanics
- ♦ Slope Engineering Case Studies
- ♦ Landslide Experimentation and Numerical Modeling

Contact Us

1. **Prof. Qi Zhao (Chair)**, qi.qz.zhao@polyu.edu.hk
2. **Dr. Zhiqian Liu (Event Secretary)**, zhiqian.liu@polyu.edu.hk

2nd International Symposium on Tailings Storage Facilities, March 11 to 13, 2026, Hermosilo, Sonora, Mexico, https://2sisdj-hermosillo-2026.com.mx/en/index.php

Observational Method Conference
Perspectives and feedback from academics, consultants, contractors, clients, and technical committees
17 Mar 2026, London, United Kingdom
www.omconference2026.com

The Observational Method (OM) remains a cornerstone of modern geotechnical practice, providing a framework to manage geotechnical uncertainties through adaptive design and construction. This Observational Method Conference, is hosted by TC206 at Imperial College and brings together perspectives from academia, consultancy, contracting, and client organisations to explore recent developments and challenges in implementing OM across disciplines.

CIRIA have recently let a contract to Arup and Mott Macdonald to update the OM Guide R185 on OM. This Conference provides an opportunity to obtain industry feedback on OM for this Guide. A goal is also to promote interaction with other Technical Committees such as TC220 (I&M), TC204 (Tunnels), and TC309 (Machine Learning), where OM is already practised.

Keynotes presentations addressing statistical control of uncertainty, reliability of instrumentation, and lessons from tunnelling practice. Subsequent sessions highlight progress in real-time back analysis (RTBA), surrogate modelling, and data bases. A session is also planned on how tunnelling, piling and ground treatment works are using data-driven methods to influence designs during construction.

CONTACT US

Chair of TC206: Duncan Nicholson Duncan.Nicholson@arup.com

Organisers:

Truong Le truong.le@mottmac.com
Franz Tschuchnigg franz.tschuchnigg@TUGraz.at

GEOMOS26 2nd International Scientific and Practical Conference on Soil Mechanics, Geotechnics and Foundation Engineering INTELLIGENCE ON GUARD OF MECHANICAL SAFETY, March 17-20, 2026, Moscow, Russia, https://geomos.rssmgfe.ru/en/

3rd Annual Conference on Foundation Decarbonization and Re-use, March 24-26 2026, Amsterdam, The Netherlands https://foundationreuse.com

3rd Annual Conference on Foundation Decarbonization and Re-use, March 24-26 2026, Amsterdam, The Netherlands, https://foundationreuse.com

GROUND ENGINEERING BASEMENTS AND UNDERGROUND STRUCTURES

Beneath the Surface, Beyond the Future
24 March 2026, London, United Kingdom
https://basements.geplus.co.uk/GEBA2026/en/page/home

Beneath the Surface, Beyond the Future.

Ground Engineering is proud to present the **18th Basements and Underground Structures Conference,** a pivotal gathering showcasing technical resilience, adaptive reuse, and the futureproofing of subterranean infrastructure.

Spanning infrastructure, commercial, and residential projects, this year's event brings together UK and international case studies, revealing the engineering, sequencing, monitoring, and waterproofing strategies driving success in the most constrained urban environments. Delegates will gain insight into landmark projects like CERN's Future Circular Collider, explore the latest in subsurface mapping and digital twins, and engage directly with the Building Safety Regulator on compliance challenges reshaping project delivery.

Across the day, sessions will cover sustainability and embodied carbon reduction, adaptive reuse of heritage basements, innovations in monitoring and ground data transformation, and visionary futures such as geothermal energy, data centres, and underground living. Networking opportunities with asset owners, Tier 1 contractors, consulting engineers, spe-

cialists, and suppliers ensure valuable connections that can shape upcoming tenders and collaborations.

This programme is designed to give you the knowledge, insights, and partnerships needed to thrive in today's fast-changing market.

This year's programme responds directly to today's market challenges: projects delayed under tighter budgets, new Building Safety Regulator requirements reshaping delivery, and a drive to reduce carbon while embracing digital tools. Through expert-led sessions, real-world case studies, and panel discussions, we will explore:

- Engineering in constrained environments beneath heritage assets and live transport hubs
- Subsurface mapping and monitoring data to inform design and risk management
- Navigating compliance and the Building Safety Act in subterranean works
- Innovation, adaptive reuse, and 2050 visions for basements as energy, data, and resilience hubs

Across a full day of knowledge exchange, delegates will gain practical insights from major UK and international projects, connect with key decision makers, and leave equipped to deliver high-performance basements and underground structures in an increasingly complex landscape.

Topics of interest can include but are not limited to:

- **Adaptive reuse and repurposing**: Innovative approaches to transforming existing underground spaces into energy hubs, data centres, or multi-use facilities.
- **Sustainable and resilient engineering:** Techniques and technologies that improve environmental performance, reduce carbon footprint, and enhance infrastructure resilience.
- **Digital and monitoring innovation:** Novel applications of digital twins, real-time monitoring, and data-driven design feedback loops to improve construction safety and performance.
- **Futureproofing underground infrastructure:** Concepts addressing long-term challenges, including climate adaptation, urban densification, and integrated subterranean networks.

For assistance with submissions or questions, please contact:
Marlene Cowlard +44 (0)203 953 2989
marlene.cowlard@emap.com

PMGEC LEBANON 2026 Pan Mediterranean Geotechnical Engineering Conference, 25 - 28 March 2026, Phoenicia Bei-rut IHG, Lebanon https://pmgec-leb.com

Sixth International Conference on Geotechnical Engineering – Iraq (6ICGE-Iraq 2026)
April 8–9, 2026, Baghdad, Iraq
https://icge-iraq.uobaghdad.edu.iq/

The Sixth International Conference on Geotechnical Engineering – Iraq (6ICGE-Iraq 2026) will be held in Baghdad, Iraq, from April 8–9, 2026. This major event is jointly organized by the Iraqi Scientific Geotechnical Society (ISGS), in collaboration with the Department of Reconstruction and Projects/University of Baghdad, the Faculty of Engineering/Koya University, Komar University of Science and Technology, and Moscow State University of Civil Engineering. As one of the most prestigious scientific gatherings in the region, 6ICGE-Iraq 2026 will offer a vibrant platform for researchers, engineers, and industry professionals to exchange knowledge and share the latest advancements across a wide range of disciplines including geotechnical engineering, civil engineering, mechanical engineering, energy, architectural engineering, water resources, environmental engineering, and petroleum engineering. The primary goal of 6ICGE-Iraq 2026 is to strengthen international collaboration between Iraq and the global scientific community, fostering partnerships that enhance innovation, research excellence, and the exchange of expertise. By bringing together distinguished experts from academia, research institutions, and industry, the conference aims to promote productive dialogue on emerging challenges, sustainable solutions, and technological innovations shaping the future of engineering. This event will serve as a catalyst for knowledge transfer and interdisciplinary cooperation, supporting the development of joint research initiatives and advancing applications in engineering sciences, energy systems, and applied mechanics. Participants will have the opportunity to present pioneering research, explore cross-disciplinary innovations, and engage in high-level scientific discussions addressing complex engineering and environmental issues. Ultimately, 6ICGE-Iraq 2026 aspires to play a leading role in advancing scientific excellence, fostering global cooperation, and integrating modern technologies into geotechnical and civil engineering practice for a more resilient and sustainable future.

Themes of the Conference

1. Soil Mechanics and Geotechnical Engineering (SMGE)
2. Structural Engineering and Mechanics (SEM)
3. Construction and Sustainability (CS)
4. Urban Development and Architecture (UDA)
5. Water Resources Engineering and Environment (WREE)
6. Mechanical Engineering and Energy Sciences (MEES)

Contact

Email: icge@uobaghdad.edu.iq, Issmfe.conference@gmail.com

Tel: +964 7860005410 (Asst. Prof. Shaimaa Muthana AbdulRahman)
+964 790 256 2401 (Dr. Maher M. Jebur)
+964 770 275 5346 (Asst. Lecturer Afrah Abdulelah Hamza)

Join us on Telegram Group:
https://t.me/+S_8Ox0UBK00zMmZi

3rd International Conference on Advances in Rock Mechanics (TuniRock 2026), 09-12 April, 2026, www.tunirock2026.com

International Conference on Geotechnics, Civil Engineering and Structures (CIGOS) 2026 Innovation in Planning, Design and Civil Infrastructure for Resilient and Sustainable Transformation, April 16 & 17, 2026, Ho Chi Minh City, Vietnam https://cigos2026.sciencesconf.org

LANDSLIDES 2026 Landslide Geo-Education and Risk (LaGER), 27 April - 1 May 2026, Queenstown, New Zealand http://landsliderisk.nz

15th International Conference "Modern Building Materials, Structures and Techniques", May 12-15, 2026, Vilnius, Lithuania, https://vilniustech.lt/332107

ITA-AITES WTC 2026 World Tunnel Congress, May 15 to 21, 2026, in Montreal, Quebec, Canada, https://wtc2026.ca

94th Annual Meeting & International Symposium on Large Dams - Water, Energy and Society: The Evolving Role of Dams in a Changing World, May 21 to 29, 2026, Guadalajara, Mexico, www.icoldmexico2026.com

ICPMG 2026 Physical Modelling in Geotechnics, 8–12 June 2026, ETH Zürich, Switzerland, https://tc104-issmge.com/icpmg-2026

8th International Young Geotechnical Engineers Conference - 8iYGEC, 11. - 14. June 2026, Graz, Austria, www.tugraz.at/institute/ibg/events/8iygec

21st International Conference on Soil Mechanics and Geotechnical Engineering Geotechnical Challenges in a Changing Environment, 14 – 19 June 2026, Vienna, Austria, www.icsmge2026.org/en

3rd International Geotechnical Innovation Conference - Shaping the World Beneath: Fostering Sustainability, Innovation and Resilience in Geotechnics, 15 - 16 June 2026, Jeddah, Saudi Arabia, https://geotechnicalinnovationconference.com Email info@creativeconnectionevents.com

ICONHIC 2026 International Conference on Natural Hazards & Infrastructure, 29 June – 2 July 2026, Chania, Greece https://iconhic.com/2026

ISFMG 2026 12th International Symposium on Field Monitoring in Geomechanics, 06 -10 August 2026, Indian Institute of Technology Indore, India, https://sites.google.com/view/isfmg2026/home

Soft Soils 2026 International Conference on Advances and Innovations in Soft Soil Engineering 2026, 24-26 August 2026, Delft, Netherlands https://softsoils2026.dryfta.com

ICGE Colombo 2026 4th International Conference on Geotechnical Engineering, 24-26 August 2026, Colombo, Sri Lanka, https://icgecolombo2026.org/

X Latin American Congress on Rock Mechanics 26 - 28 Aug, 2026, Brsasilia, Brazil, https://larms2026.com

CREST 2026 3rd International Conference on Construction Resources for Environmentally Sustainable Technologies, Sep 07-08, 2026, Cambridge, England-United Kingdom https://engage-events.ifm.eng.cam.ac.uk/IC-CREST2026#/

13 ICG - 13th International Conference on Geosynthetics (13 ICG), 13-17 September 2026, Montréal, Canada, www.13icg-montreal.org

Eurock 2026 Risk Management in Rock Engineering - an ISRM Regional Symposium, 15-19 September 2026, Skopje, Republic North Macedonia, https://eurock2026.com

ECEE2026 18th European Conference on Earthquake Engineering Shaping the Future of Earthquake Engineering, 14 – 1 September 2026, Berlin, Germany, https://ecee2026.eu

ISRM Regional Symposium – EU-ROCK 2026, September 15–19, 2026, in Skopje, N. Macedonia, https://eurock2026.com

4th International Symposium Preservation of Monuments & Historic Sites, 16 – 18 September 2026, Athens, Greece https://tc301-athens.com

2nd International Conference on
Insitu Measurement of Soil Properties
and Case Histories
INSITU 2026
September 21 - 23, 2026, Bali, Indonesia
https://www.insitu2026.com/

Greetings!

It is our great pleasure to welcome you to the 2nd International Conference on In Situ Measurement of Soil Properties and Case Histories (INSITU 2026), which will be held in Bali, Indonesia, on September 21–23, 2026.

INSITU 2026 is hosted by Universitas Katolik Parahyangan (UNPAR) under the auspices of TC 102, the International Society for Soil Mechanics and Geotechnical Engineering (ISSMGE) and the Indonesian Society for Geotechnical Engineering – Himpunan Ahli Teknik Tanah Indonesia (HATTI).

We warmly invite researchers, industry professionals, and policymakers from around the world to participate in this important forum to share insights, exchange experiences, and explore innovations in in situ testing, site characterization, and geotechnical design.

We look forward to welcoming you to INSITU 2026.

Conference Themes

1. Site Characterization by In Situ Test and Geophysical Method
2. Interpretation of In Situ Test Results

3. In Situ Measurement of Shear Strength, Deformation Characteristics, Initial Stress, and Stress History
4. In Situ Measurement of Ground Water Flow Characteristics in Unsaturated and Saturated Soils
5. In Situ Test in Soft Clays and Peats
6. CPTu and DMT in Underconsolidating Soils
7. In Situ Measurement of Consolidation Characteristics and Permeability
8. In Situ Test for Seismic Analysis
9. In Situ Test for Foundation Design and Geotechnical Analysis
10. Interpretation of In Situ Test in Residual Soils, Volcanic Soils, and Problematic Soils
11. Technological Developments in Geotechnical Field Testing Instruments and Procedures
12. Liquefaction Risk Assessment by Insitu Tests
13. Rock Properties and Geophysical Investigation for Site Characterization
14. Case Histories on Landslide
15. Case Histories on Ground Improvement
16. Case Histories on Seismic Problems
17. Case Histories on Foundation Problems and Advancement
18. Case Histories on Geotechnical Failures
19. Geotechnical Forensic Engineering by Insitu Test

Secretariat INSITU 2026

For further info contact us insitu2026@gmail.com

6th International Conference on Information Technology in Geo-Engineering JTC2 Conference, 13-16 October 2026, Graz, Austria, www.icitg2026.com

Adapting to change ~ Embracing opportunities
14-16 October 2026, Bologna, Italy

We are pleased to announce that the HYDRO 2026 conference and exhibition will take place in Bologna, Italy from 14 to 16 October 2026, with the overall theme 'Adapting to change ~ Embracing opportunities'.

The Call for Papers brochure can be found on our website here. We welcome abstracts on any of the topics listed in the brochure, or related topics, as soon as possible and by 16 March 2026 at the latest. Please make sure to follow the guidelines on the final page of the brochure when submitting an abstract - thank you.

A brief initial report of the previous event in this series, HYDRO 2025, held recently in Thessaloniki, Greece is available on our website here. A more detailed report will be published soon in Hydropower & Dams journal.

For any enquiries about the HYDRO 2026 conference programme, please contact us at: Hydro2026@hydropower-dams.com

For enquiries about the HYDRO 2026 Exhibition, please contact: Sales@hydropower-dams.com

More information about HYDRO 2026 will be uploaded to a dedicated part of our website soon, and then this micro-site will be regularly updated in the coming months. Meanwhile, please mark the dates in your calendar for next year, and we hope to welcome you in Bologna.

EWRWSE – 2026 7th International Conference on Environmental Geotechnology, Recycled Waste Materials and Sustainable Engineering, 22-25 October 2026, Surat, Gujarat, India www.egrwse2026.com

SLOPE STABILITY 2026 Slope for Safety Performance an ISRM Specialized Conference, 26 – 29 October 2026, Lima, Peru www.slopestability2026.com/en

PBD-V Chile International Conference on Performance-Based Design in Earthquake Geotechnical Engineering, November 4th to 6th, 2026, Puerto Varas, Chile www.pbd-v-chile.com

ARMS 14 Fukuoka 2026 - 14th Asian Rock Mechanics Symposium Rock Mechanics for the Next Generation –Innovations, Sustainability, and Resilience – an ISRM Regional Symposium, 22-26 November 2026, Fukuoka, Japan, www.ec-convention.com/ARMS14/

GEOTEC HANOI 2026, The 6th International Conference on Geotechnics for Sustainable Infrastructure Development, November 26 - 27, 2026, Hanoi, Vietnam, https://geotechn.vn/

7th International Conference on Grouting and Deep Mixing, March 17 - 19, 2027 | Florence, Italy, https://dfi-events.org/grout27/index.html

IS-GI LYON 2026 International Symposium on Ground Improvement, April 12 to 14, 2027, Lyon, France, www.menard-group.com/isgi-lyon2027

ITA World Tunnel Congress 2027 - Antwerp (WTC 2027)
Underground Creativity to Meet Societal Needs
23-29 April 2027, Antwerp, Belgium

The World Tunnel Congress 2027, scheduled to take place in Antwerp from the 23rd to the 29th of April 2027, is a leading event in the field of tunnel construction, underground building, and technology. Professionals from around the world gather to exchange knowledge, present innovations, and discuss the future of the tunnel industry. The event attracts experts, researchers, policymakers, and companies from various sectors, including civil engineering, construction, transportation, and infrastructure.

International Symposium
Cone Penetration Testing CPT '27
May 12 - 14 2027, Vancouver, Canada
www.cpt27.org

CPT'27, an International Symposium on Cone Penetration Testing will be held in Vancouver, Canada in 2027. Organized under the auspices of ISSMGE TC102, we hope to bring together industry leaders in industry, practice and research to share their knowledge and experience in cone testing across the globe.

XVIII DECGE Danube-European Conference on Geotechnical Engineering, 9–12 June 2027, Budapest, Hungary, https://18decge.hu/

11th European Conference on Numerical Methods in Geotechnical Engineering, 21 – 24 September 2027, Graz, Austria, www.tugraz.at/events/numge2027/home

16th International Congress on Rock Mechanics Innovations in Rock Mechanics and Rock Engineering for a Sustainable Future, 17-23 October 2027, Seoul, Korea, https://isrm2027.com

Eurock2028 -
Advances in rock mechanics and rock engineering to cope with increasingly extreme conditions - an ISRM Regional Symposium
25 - 30 Jun, 2028, Aix-en-Provence, France

"Connecting Continents Through Geotechnical Innovations"
04-08 September 2028, Istanbul, Turkey
https://zmgm.org.tr/en

Conference Topics

01 Modelling and Experimental Assessment of Geomaterials
02 Geohazards, Earthquakes and Risk Mitigation
03 Development of Resilient and Sustainable Geosystems
04 Geotechnical Construction and Soil Improvement
05 Geotechnical Engineering of Multiscale Observations, Sensors and Monitoring
06 Energy Geotechnologies
07 Technological Innovation
08 Geo Education, Standards And Codes

Contact

R. Duzceer
(President of Turkish National Society for ISSMGE)
irduzceer@gelisim.edu.tr

ΕΝΔΙΑΦΕΡΟΝΤΑ ΓΕΩΤΕΧΝΙΚΑ ΝΕΑ

Έργα υπογειοποίησης ηλεκτρικού σιδηροδρόμου στην Αθήνα το 1928

Γ' Σεπτεμβρίου και Μάρνη 1928. Έργα υπογειοποίησης ηλεκτρικού σιδηροδρόμου. Δεξιά διακρίνεται μεγάλης διαμέτρου αγωγός ομβρίων υδάτων. Η οδός Μάρνη (και όχι Μάρνης) ήταν ένας βαθύς χείμαρρος επάνω στον οποίο δημιουργήθηκε η ομώνυμη οδός. Αυτός είναι και ο λόγος που η Μάρνη δεν διασχίζει καθέτως τις οδούς από τις οποίες διέρχεται, αλλά τις τέμνει διαγωνίως, σύμφωνα με τον ρου του χειμάρρου.

Αλέξανδρος Γέροντας (facebook)

10 longest tunnels used by trains in the world

The Gotthard Base Tunnel in Switzerland is the longest railway tunnel at 57.1 km. Japan's Seikan Tunnel and the Channel Tunnel follow close behind. These long tunnels improve global rail connectivity efficiently

Gotthard Base Tunnel, Switzerland - 57.1 km

(Photograph: Wikimedia Commons)

The Gotthard Base Tunnel is the longest railway tunnel in the world, running 57.1 kilometres beneath the Swiss Alps. Opened in 2016, it connects northern and southern Europe, easing freight and passenger transport. High rock pressure and underground water were key challenges overcome with advanced engineering.

Seikan Tunnel, Japan - 53.85 km

(Photograph: Wikimedia Commons)

Connecting the islands of Honshu and Hokkaido, the Seikan Tunnel spans 53.85 km, with 23.3 km under the seabed. Opened in 1988, it's the longest undersea rail tunnel globally and serves both high-speed and regional trains.

Channel Tunnel, UK-France - 50.45 km

(Photograph: Wikimedia Commons)

The Channel Tunnel runs 50.45 km beneath the English Channel. Opened in 1994, it links Folkestone in the UK with Coquelles in France, facilitating passenger and cargo rail traffic through one of Europe's busiest transport corridors.

Yulhyeon Tunnel, South Korea - 50.3 km

Opened in 2016, Yulhyeon Tunnel is a 50.3 km double-track railway tunnel on the Seoul Metropolitan Subway. It is one of Asia's longest urban underground railway tunnels, handling high commuter traffic.

(Photograph: Wikimedia Commons)

Swiss Lötschberg Base Tunnel - 34.6 km

This tunnel in the Swiss Alps has a length of 34.6 km, serving the Lötschberg railway line since 2007. It is an important freight and passenger route enhancing transalpine transport.

New Guanjiao Tunnel, China - 32.7 km

(Photograph: Wikimedia Commons)

Located on the Qinghai Tibet Railway, it measures 32.7 km. Opened in 2014, it passes through mountain passes at high altitudes and helps connect Tibet to the Chinese railway network.

Songshan Lake Tunnel, China - 38.82 km

One of China's longest national railway tunnels, Songshan Lake Tunnel lies on the Guangzhou-Shenzhen railway and stretches 38.82 km. It started service in 2017, with six underground stations along its length.

(Photograph: Wikimedia Commons)

Pajares Base Tunnel, Spain - 24.67 km

(Photograph: Wikimedia Commons)

Pajares Base Tunnel links Asturias and León regions, facilitating high-speed rail traffic. Opened in 2023, it has improved connectivity in northern Spain.

Guadarrama Tunnel, Spain - 28.4 km

(Photograph: Wikimedia Commons)

Part of Spain's high-speed rail network since 2007, the Guadarrama Tunnel stretches 28.4 km beneath mountain ranges, supporting fast train services in the Madrid metropolitan area.

Taihang Tunnel, China - 27.8 km

Used since 2007 on the Shijiazhuang–Taiyuan high speed railway, Taihang Tunnel is 27.8 km and is one of the longest

in Chinese high-speed rail, reducing travel time across difficult terrain.

(Photograph: Wikimedia Commons)

(Abhinav Yadav / WION, Nov 09, 2025, 09:13 IST | Updated: Nov 09, 2025, 09:13 IST)

ଓ ଌ

THE BRUNEL MUSEUM THAMES TUNNEL

Monday 10 November 2025 is the 198th anniversary of an extraordinary dinner, held under the waters of the River Thames in the Thames Tunnel!

But it was by no means the only one...

Following her exciting discovery of a file of RSVPs sent to the Brunels in 1827, Museum volunteer Sue Thomas reveals a raft of new information about the (in)famous dinner, and others which followed it in the 1800s and again in 1997.

Read now on our blog: **https://vist.ly/4dm6x**

The Brunel Museum, Nov. 10, 2025

ଓ ଌ

The world's first EPB TBM

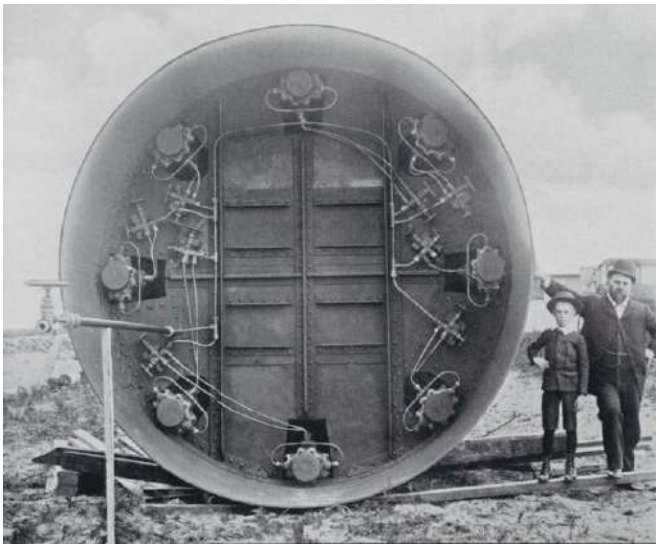

The photograph dates from 1894. The machine was designed by the British engineer James Henry Greathead (1844–1896) and was named "The Greathead Shield." It was based on the original idea of the French engineer Marc Isambard Brunel and on the patents of the British civil engineer Peter William Barlow.

It was used in the construction of a sewer tunnel in Melbourne, Australia, under the Yarra River. The shield had a diameter of 3.4 m, and its advancement was achieved through hydraulic jacks. As the shield moved forward, prefabricated cast-iron segments were installed in ring form and bolted together. Later, a 30 cm layer of concrete was cast behind the lining, forming the permanent tunnel structure.

The workers operated inside the shield under compressed air at a pressure of two to three atmospheres (bar). Unfortunately, during the night shift on April 12, 1895, a sudden inrush of water from the Yarra River flooded the tunnel, resulting in the drowning of one engineer and three workers. Three other workers, waiting in the pressurized chamber to enter the tunnel, were forced to watch helplessly through the chamber's window as their colleagues perished.

The project was later continued by another contractor and was completed 12 months later.

Georgios Milionis' Post LinkedIn

ΕΝΔΙΑΦΕΡΟΝΤΑ - ΣΕΙΣΜΟΙ & ΑΝΤΙΣΕΙΣΜΙΚΗ ΜΗΧΑΝΙΚΗ

What are the signs that nature is telling us?' Scientists are triggering earthquakes in the Alps to find out what happens before one hits

Researchers are deliberately setting off real (small) earthquakes to understand how to gauge the danger of a fault line before it breaks.

Researchers prepare to set off a small earthquake underneath the Alps. The results will help them understand how to better monitor fault lines. (Image credit: Bedretto Underground Laboratory for Geosciences and Geoenergies)

Scientists are deliberately triggering earthquakes from a tunnel deep beneath the Alps. Although it may sound like something out of a James Bond movie, the goal isn't turmoil and destruction. Rather, researchers with the Fault Activation and Earthquake Rupture (FEAR) project are looking for ways to determine the danger of an earthquake before it strikes.

Despite an increasing amount of monitoring on fault lines worldwide, researchers still don't understand the immediate triggers of earthquakes. Nor do they know why some ruptures happen on short segments of fault lines while others run for many miles, causing greater destruction. Right now, geoscientists are limited to studying these events only after they happen, Domenico Giardini, professor of seismology and geodynamics at ETH Zürich, told Live Science.

"What are the signs that nature is telling us?" Giardini said. "Invariably, they become clear after the quake, not before, so we are trying to understand much better how to see the signs."

That means they must trigger real earthquakes in controlled conditions with thousands of monitors right on a fault — not an easy prospect. But Giardini and his colleagues are taking advantage of the massive power of the Alps themselves. These mountains, on the border of Switzerland and Italy, are deeply faulted; the zigzagging networks of cracks beneath them are the legacy of millions of years of tectonics. Just the compressional force of the towering mountains above is enough to fracture the rocks 0.6 to 1.2 miles (1 to 2 kilometers) below the surface.

A researcher monitors data from the experiments. (Image credit: Bedretto Underground Laboratory for Geosciences and Geoenergies)

The rocks on the sides of these faults do occasionally slip, giving off mostly small quakes. Using a preexisting tunnel that was once used in the construction of a railway project, the FEAR project is getting up close and personal with one of these faults and pumping water into them to trigger it to release earthquakes on a convenient time schedule.

"They would have taken place sooner or later in the history of the Alps, but we make sure they happen next week," Giardini said.

The process is similar to what happens when oil and gas companies inject wastewater from wells into faulted areas in places like Oklahoma and Texas. This water lubricates the faults, thus reducing the friction required for them to rupture.

The difference is that Giardini and his team have a dense network of seismometers and accelerometers right on the fault, so they can measure exactly how it moves in response to this decrease in friction. The team has already triggered hundreds of thousands of quakes up to magnitude zero. (Because earthquakes are measured on a nonlinear, logarithmic scale, it's possible to have very small quakes with a magnitude of zero or even with negative magnitudes.)

Next week, the researchers will begin injecting hot water into the fault to see how temperature affects the evolution of an earthquake. And in March, Giardini said, they'll start triggering earthquakes up to magnitude 1.

The idea is that if they can figure out what parameters trigger a quake of a certain size — if they can, in essence, trigger a quake of whatever size they desire — they'll eventually be

able to measure a dangerous fault in the real world before it breaks and calculate the kinds of stresses needed to trigger a quake of a certain size on that fault.

"A couple years ago [in February 2023], there was a very large quake on the border between Syria and Turkey," Giardini said. "We know that fault will continue toward the south and toward the north. We want to try to understand, is the next quake going to be a 7 or an 8 or 8.5?"

Already, he said, certain parameters, like the amount of strain in the rocks outside the fault, are proving to be important. The researchers are also starting to understand more about how quakes jump from one fault to a neighboring fault.

"We are seeing examples that we produce ourselves underground that look very much like what happens in nature," Giardini said.

(Stephanie Pappas / , Nov. 3, 2025, https://www.livescience.com/planet-earth/earthquakes/what-are-the-signs-that-nature-is-telling-us-scientists-are-triggering-earthquakes-in-the-alps-to-find-out-what-happens-before-one-hits)

Cyprus records M5.3 earthquake with rare rapid aftershock clustering near Paphos

A shallow M5.3 earthquake struck near Paphos, Cyprus, at 16:23 LT (14:23 UTC) on November 12, 2025, producing a rare rapid aftershock cluster. More than 20 aftershocks were recorded within the first hours, including M3.9 and M4.3 events occurring five and ten minutes after the mainshock. By the morning of November 13, the total number of aftershocks had reached 50. The Geological Survey Department reported that the early activity rate and the presence of two closely spaced events were unusual for the region's modern instrumental record.

Earthquakes registered by EMSC in Cyprus from November 12 to 14, 2025. Credit: TW/SAM, Google

A shallow M5.3 earthquake struck near Paphos, western Cyprus, at 16:23 LT (14:23 UTC) on November 12, at a depth of 9 km (5.6 miles). The epicenter was located approximately 15 km (9.3 miles) north-northeast of Paphos (population ~35 900) and 56 km (35 miles) west-northwest of Limassol (population ~154 000).

Records show the region was already seismically active earlier that day, with an M5.2 event occurring at 09:31 UTC and an M4.7 at 09:41 UTC.

Within minutes of the M5.3 mainshock, the region experienced an unusually dense sequence of aftershocks. An M3.9 occurred five minutes after the main event, followed by an M4.3 at the ten-minute mark.

By 15:00 LT, more than 20 aftershocks had been recorded, and by the morning of November 13, the total number had reached 50. According to the Geological Survey Department of Cyprus (GSD), several of these aftershocks were felt in the wider Paphos district.

GSD reported that the sequence was atypical for Cyprus' modern instrumental period due to the speed and concentration of early aftershocks.

Earthquakes registered by EMSC in Cyprus from November 12 to 14, 2025. Credit: TW/SAM, Google

M5.3 earthquake in Cyprus on November 12, 2025. Credit: TW/SAM, Google

M5.3 earthquake in Cyprus on November 12, 2025. Credit: TW/SAM, Google

The department noted that waveform analysis indicated the presence of two closely spaced earthquakes within the main sequence, complicating the separation of individual events. This behaviour suggests a possible double-event source, in which rupture on one fault segment influences failure on an adjacent segment on short timescales.

The Paphos region is one of the most seismically active areas in Cyprus, located within the diffuse boundary between the African and Anatolian plates. Several active faults in western Cyprus are capable of generating moderate to strong crustal earthquakes, and shallow focal depths commonly result in locally strong shaking.

Historical records include multiple significant earthquakes in the broader region, such as the 1953 M6.5 event that caused extensive damage and fatalities, the 1995 M5.9 and 1996 M6.8 events, and the 2022 M6.6 earthquake.

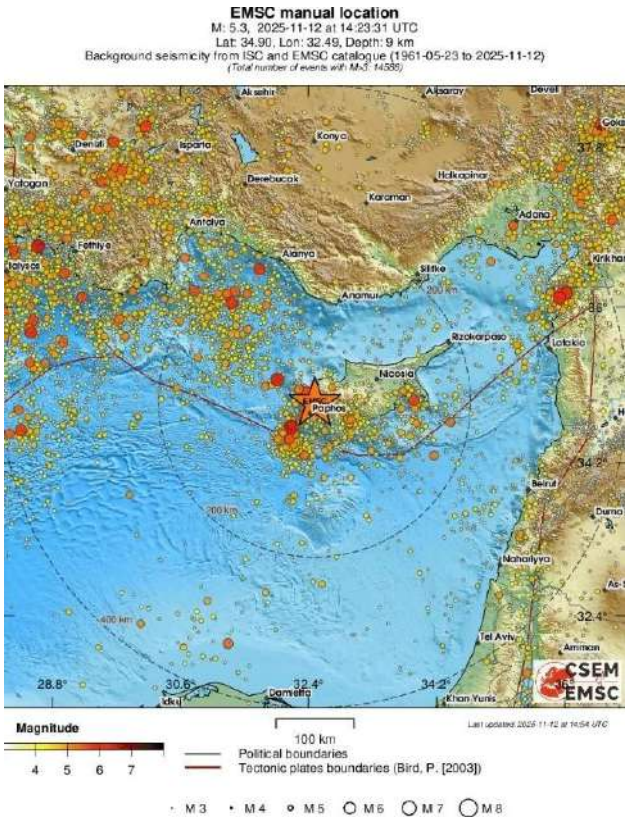

Image credit: EMSC

While multi-event sequences have occurred before, the rapid early clustering observed on November 12 is uncommon in the modern instrumental record.

Early reports show no major structural damage from the November 12 earthquake, though buildings in the Paphos district were temporarily evacuated as a precaution.

GSD stated that the aftershock activity appears to be gradually declining, but short-term forecasts remain uncertain.

(Teo Blašković / THE WATCHERS, Friday, November 14, 2025, https://watchers.news/2025/11/14/cyprus-records-m5-3-earthquake-with-rare-rapid-aftershock-clustering-near-paphos)

ΕΝΔΙΑΦΕΡΟΝΤΑ - ΓΕΩΛΟΓΙΑ

Breakup of ancient supercontinent Nuna created 'incubators' for complex life, study finds

Ancient supercontinent Nuna's breakup around 1.5 billion years ago set off a chain of events that made Earth more habitable, new research suggests.

Researchers already knew that complex life evolved during the Boring Billion, but the new research confirms the idea in unprecedented detail. (Image credit: Paige Mattsson - Videoccasions/Getty Images)

The breakup of the ancient supercontinent Nuna during Earth's "Boring Billion" years drastically shook up the planet, and the reshuffle may have created the conditions that gave rise to complex life, new research shows in unprecedented detail.

The Boring Billion refers to the period between 1.8 billion and 800 million years ago. Even though this interval encompassed the breakup and assembly of two ancient supercontinents, Nuna and Rodinia, scientists gave the period this name due to a perceived lack of upheaval.

"The term was coined to describe what appeared to be a long interval of geochemical, climatic, and biological stability in Earth's history," Dietmar Müller, a professor of geophysics at the University of Sydney who led the new research, told Live Science in an email. "However, we now know that this interval was less boring in terms of plate tectonics and evolutionary changes than previously thought."

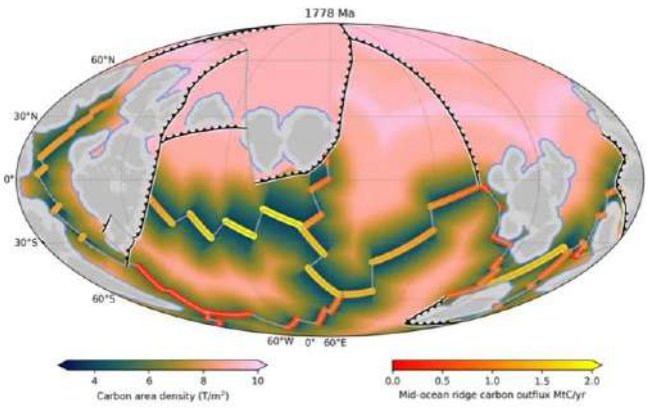

https://www.youtube.com/watch?v=tDPt3xRkiUI

Nuna's breakup set off a chain of events that made Earth more hospitable to life, according to a study published Oct. 27 in the journal Earth and Planetary Science Letters. As pieces of Nuna drifted away from the supercontinent's core, shallow seas mushroomed in the gaps between them that were more temperate and oxygen-rich than previous oceans had been, first-of-their-kind simulations revealed.

The researchers reconstructed tectonic-plate movements and related changes in carbon storage and emissions over the past 1.8 billion years, using a cutting-edge model they recently released. The novelty of the method lies in its ability to reconstruct carbon fluxes in greater detail than has been possible so far, the team wrote in the study.

Over the course of 350 million years during the Boring Billion, the total length of shallow seas around landmasses doubled to about 81,000 miles (130,000 kilometers), equivalent to more than three times Earth's circumference at the equator, the team found. At the same time, subduction zones — where one tectonic plate dives beneath another — shortened overall due to how the plates were shifting, according to the study.

Subduction zones trigger volcanic activity at the surface because they inject seawater that lowers the melting temperature of rocks into Earth's mantle, the layer that sits beneath the crust. This facilitates the formation of magma, which then rises into the crust and erupts from volcanoes along with debris and gases such as carbon dioxide (CO_2).

As subduction zones shortened, the amount of CO_2 escaping from Earth's interior into the atmosphere decreased. This cooled the planet and helped establish the oxygen-rich conditions in the newly formed shallow seas, and these relatively stable ecosystems gave rise to more complex life than had existed so far, the researchers suggested.

"We think these vast continental shelves and shallow seas were crucial ecological incubators," study co-author Juraj Farkaš, an associate professor in the School of Physics, Chemistry and Earth Sciences at the University of Adelaide in Australia, said in a statement. "They provided tectonically and geochemically stable marine environments with presumably elevated levels of nutrients and oxygen, which in turn were critical for more complex lifeforms to evolve and diversify on our planet."

Specifically, shallow seas may have sped up the diversification of eukaryotes — organisms whose cells have specialized structures called organelles and a membrane-bound nucleus that houses the DNA. All animals, plants and fungi are eukaryotes, so the emergence of eukaryotic cells during the Boring Billion was a key step in the evolution of complex life, the study authors proposed.

Researchers already knew that eukaryotes evolved during the Boring Billion thanks to fossil evidence dating to 1.05 billion years ago. But the conditions under which these organisms emerged remained unclear.

"The breakup of Nuna created a lot of new ocean floor in young ocean basins that previously did not exist," Müller explained. And this ocean floor contributed to the decline of atmospheric CO_2 already triggered by the shortening of subduction zones, he said. That's because when seawater seeps into cracks in the seabed, carbon gets stripped out to make limestone.

"This ocean floor was altered by hydrothermal fluid circulation and stored carbon in the form of carbonate cements in voids and fractures, drawing down atmospheric CO_2," Müller said.

In short, ancient supercontinent Nuna's breakup sparked three major changes that benefited complex life: It created shallow seas, diminished outgassing from volcanoes, and locked carbon away in ocean sediments, leading to a more oxygen-rich atmosphere and temperate conditions.

"The next steps will be to discover more well preserved eukaryote fossils to document their earliest evolution," Müller concluded.

(Sascha Pare / LIVESCIENCE, Nov. 10, 2025, https://www.livescience.com/planet-earth/geology/breakup-of-ancient-supercontinent-nuna-created-incubators-for-complex-life-study-finds)

ΕΝΔΙΑΦΕΡΟΝΤΑ - ΠΕΡΙΒΑΛΛΟΝ

Money and power underlie mysterious Andean 'band of holes'

The purpose of the pre-Hispanic Monte Sierpe site in Peru has long baffled researchers.

The Monte Sierpe site in Peru was probably used as a marketplace and a centre for tax collection. Credit: J. L. Bongers

The 'Band of Holes' in southern Peru is a 1.5-kilometre stretch of land dotted with thousands of carefully aligned holes that has puzzled researchers for decades. Now a team has found traces of crops and other plant material that suggest people might have filled the holes with bundles or baskets of goods. And drone images showed that the holes were organized in a pattern that resembled a khipu — a knotted-string device that the Inca used for accounting. That points to the Band as a marketplace and, later, an accounting device for recording tribute taxes under Inca rule. (Nature | 3 min read) (J. L. Bongers)

(J. L. Bongers / NATURE, 12 November 2025, https://www.nature.com/articles/d41586-025-03660-x)

Sink or swim? What will human migration look like as climate change impacts take hold

In this excerpt from "Sink or Swim," author Susannah Fisher explores the future of human migration, and what that will look like based on the difficult choices we make in the coming years.

What do we do when the worst impacts of climate change take hold? In this excerpt from "Sink or Swim: How the World Needs to Adapt to a Changing Climate" (Bloomsbury Sigma, 2025), author Susannah Fisher, who leads an international research program on climate adaptation at University College London, looks at the future of human migration. In it, she argues that as parts of the planet become uninhabitable, hard choices will need to be made to manage the movement of people — be it through organized relocation or sudden displacement. But what will these choices look like 45 years in the future?

Coastal erosion is accelerating as sea levels rise, resulting in the loss of homes and infrastructure. (Image credit: West-WindGraphics/Getty Images)

What does it look like to sink or swim?

Imagine it is 2070 and the world has battened down the hatches. People are moving in large numbers away from storms, droughts, floods and fires usually within their own countries and ending up in large displaced-people camps. The camps are in the middle of nowhere in some cases, or in huge areas of urban sprawl in others, with few amenities or avenues for support. The people struggle to make new lives but there is little left to go back for.

Those who try to move further hit up against heavily fortified internal or national borders with armed patrols. The humanitarian organizations do monthly drops of food and drinking water to the worst-affected areas, and the United Nations (U.N.) teaches communities about collecting rainwater and cooling their houses — but it is not enough.

Regional agreements allow people to move locally when disasters hit, but this does not help with the slow onset changes that have made life so hard. There are now two global political alliances that go beyond national borders — people living in the habitable zone and those outside it.

The U.S. has put up a border around the southwestern states that have run out of water to keep people out. The states have turned on each other as they fight for the last flows of the Colorado River. Those living in the "nonhab" zone increasingly do not bother with the U.N. or their own governments. Instead they strategize together on how to use technology such as solar geoengineering to reinvigorate their regions.

Cities in the habitable zone continue to lack people due to demographic shifts, but the process to migrate there is extensive and the local communities do not welcome "non-hab" applications.

Or another set of choices. A hurricane hits the coast of a small Caribbean country. The government had everything prepared — the early warning systems sounded and people went to the shelters before the storm ravaged the island. The day after the hurricane, the rapid attribution study is published and certified by the U.N., showing that the hurricane winds were made much more severe due to climate change.

The government issues a set of climate passports and people are able to choose from a set of countries to host them. These countries include historical carbon emitters that accept their responsibility for worsening the hurricane.

People can claim relocation grants from the fossil fuel companies, which were forced to pay out after a groundbreaking legal case. The storm was a scary one, and many people choose to go, taking the chance of a better life over the risk of another storm next month. The move might be temporary or longer-term but it buys people time to recover and continue their businesses, education or training while the rebuilding goes on.

Flooding risk in Bangladesh is increasing due to climate change. (Image credit: Michael Hall/Getty Images)

Over in Bangladesh, communities living in the delta are being hit again and again by cyclones and flooding. A young family decides they want more stability for the education of their children. They wanted to go to Dhaka but have heard it is crowded and still has flooding most monsoons. Instead, they apply to the U.N. displacement facility, where they hear about the secondary cities that have space for new migrants. They weigh up proximity to their family, the educational opportunities and the retraining on offer and decide on a small city with a vibrant cultural life. They enroll on a scheme of training for a new life in their chosen home. They are able to return regularly to family in their old neighborhood and live between the two locations.

In the U.K., a community of 400 families from a coastal area in Norfolk are settling into their new homes in the Peak District. The whole community, mostly low-income families with strong ties, were moved from a location where they were constantly at risk from floodwaters, storms and seeping damp into their houses. Many did not want to go, but a wilderness company wanted to buy their land to set up flooding tourism and adventure tours.

They applied to the government relocation scheme and developed a plan, mapping out what was important to them and how they would like to spend the money available. The community negotiated with the government agencies and finally a plan was agreed for all residents. Some are happy with the move, others have moved back close to the old land and take people on canoes past their old flooded homes.

In a small island developing state, the government has invested heavily in floating platforms and reclaiming land from the sea. This works for some islanders who have the money to buy the new properties and embrace the new way of life. They work hard on bringing new forms of tourism to the area through low-carbon transportation. Some islanders were not able to wait and moved away, with the support of the U.N. displacement facility.

These islanders send money back and remain citizens of their island home as well as their new country. They come back for cultural festivals and see themselves as belonging to the island as well as making new connections elsewhere. They call the country a "network nation" — linked to the sea and to many new areas of land and opportunity like spokes of a wheel.

These thought experiments raise vital questions that we as individuals, as communities and as voters need to consider. There are also choices for citizens in countries that could host migrants, and governments considering their interests in the regional or international system.

There is no single answer, and many choices have high political costs in the short term, but we will need to face up to these hard choices to find a way of living well under climate change.

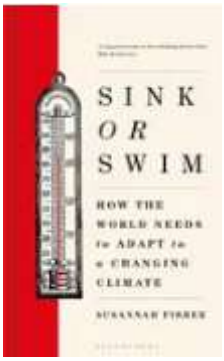

Sink or Swim: How the world needs to adapt to a changing climate

The world needs to adapt to climate change – but how? What are the key problems and hard choices that lie ahead for the global community? This book reveals all.

(Susannah Fisher / LIVESCIENCE, Nov. 4, 2025, https://www.livescience.com/planet-earth/climate-change/sink-or-swim-what-will-human-migration-look-like-as-climate-change-impacts-take-hold)

ΕΝΔΙΑΦΕΡΟΝΤΑ - ΛΟΙΠΑ

Θεοδόσης Τάσιος: «Στη χώρα μας έχουμε 30 συνώνυμα της λέξης "λάδωμα"»

Δείτε τον Θεοδόση Τάσιο να μιλάει στον Γιάννη Πανταζόπουλο και στο site 👉https://bit.ly/4mq6EQe

Ο ομότιμος καθηγητής του ΕΜΠ και ένας από τους σημαντικότερους στοχαστές της σύγχρονης Ελλάδας μιλάει ανοιχτά για τα μεγάλα αδιέξοδα και τα κακώς κείμενα της κοινωνίας μας.

Γιατί η διαπλοκή παραμένει διαχρονική πληγή στην Ελλάδα; Ποια είναι τα χαρακτηριστικά του νεοέλληνα σήμερα και τι συμβαίνει με του νέους; Πόσο κινδυνεύουν η δημιουργικότητα και η πνευματική ανεξαρτησία από την τεχνητή νοημοσύνη; Ο Θεοδόσης Τάσιος, ο σπουδαιότερος Έλληνας πολιτικός μηχανικός και ένας από τους μεγαλύτερους σύγχρονους διανοητές και φιλοσόφους, μας καλεί να δούμε τη χώρα και τον εαυτό μας με πιο καθαρό βλέμμα.

Με τον χαρακτηριστικά αιχμηρό και αιρετικό λόγο του μιλά για τη βαθιά ριζωμένη διαφθορά στην Ελλάδα και για τον λόγο που η χώρα παραμένει «ουραγός στην αξία του σεβασμού προς τον διπλανό». Εξηγεί γιατί η Αθήνα έχει μετατραπεί σε μια απέραντη τσιμεντούπολη, πώς βλέπει τη ζωή, τον θάνατο και τι θεωρεί πιο δύσκολο να αποδεχτεί μεγαλώνοντας. Αναφέρεται στον ρόλο που παίζει ο έρωτας στη ζωή μας και στη σημασία της διαρκούς προσωπικής μάχης, ακόμα κι όταν όλα μοιάζουν μάταια. Τέλος, παραμένει «αγωνιστικά απαισιόδοξος» και μας θυμίζει με φιλοσοφική απλότητα: «Έτσι κι αλλιώς, είμαστε αστρόσκονη».

Ο Θεοδόσης Τάσιος γεννήθηκε στην Καστοριά και μεγάλωσε στα Μέγαρα. Σπούδασε στο Εθνικό Μετσόβιο Πολυτεχνείο και στο Παρίσι. Ακαδημαϊκός και ομότιμος καθηγητής του ΕΜΠ σήμερα, παραμένει μια δεσπόζουσα προσωπικότητα στην επιστημονική και πνευματική μας ζωή.

Δημοσιογραφική επιμέλεια: Γιάννης Πανταζόπουλος
https://www.youtube.com/watch?v=hOi-mXrhGDM

How Did a Brand-New Bridge Collapse in China? Experts Blame Speed Over Safety

Yunnan bridge failure raises concerns about rushed construction and oversight gaps

Collapsed section of the Hongqi Bridge in Sichuan, China, seen on 11 November—just months after opening. A landslide triggered by slope failure caused the collapse, prompting renewed scrutiny of China's rapid infrastructure expansion. No casualties were reported. Screenshot from X

A section of the Hongqi Bridge in Sichuan province collapsed on 11 November 11, just months after opening, following a mountain slope failure that triggered a landslide. The bridge, part of National Highway 317 in Maerkang City, had shown signs of instability the day before, prompting emergency closures. While no casualties were reported, the incident has reignited concerns about the pace and oversight of China's infrastructure development.

Early Warning Signs and Emergency Response

On Monday afternoon, local authorities detected slope deformation on the right bank of the Hongqi Bridge. By 5:25 p.m., officials had identified potential risks and activated an emergency response. Teams from public security, transportation, and natural resources departments arrived on-site, evacuating stranded vehicles and installing warning signs to prevent unauthorised access.

Despite these precautions, the situation worsened rapidly. By Tuesday afternoon, the slope gave way, triggering a landslide that collapsed the bridge's approach section and roadbed. Videos posted online show bridge piers and decks crumbling amid clouds of smoke and dust.

A Bridge Built for Speed, Not Stability?

The Hongqi Bridge had only recently been completed in early 2025. Promotional materials from the contractor, Sichuan Road & Bridge Group, emphasised the project's scale and strategic importance in connecting China's heartland to Tibet. However, experts say the collapse reflects deeper issues in China's infrastructure model, particularly in the prioritisation of speed over safety.

In a 2024 peer-reviewed study published in MDPI, researchers Dina Tang and Minshui Huang of Wuhan Institute of Technology identified recurring vulnerabilities in Chinese bridge projects. These include rushed construction timelines, insufficient slope analysis, and inadequate geotechnical surveys—especially in mountainous regions like Sichuan, where terrain is complex and prone to geological shifts. The authors argue that long-term resilience is often sacrificed in favour of rapid delivery, increasing the risk of catastrophic failures in structurally sensitive zones (Tang & Huang, 2024).

Environmental Stressors and Hydropower Context

The bridge's proximity to the Shuangjiangkou Hydropower Station reservoir may have introduced environmental stressors such as fluctuating water levels, sedimentation, and terrain instability, which are factors that often complicate infrastructure resilience in mountainous regions.

The bridge was intended to enhance regional connectivity and economic development; its failure has raised questions about whether environmental risks were properly accounted for during planning and execution.

Public Reaction and Accountability

The collapse has unleashed a torrent of commentary across social media, where users have responded with sarcasm, scepticism, and satire. Posts range from quips like 'the bridge does that when it's nervous' and 'made of only the best tofu' to jabs at China's rapid development model, with one user remarking, 'everything looks futuristic when you strap colourful LED lights to it.' Others speculated wildly, joking about self-destruct features, ChatGPT engineers, and phantom bridge experts. Beneath the humour, however, runs a thread of public distrust. Many users are questioning whether speed and spectacle have overtaken safety and accountability in China's infrastructure boom.

Local authorities have yet to provide a timeline for reopening the highway. Detour routes have been announced, and investigations into the collapse are underway. Officials have not confirmed whether design flaws, construction errors, or environmental triggers were the primary cause.

A Pattern of Failures?

This incident adds to a growing list of infrastructure failures in China, including bridge collapses in Guangxi and Henan provinces. While each case has unique circumstances, experts warn that systemic issues such as rushed execution, limited oversight, and environmental neglect are recurring themes.

As China continues to expand its infrastructure footprint, the Hongqi Bridge collapse serves as a stark reminder that durability and safety must not be sacrificed for speed. Long-term resilience, especially in geologically sensitive regions, demands more than engineering ambition—it requires accountability, transparency, and time.

(Bernadette B. Tixon / INTERNATIONAL BUSINESS TIMES UK, 11 November 2025, https://www.ibtimes.co.uk/how-did-brand-new-bridge-collapse-china-experts-blame-speed-over-safety-1754244)

Γέφυρες στην Ελλάδα: Δεν ξέρουμε πόσες είναι – Ακόμη τις μετράμε

Η HuffPost ανοίγει έρευνα για τις γέφυρες στην Ελλάδα και κυρίως των αυτοκινήτων. Πόσες είναι; Ποιός ή ποιοι έχουν την ευθύνη τους; Πόσο ασφαλείς είναι; Ποιός φορέας τις ελέγχει; Τι καινούργια μέτρα λαμβάνονται;

Το φετινό περιστατικό στην Αχαΐα και το πολύ πρόσφατο στη Κίνα, μας αναγκάζει να βρούμε και να δημοσιεύσουμε τα όποια διαθέσιμα στοιχεία για τις γέφυρες στην Ελλάδα, που αφορά πάνω απ' όλα, την ασφάλεια των πολιτών. Στο πρώτο κεφάλαιο αναζητήσαμε αριθμούς. Πόσες γέφυρες υπάρχουν στην χώρα; Και πόσες, ειδικότερα, στην μεγαλύτερη Περιφέρεια, την Αττική; Η απάντηση είναι σοκαριστική. Και απόλυτα «ελληνική». Ξέρουμε κατ' εκτίμηση, αλλά όχι με ακρίβεια. Δεν υπάρχει ακόμη επίσημος "τελικός" αριθμός δημοσιευμένος.

Γιατί δεν υπάρχει "απόλυτος" αριθμός; Το κράτος υλοποιεί το Εθνικό Μητρώο Γεφυρών μέσα από το «Εθνικό Σύστημα Εποπτείας Γεφυρών», ώστε να καταγραφούν όλες οι γέφυρες και να βγαίνει ακριβής απογραφή. Ως έργο βρίσκεται σε φάση υλοποίησης/τροποποίησης και δεν έχει δοθεί δημοσίως πλήρης τελική καταμέτρηση. Πιο συγκεκριμένα:

Έναρξη έργου: 03/03/2025 **Λήξη έργου:** 02/11/2025

Γεωγραφική Περιοχή: Όλη η Ελλάδα

Φορέας Ευθύνης: ΥΠΟΥΡΓΕΙΟ ΨΗΦΙΑΚΗΣ ΔΙΑΚΥΒΕΡΝΗΣΗΣ

Φορέας Υλοποίησης: ΚΟΙΝΩΝΙΑ ΤΗΣ ΠΛΗΡΟΦΟΡΙΑΣ Μ.Α.Ε

Προϋπολογισμός Ταμείου: 400.200 €

Συνολικός Προϋπολογισμός: 496.248 €

Άρα λογικά πρέπει να είμαστε κοντά στον ακριβή αριθμό των γεφυρών. Προς το παρόν, οι καλύτερες δημόσιες εκτιμήσεις δείχνουν:

6.000 οδικές γέφυρες που περνούν οχήματα (με άνοιγμα >6 μ.). 3.000 σε αυτοκινητοδρόμους και >3.000 στο παλιό εθνικό/επαρχιακό δίκτυο. Πρόκειται για **εκτίμηση** που έχει διατυπωθεί δημόσια από περιφερειακούς φορείς με αναφορά σε εθνικά στοιχεία.

17.000 γέφυρες συνολικά στη χώρα (δρόμου + σιδηροδρομικές, πιθανώς και κάποιες πεζογέφυρες), σύμφωνα με μελέτες που επικαλούνται ο ΣΠΜΕ/διαΝΕΟσις και επαναλαμβάνονται σε πλήθος δημοσιευμάτων. Αυτός ο αριθμός δεν είναι μόνο για οδικές.

ΑΤΤΙΚΗ

Πόσες οδικές γέφυρες έχει η Αττική; Τεκμηριωμένο «ελάχιστο»: τουλάχιστον 254 απ' όπου περνούν οχήματα, αλλά ο πραγματικός αριθμός είναι υψηλότερος

Τι γνωρίζουμε με βεβαιότητα (χωρίς διπλομετρήσεις):

- Αττική Οδός: 100 οδικές άνω διαβάσεις + 25 κάτω διαβάσεις + 21 γέφυρες ρεμάτων = 146 οχηματοφόρες γέφυρες/τεχνικά στο δίκτυό της.

- Γέφυρες αρμοδιότητας Περιφέρειας Αττικής: Έγιναν βασικές επιθεωρήσεις σε 108 τεχνικά (άνω/κάτω διαβάσεις, οδικές γέφυρες) και συγκροτήθηκε μητρώο· πρόκειται για ξεχωριστό «καλάθι» από την Αττική Οδό.

Άλλα στοιχεία που «ανεβάζουν» τον πραγματικό αριθμό:

- Ολυμπία Οδός (Α8) και ΑΘΗΕ (Νέα Οδός) έχουν πρόσθετες γέφυρες μέσα στα διοικητικά όρια της Αττικής, αλλά δεν υπάρχει δημόσια ανάλυση/σπάσιμο ανά Περιφέρεια. Άρα δεν τις προσμετράμε στο «254», όμως πρέπει να συνυπολογιστούν για το πραγματικό σύνολο.

- Θεσμικά, όπως γράφουμε ανωτέρω, το Εθνικό Σύστημα Εποπτείας Γεφυρών (Εθνικό Μητρώο) βρίσκεται σε εξέλιξη. Αναμένουμε το πότε θα δημοσιευθούν πλήρη στοιχεία.

- Το 2025 μεταφέρθηκαν στην Περιφέρεια αρμοδιότητες για 108 «αδέσποτες» γέφυρες στην Αττική, γεγονός που δείχνει ότι η καταγραφή/ιδιοκτησία ακόμη τακτοποιείται.

ΘΕΣΣΑΛΟΝΙΚΗ

Από τις 3 Νοεμβρίου 2025, η Περιφέρεια Κεντρικής Μακεδονίας ξεκίνησε επίσημη απογραφή και τεχνική αξιολόγηση όλων των γεφυρών της, ώστε να ενταχθούν στο Εθνικό Μητρώο Γεφυρών. Μέχρι να ολοκληρωθεί, δεν υπάρχει αριθμός «τελικός» ανά Π.Ε. (όπως Θεσσαλονίκης). Τι ξέρουμε σήμερα (τεκμηριωμένα):

- Η ΠΚΜ εγκατέστησε συστήματα μόνιμης παρακολούθησης σε 16 σημεία και «τρέχει» την καταγραφή σε οδικό και σιδηροδρομικό δίκτυο της Κεντρικής Μακεδονίας (μέρος των οποίων στη Θεσσαλονίκη). Αυτό αποδεικνύει την εξέλιξη του καταλόγου, αλλά όχι το συνολικό πλήθος.

- Ο Δήμος Θεσσαλονίκης δηλώνει αρμοδιότητα ελέγχου/συντήρησης για γέφυρες & πεζογέφυρες στο δημοτικό οδικό δίκτυο, αλλά δεν δημοσιεύει αριθμό.

ΑΝ.ΜΑΚΕΔΟΝΙΑ – ΘΡΑΚΗ

Σε αυτή την χρονική στιγμή, δεν υπάρχει ανοιχτά διαθέσιμος συνολικός αριθμός οδικών γεφυρών της ΠΑΜΘ. Η Περιφέρεια «τρέχει» καταγραφή στο Εθνικό Μητρώο Γεφυρών και εντάσσεται στο εθνικό σύστημα εποπτείας. Ως σαφώς τεκμηριωμένο υποσύνολο, έχουν ονομαστικά προτεραιοποιηθεί 20 γέφυρες για αισθητήρες/real-time monitoring.

ΔΥΤΙΚΗ ΜΑΚΕΔΟΝΙΑ

Τι ξέρουμε με βεβαιότητα για τις εκεί γέφυρες, αν και στην ουσία δεν ξέρουμε, όχι πολλά, αλλά ίσως και… τίποτα!

- Σε εξέλιξη η απογραφή στην ΠΔΜ: Η Περιφέρεια έχει επίσημα δρομολογήσει Μητρώο Γεφυρών για το εθνικό και επαρχιακό δίκτυο της Δυτικής Μακεδονίας.

- Συμβάσεις "Έξυπνων Γεφυρών": Υπάρχει εκτελεστική σύμβαση ΤΕΕ για το υποέργο «Θεσσαλίας, Δυτικής Μακεδονίας & Νοτίου Αιγαίου», στο πλαίσιο του εθνικού προγράμματος.

- Αριθμός υποσυνόλου – 16 γέφυρες: Δημοσιευμένη ονομαστική λίστα για τη Δυτική Μακεδονία αναφέρει 16 γέφυρες που καλωδιώνονται με αισθητήρες (ενδεικτικά: γέφυρες στον Αλιάκμονα, Ρύμνιο, κόμβους Κοζάνης–Φλώρινας κ.ά.). Πρόκειται για υποσύνολο και όχι για το σύνολο των οδικών γεφυρών της Περιφέρειας.

ΠΕΛΟΠΟΝΝΗΣΟΣ

Πόσες οδικές γέφυρες έχει η Περιφέρεια Πελοποννήσου; Τεκμηριωμένο «ελάχιστο»: 341 γέφυρες (μήκος >6 μ.) στο εθνικό & επαρχιακό οδικό δίκτυο. Πιό συγκεκριμένα, στις 18 Απριλίου 2022 ολοκληρώθηκε και διαβιβάστηκε στην Περιφέρεια το μητρώο γεφυρών που εκπόνησε το ΤΕΕ. Με βάση αυτό, καταγράφηκαν 341 οδικές γέφυρες με άνοιγμα πάνω από 6 μέτρα στο εθνικό και επαρχιακό οδικό της Πελοποννήσου.

Ανά Περιφερειακή Ενότητα (Π.Ε.)

- Αργολίδα: 82
- Αρκαδία: 59
- Κορινθία: 44
- Λακωνία: 79
- Μεσσηνία: 77

ΔΥΤΙΚΗ ΕΛΛΑΔΑ

Σήμερα το ακριβές "πόσες" γέφυρες για τη Δυτική Ελλάδα, δεν έχει δημοσιευθεί επίσημα. Τεκμηριωμένο ελάχιστο για το ρεπορτάζ: 20 γέφυρες ήδη ενταγμένες σε μόνιμη παρακολούθηση (smart), ενώ η ευρεία απογραφή όλων των οδικών γεφυρών (>6 μ.) είναι σε εξέλιξη.

ΗΠΕΙΡΟΣ

Η Ήπειρος έχει πυκνό δίκτυο οδικών γεφυρών (εθνικό, επαρχιακό, αυτοκινητόδρομοι όπως η Εγνατία), όμως η ακριβής απογραφή «όσων φέρουν οχήματα» θα προκύψει όταν ολοκληρωθεί και δημοσιοποιηθεί το Εθνικό Μητρώο Γεφυρών.

ΚΕΝΤΡΙΚΗ ΕΛΛΑΔΑ

Στις 26 Αυγούστου 2025 η Περιφέρεια Στερεάς Ελλάδας ανακοίνωσε ονομαστικά 21 σημεία (οδικές γέφυρες σε Βοιωτία, Εύβοια, Φθιώτιδα, Φωκίδα, Ευρυτανία) όπου εγκαθίσταται RT-SHM. Αυτό είναι το υποσύνολο, γιατί ο συνολικός αριθμός οδικών γεφυρών θα προκύψει από το Εθνικό Μητρώο Γεφυρών όταν δημοσιευθούν τα πλήρη στοιχεία. Προς το παρόν, πιό αναλυτικά, ξέρουμε με βεβαιότητα τα εξής:

- 21 "έξυπνες" γέφυρες: επίσημη λίστα της Περιφέρειας (π.χ. Βασιλικό–Λήλας, Καστέλλα–Μεσσάπιος, Κορίνθου–Νηλέας, Οξύλιθος–Μανικιάτης, Σπερχειός, Δελφών, Τατάρνα κ.ά.).

- Κλίμακα εξοπλισμού: η σύμβαση του ΤΕΕ για το υποέργο «Έξυπνες Γέφυρες… Πελοποννήσου, Στερεάς Ελλάδας κ.ά.» προβλέπει για τη Στερεά 42 καταγραφικούς σταθμούς, 252 μετρητές παραμόρφωσης, 42 επιταχυνσιόμετρα και έως 10 αισθητήρες στάθμης υδάτων που τροφοδοτούν ενιαία πλατφόρμα. (Δείκτης μεγέθους, όχι συνολική καταμέτρηση γεφυρών)

ΚΡΗΤΗ

Πόσες οδικές γέφυρες έχει η Περιφέρεια Κρήτης; Ούτε και εδώ έχουμε ακριβή απάντηση του δεδομένου ότι δεν έχει δημοσιευτεί ακόμη πλήρης, επίσημη καταμέτρηση. Η απογραφή τρέχει κεντρικά μέσω του Εθνικού Μητρώου Γεφυρών/Εθνικού Συστήματος Εποπτείας Γεφυρών. Όταν ανοίξουν τα συγ-

κεντρωτικά δεδομένα ανά Περιφέρεια θα υπάρξει ακριβής αριθμός για την Κρήτη. Δεν παύει, όμως, να ξέρουμε μερικά πολύ χρήσιμα στοιχεία

- 18 «έξυπνες» γέφυρες ήδη επιλεγμένες για RT-SHM στην Κρήτη (πρώτη φάση εγκαταστάσεων). Ενδεικτικά: Ταυρωνίτης, χαραδρογέφυρες Ρεθύμνου, Αράδαινας, Παλαιόκαστρου, Παντάνασσας, Γιόφυρου, Καρτερού, Χαμεζίου κ.ά.

- Η Περιφέρεια αναφέρει ότι οι 18 θα γίνουν 27 με επέκταση της σύμβασης, με κατανομή 11 στον ΒΟΑΚ και 7 στο επαρχιακό δίκτυο (Πόμπια, Αναποδάρης, Πέραμα, Ροδάκινο, Πλεμενιανά, Καλλιθέρα, Αράδαινα).

- Σε επίσημο έγγραφο της Π.Κ. ορίζεται ότι μέγιστος αριθμός γεφυρών που μπορεί να προτείνει η Κρήτη στο πρόγραμμα είναι 36 (όριο προτάσεων του έργου «Έξυπνες Γέφυρες», όχι σύνολο γεφυρών στην Κρήτη).

- Παράλληλα «τρέχουν» επισκευές σε 11 γέφυρες του ΒΟΑΚ (Ηρακλείου–Ρεθύμνου), ένδειξη του μεγέθους του αποθέματος τεχνικών – αλλά και αυτό είναι υποσύνολο.

(*HUFFPOT* / ΔΗΜΟΣΙΟΓΡΑΦΙΚΗ ΕΠΙΜΕΛΕΙΑ: ΤΕΡΕΝΣ ΚΟΥΙΚ, 13 Νοεμβρίου 2025, https://www.huffingtonpost.gr/kinonia/gefyres-stin-ellada-den-xeroume-poses-einai-akomatis-metrame/

Δεν γίνονται έλεγχοι δομικών έργων

Ο Ιάπωνας Γιοσινόρι Μοριγουάκι κατήγγειλε την Τουρκία για την έλλειψη μέτρων ασφαλείας προκειμένου να προστατευτεί από επικείμενο μεγάλο σεισμό

Ο Ιάπωνας Γιοσινόρι Μοριγουάκι δεν δίστασε να μιλήσει στη σκληρή γλώσσα της αλήθειας για το **σεισμικό κίνδυνο** που υπάρχει στην **Τουρκία** και το Αιγαίο, σε συνέδριο που διοργανώθηκε από τη Σχολή Επιστημών Υγείας του Πανεπιστημίου Σελτσούκ. Ο ειδικός σεισμολόγος είπε ότι ζει 35 χρόνια στην Τουρκία και τα λόγια του σε ό,τι αφορά τα μέτρα ασφάλειας που λαμβάνουν στη χώρα για να προστατευτούν από τα ρήγματα, είναι ωμά. "Με λύπη το λέω: σε απώλειες ζωών, **η Τουρκία είναι στην τρίτη θέση παγκοσμίως**. Πρέπει να ντραπούμε και να το διορθώσουμε αυτό. Γι' αυτό είμαι 35 χρόνια στην Τουρκία", ήταν μια χαρακτηριστική δήλωσή του.

Ο Μοριγουάκι έχει εντοπίσει μέρος του προβλήματος στα αυθαίρετα, αλλά και στην έλλειψη ελέγχου δομικών έργων. Ο νόμος περί Ελέγχου μετράει 24 χρόνια, ωστόσο ο Ιάπωνας σεισμολόγος ισχυρίζεται: "Υπάρχουν επαρχίες που, ενώ είναι ζώνες πρώτου βαθμού σεισμικής επικινδυνότητας, μέχρι σήμερα δεν έχει πραγματοποιηθεί έλεγχος δομικών έργων". Επιπλέον, αναφέρει ότι σε ποσοστό περισσότερο του 50%, τα κτίρια στη χώρα είναι αυθαίρετα: "**Το 50% του κτιριακού αποθέματος της Τουρκίας, το οποίο ξεπερνά τα 21 εκατομμύρια κτίρια, είναι αυθαίρετα**".

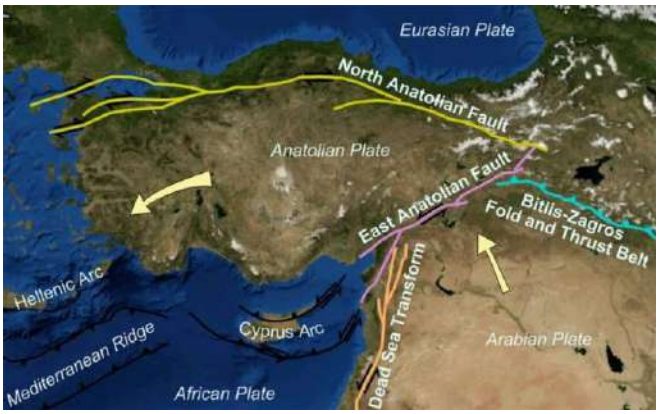

Ο Ιάπωνας σεισμολόγος μπορεί να μίλησε εξαιτίας **των σεισμών στο Μπαλικεσίρ**, ωστόσο τόνισε ότι "δεν περιμένω μεγάλο σεισμό εκεί". Αντιθέτως, "κόκκινο συναγερμό" βάρεσε για δύο πόλεις: την Μπαντίρμα και την Προύσα. Η πρώτη είναι... γειτονάκι του **Αιγαίου**, το οποίο ο Μοριγουάκι έφερε "στην κορυφή του κινδύνου. Τα ρήγματα εκεί συμπυκνώνουν ένα "δίκτυο" το οποίο καθιστά την κατάσταση περίπλοκη. Όπως είναι η Τουρκία, τουλάχιστον σε σχέση με την Ιαπωνία. "Η Τουρκία και η Ιαπωνία έχουν παρόμοια χαρακτηριστικά όσον αφορά τους σεισμούς. **Η Ιαπωνία έχει 4 σεισμικές πλάκες, η Τουρκία έχει 6**. Η Τουρκία είναι πιο πολύπλοκη". Σε ό,τι αφορά το ρήγμα της Βόρειας Ανατολίας, είπε ότι είναι από τα πιο μεγάλα στον πλανήτη.

Σε ό,τι αφορά τις ασφαλείς πόλεις, μίλησε για τη γειτόνισσα της Θράκης, δηλαδή το Κιρκλαρελί, το Ικόνιο -παρά τους μικροσεισμούς που σημειώθηκαν, τη Νίγδη και την Καραμάν. Ωστόσο, εξαίρεσε τη Σαμψούντα από τον Εύξεινο Πόντο, τον οποίο επίσης χαρακτήρισε περιοχή χαμηλότερου κινδύνου.

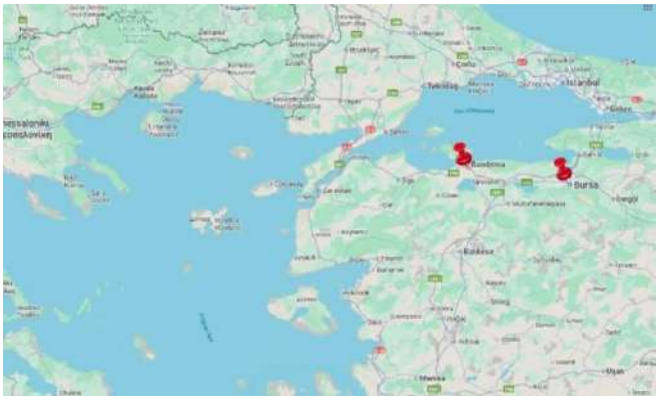

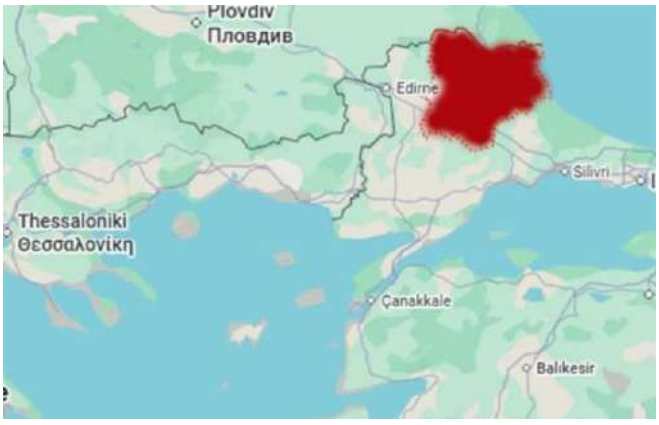

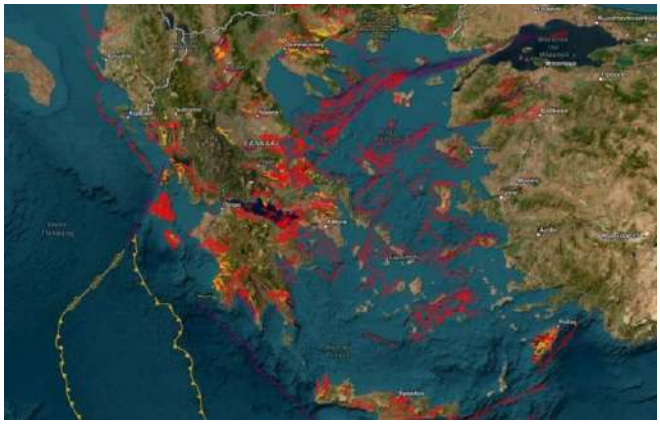

(Parapolitika Newsroom, 27.11.2025, https://www.parapolitika.gr/diethni/article/1645560/kokkinos-sunagermos-apo-iapona-seismologo-stin-tourkia-to-aigaio-kinduneuei-au-thaireta-21-ekatommuria-ktiria-hartes/)

Εφαρμογές οπλισμένου σκυροδέματος σε κτήρια της Κρήτης

Κώστας Κάπος (facebook)

ΝΕΕΣ ΕΚΔΟΣΕΙΣ ΣΤΙΣ ΓΕΩΤΕΧΝΙΚΕΣ ΕΠΙΣΤΗΜΕΣ

Microtunnelling and Auger Boring

Publication no: ATS-4541-25

Austroads Technical Specification ATS 4541 sets out the requirements for the installation of pipes by Microtunnelling or Auger Boring, which are types of trenchless technology that are launched from an excavated pit. The pipes may be for the purpose of moving fluids or gases or for the protection of telecommunications/electrical cables.

PDF (free) Download

(Austroads, 26 November 2025)

ΗΛΕΚΤΡΟΝΙΚΑ ΠΕΡΙΟΔΙΚΑ

INTERNATIONAL JOURNAL OF GEOENGINEERING CASE HISTORIES

An official journal of the International Society for Soil Mechanics and Geotechnical Engineering

NEW ISSUE PUBLISHED

Special Issue on Environmental Geotechnics by ISSMGE TC215 Published

The Case Histories Journal is pleased to announce the Special Issue #3 of Volume #8 of the International Journal of Geoengineering Case Histories, an official Journal of the International Society for Soil Mechanics and Geotechnical Engineering (ISSMGE).

This Special Issue of the ISSMGE International Journal of Geoengineering Case Histories, edited by Guest Editor Prof. Andrea Dominijanni, ISSMGE TC215 Chair, focuses on the broader area of environmental geotechnics and soil behavior. Originally envisioned as an opportunity to publish case histories presented at the 9th International Congress on Environmental Geotechnics, held in Chania, Crete, on June 2528, 2023, the issue was later expanded through a public call for papers to include contributions addressing soil behavior issues associated with the built environment.

Papers published in this refereed journal are freely available in color and are accompanied by databases that include the electronic data presented in the paper as well as additional figures (as necessary). The locations of the case histories are also positioned in the IJGCH Geographic Database.

The contents of the Special Issue and direct access to the papers are provided below.

On behalf of the Case Histories Journal,
Dimitrios Zekkos, University of California at Berkeley,
Editor-in-Chief

Volume 8, Issue 3 - Table of Contents

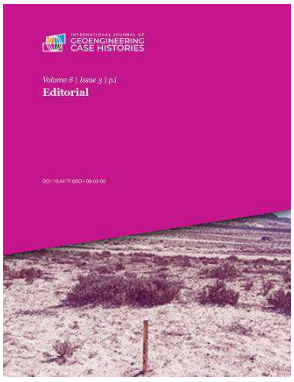

Editorial Andrea Dominijanni ; Dimitrios Zekkos

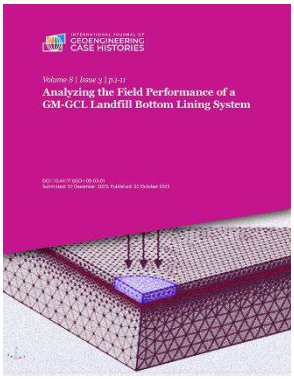

Analyzing the Field Performance of a GM-GCL Landfill Bottom Lining System Leslie Okine ; Poyu Zhang ; Tarek Abichou ; Jiannan Chen

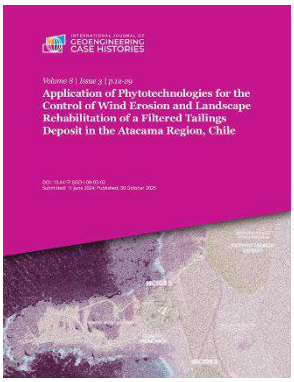

Application of Phytotechnologies for the Control of Wind Erosion and Landscape Rehabilitation of a Filtered Tailings Deposit in the Atacama Region, Chile Pamela Valenzuela ; Juan Palma ; Osvaldo Moreno ; Claudia Ortiz ; Claudio Masson

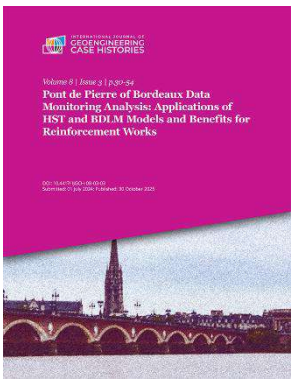

Pont de Pierre of Bordeaux Data Monitoring Analysis: Applications of HST and BDLM Models and Benefits for Reinforcement Works Gilles Valdeyron

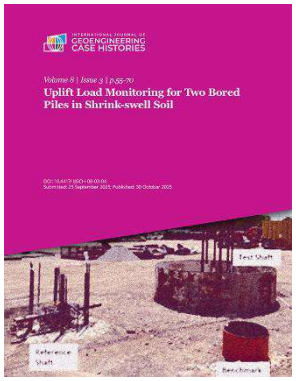

Uplift Load Monitoring for Two Bored Piles in Shrink-swell Soil Jean-Louis Briaud ; Jerome Sfeir

View Issue in Volume

INTERNATIONAL GEOSYNTHETICS SOCIETY

November 2025

Helping the world understand the value and appropriate use of geosynthetics

IGS Geosynthetics Handbook Available To Buy Now

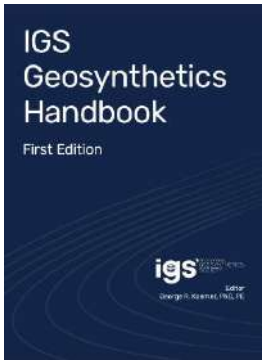

The long-awaited **IGS Geosynthetics Handbook** is now available to buy. A one-stop technical reference guide suitable for all levels of experience in geosynthetics. The handbook offers a concise yet comprehensive summary of the fundamental applications of geosynthetics and is an essential reference guide for student, instructor or civil engineering professional alike.

Non member price: $200 USD
Member price: $150 USD

IGS Chapters can access a bulk buy discount of 30 copies or more at $75 USD per copy, for this option only, contact igssec@geosyntheticssociety.org.

Get Your Handbook Today

Call for Candidates

Nominations are now open to elect the next IGS President, Vice President and 10 Council Members.

Could you be part of the next leadership team to further the Society's mission and goals? These important positions need dedicated members looking to take the next step in their industry journey by playing a leading role in one of the most prestigious membership organizations in geosynthetics.

Nominations must be sent to IGS Secretariat Manager Elise Oatman at igssec@geosyntheticssociety.org by December 31, 2025. Candidates can nominate themselves – no proposer or seconder is needed – and current IGS Council members can reapply.

"Serving on the IGS Council is inspiring because it allows us to look at geosynthetics in 360 degrees and turn that broader view into action. This role helps to grow awareness and foster cooperation between practitioners, researchers, and stakeholders worldwide." - Giulia Lugli, IGS Council Member

IGS at Industry Events

We attended Tailings & Mine Waste in Canada (2–5 Nov 2025). Where we were joined by Premium Corporate Member representatives, Macaferri, TRI Environmental and Strata Global. Thank you to our Premium Corporate Members for supporting the IGS in attending these insightful events and helping us expand awareness of how geosynthetics contribute to resilient and sustainable infrastructure. We are currently confirming which 2026 industry events we will be attending and look forward to sharing that update soon.

IGS Chapter News

Welcome to IGS Iraq!

Led by Professor Mahdi Karkush, President of the Iraqi Scientific Geotechnical Society, the new Chapter was formally approved by the IGS Council at the recent EuroGeo8 conference in September following around two years of development. Learn more about IGS Iraq and read a 10 Questions with the IGS Iraq President.



My Engineer Life With Ness Di Battista

Read Ness's story to discover how a passion for geosynthetics engineering led her from mining sites to Antarctic research, and even influences how she bakes her pies. Read the full the interview on our website.

A Look Back at our Interview with IGS Panama

A revitalized IGS Panama launched last year with greater foci on student engagement, sustainability and technical expertise, with strategic plans shared by Chapter Secretary Ken-

neth Thompson in a revealing Q&A. Read the full interview on our website.

Call for IGS Awards - Coming Soon!

Next month we will be putting out a call for nominations for the IGS Awards to recognize the achievements completed between January 1 2022- December 31 2025.

Why does diversity matter in geosynthetics?

In this new interview, IGS President Samuel Allen joins Jabulile Msiza from the IGS Diversity Committee (DEI) to reflect on how inclusion is shaping the future of our profession and the global work of the IGS. Watch the full interview on YouTube. If you missed it, you can read about the EuroGeo8 DE&I session delivered by Daniela Felletti.

Upcoming Events

Explore the upcoming IGS events, industry events we will be attending and events delivered by IGS Chapters.

04–06 Feb 2026 ASTM D35 Meeting Atlanta, Georgia, USA

Committee meeting on geosynthetics standards, useful for practitioners involved in test methods and specifications. Event page

30 Jun–02 Jul 2026 CEN TC 189 Meetings Copenhagen, Denmark

European standards committee meetings on geosynthetics, relevant for European practitioners and manufacturers. Event page

13–17 Sep 2026 13th International Conference on Geosynthetics Montreal, Canada

The conference theme, **"Legacy, Evolution & Revolution in Geosynthetics,"** emphasizes innovation, sustainability, and global collaboration. Scheduled at the Palais des congrès de Montréal, attendees can access technical sessions, workshops, and networking opportunities. Event page

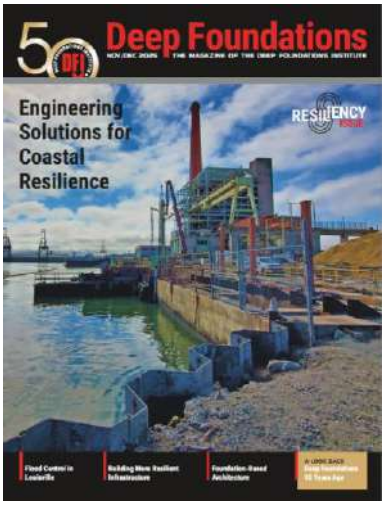

Highlights of the Nov/Dec Issue
https://mailchi.mp/dfi/dfi-enews-august-10985483?e=c89e58da1f

This is a special issue on Resiliency. From landslides to high tides and everything in between, the deep foundation industry is increasingly on the front line when it comes to defense against as well as recovery from environmental changes. This special issue highlights what the industry can offer in response to the ever-increasing threats of climate change, seismic activity and geohazards.

Cover Story: Engineering Solutions for Coastal Resilience in San Francisco Bay

Defense Against Rising Waters: A New Era for Louisville's Flood Control

Building the Foundations of Resilience

Foundation-Based Architecture: A New Approach for Realizing Infrastructure From the Ground Up

A Look Back: A Vision for the Future of Foundation Engineering and Construction

Member Profile: Ramin Motamed, Ph.D., P.E., Prolific Teacher, Researcher, Author, Presenter

Foundations for a Sustainable Future: Sustainability and Resiliency: Alike but Different

Legally Speaking: Sustainable Design and Construction Legal Framework and Issues

ΕΚΤΕΛΕΣΤΙΚΗ ΕΠΙΤΡΟΠΗ ΕΕΕΕΓΜ (2023 – 2026)

Πρόεδρος	:	Μιχάλης ΜΠΑΡΔΑΝΗΣ, Δρ. Πολιτικός Μηχανικός, ΕΔΑΦΟΣ ΣΥΜΒΟΥΛΟΙ ΜΗΧΑΝΙΚΟΙ Α.Ε. mbardanis@edafos.gr, lab@edafos.gr
Α' Αντιπρόεδρος	:	Σταυρούλα ΚΟΝΤΟΕ, Δρ. Πολιτικός Μηχανικός, Αναπληρώτρια Καθηγήτρια Τμήμα Πολιτικών Μηχανικών Πανεπιστήμιο Πατρών skontoe@upatras.gr
Β' Αντιπρόεδρος	:	Νίκος ΚΛΗΜΗΣ, Δρ. Πολιτικός Μηχανικός, Καθηγητής Τμήμα Πολιτικών Μηχανικών, Πολυτεχνική Σχολή, Δημοκρίτειο Πανεπιστήμιο Θράκης nklimis@civil.duth.gr, nsklimis@gmail.com
Γενικός Γραμματέας	:	Γιώργος ΜΠΕΛΟΚΑΣ, Δρ. Πολιτικός Μηχανικός, Επίκουρος Καθηγητής Τμήμα Πολιτικών Μηχανικών Σχολή Μηχανικών Πανεπιστημίου Δυτικής Αττικής gbelokas@uniwa.gr, gbelokas@gmail.com
Ταμίας	:	Χρήστος ΣΤΡΑΤΑΚΟΣ, Πολιτικός Μηχανικός, NAMALAB Α.Ε. stratakos@namalab.gr
Έφορος	:	Τάσος ΑΝΑΣΤΑΣΙΑΔΗΣ, Δρ. Πολιτικός Μηχανικός, Καθηγητής Τμήμα Πολιτικών Μηχανικών Αριστοτελείου Πανεπιστημίου Θεσσαλονίκης anas@civil.auth.gr
Μέλη	:	Γιώργος ΝΤΟΥΛΗΣ, Πολιτικός Μηχανικός, ΕΔΑΦΟΜΗΧΑΝΙΚΗ Α.Ε.- ΓΕΩΤΕΧΝΙΚΕΣ ΜΕΛΕΤΕΣ Α.Ε. gdoulis@edafomichaniki.gr
		Μαρίνα ΠΑΝΤΑΖΙΔΟΥ, Δρ. Πολιτικός Μηχανικός, Αναπληρώτρια Καθηγήτρια Σχολή Πολιτικών Μηχανικών Ε.Μ.Π. mpanta@central.ntua.gr
		Χρήστος ΤΣΑΤΣΑΝΙΦΟΣ, Δρ. Πολιτικός Μηχανικός, ΠΑΝΓΑΙΑ ΣΥΜΒΟΥΛΟΙ ΜΗΧΑΝΙΚΟΙ Ε.Π.Ε. editor@hssmge.gr, ctsatsanifos@pangaea.gr
Αναπληρωματικά Μέλη	:	Γιάννης ΖΕΥΓΩΛΗΣ, Δρ. Μηχανικός Μεταλλείων - Μεταλλουργός, Αναπληρωτής Καθηγητής Σχολή Μεταλλειολόγων - Μεταλλουργών Μηχανικών ΕΜΠ izevgolis@metal.ntua.gr Δημήτρης ΠΙΤΙΛΑΚΗΣ, Δρ. Πολιτικός Μηχανικός, Αναπληρωτής Καθηγητής Τμήμα Πολιτικών Μηχανικών Αριστοτελείου Πανεπιστημίου Θεσσαλονίκης dpitilakis@civil.auth.gr Χάρης ΛΑΜΑΡΗΣ, Πολιτικός Μηχανικός, ΧΑΡΗΣ Π. ΛΑΜΑΡΗΣ ΚΑΙ ΣΥΝΕΡΓΑΤΕΣ ΙΚΕ h.lamaris@lamaris.gr Πρόδρομος ΨΑΡΡΟΠΟΥΛΟΣ, Δρ. Πολιτικός Μηχανικός prod@central.ntua.gr
Εκδότης	:	Χρήστος ΤΣΑΤΣΑΝΙΦΟΣ, Δρ. Πολιτικός Μηχανικός, ΠΑΝΓΑΙΑ ΣΥΜΒΟΥΛΟΙ ΜΗΧΑΝΙΚΟΙ Ε.Π.Ε. editor@hssmge.gr, ctsatsanifos@pangaea.gr

ΕΕΕΕΓΜ

Τομέας Γεωτεχνικής
ΣΧΟΛΗ ΠΟΛΙΤΙΚΩΝ ΜΗΧΑΝΙΚΩΝ
ΕΘΝΙΚΟΥ ΜΕΤΣΟΒΙΟΥ ΠΟΛΥΤΕΧΝΕΙΟΥ
Πολυτεχνειούπολη Ζωγράφου
15780 ΖΩΓΡΑΦΟΥ

Τηλ. 210.7723434
Τοτ. 210.7723428
Ηλ-Δι. secretariat@hssmge.gr ,
geotech@central.ntua.gr
Ιστοσελίδα www.hssmge.org (υπό κατασκευή)

«ΤΑ ΝΕΑ ΤΗΣ ΕΕΕΕΓΜ» Εκδότης: Χρήστος Τσατσανίφος, τηλ. 210.6929484, τοτ. 210.6928137, ηλ-δι. ctsatsanifos@pangaea.gr, editor@hssmge.gr, info@pangaea.gr

«ΤΑ ΝΕΑ ΤΗΣ ΕΕΕΕΓΜ» «αναρτώνται» και στην ιστοσελίδα www.hssmge.gr